First-Principles Study of Metastable Phases and Structural Anomalies of Fe, Al, Zn and Cd under Pressure

by

Florin Apostol

A Dissertation Submitted to the Faculty of

The Charles E. Schmidt College of Science

in Partial Fulfillment of the Requirements for the Degree of

Doctor of Philosophy

Florida Atlantic University

Boca Raton, Florida

December 2008

First-Principles Study of Metastable Phases and Structural Anomalies of Fe, Al, Zn and Cd under Pressure

by

Florin Apostol

This dissertation was prepared under the direction of the candidate's dissertation advisor, Dr. Shen Li Qiu, Department of Physics, and has been approved by the members of his supervisory committee. It was submitted to the faculty of The Charles E. Schmidt College of Science and was accepted in partial fulfillment of the requirements for the degree of Doctor of Philosophy.

SUPERVISORY COMMITTEE:

Shen Li Qiu, Ph.D.
Dissertation Advisor

Robin Jordan, Ph.D.

Fernando Medina, Ph.D.

Warner A. Miller, Ph.D.
Chair, Department of Physics

Korey Sorge, Ph.D.

Gary W. Perry, Ph.D.
Dean, The Charles E. Schmidt College of Science

Yuan Wang, Ph.D.

Barry T. Rosson, Ph.D.
Dean, Graduate College

October 10, 2008
Date

Acknowledgements

I wish to express my sincere gratitude to my advisor Dr. Shen Li Qiu for his extensive guidance and assistance through the whole project and in the preparation of this dissertation. Appreciation also goes to Dr. Paul M. Marcus at T. J. Watson Research Center for his instruction, enlightening discussions, and generous help.

I would like to thank all of my committee members Dr. Warner Miller, Dr. Robin Jordan, Dr. Fernando Medina, Dr. Korey Sorge and Dr. Yuan Wang for their time and useful comments. I would also like to thank all other faculty, staff, and graduate students in the Department of Physics for the help that I have received through these years.

I would like to thank Department of Physics for admitting me to FAU and continuous financial support. Gratitude is also extended to the Daniel Newell and Aurel Newell Doctoral Fellowship for the financial support. I also thank the Center for High-Performance Computing at Florida Atlantic University, funded by National Science Foundation under the grant CNS-0521410, for providing computational resources.

Finally, I would like to thank my parents. Without their love, encouragement and support, I could not have come to the United States and could not have finished the study here. I thank them for everything they have done for me.

Abstract

Author:	Florin Apostol
Title:	First-Principles Study of Metastable Phases and Structural Anomalies of Fe, Al, Zn and Cd under pressure
Institution:	Florida Atlantic University
Dissertation Advisor:	Dr. Shen Li Qiu
Degree:	Doctor of Philosophy
Year:	2008

Stable and metastable phases of Fe and Al and structural anomalies of Zn and Cd have been studied by epitaxial Bain path (EBP) and minimum path (MNP) first-principles procedures, based on finding equilibrium structures from minimizing the Gibbs free energy G with respect to structure at a given hydrostatic pressure p and temperature T. The main accomplishments are as follows. (1) This dissertation illustrates the effectiveness of the MNP procedure for finding stable and metastable phases of an element by studying four Bravais phases of Fe including body-centered tetragonal (bct), body-centered cubic (bcc), face-centered cubic (fcc) and rhombohedral (*rh*) phases. The determination of absolute stability using MNP is new; MNP finds all the elastic constants c_{ij} of a given state and the eigenvalues of the elastic constants matrix, which determine the absolute stability of the state. (2) We have extended our search for stable and metastable phases from zero temperature to finite temperature, which requires the

calculations of the Debye temperature θ_D from c_{ij} in the case of no symmetry. The Debye theory is modified by introducing a parameter β_z that gives the fraction of the full Debye zero-point energy possessed by the actual dispersive mode frequencies. The value of the lattice parameter of fcc Al at low temperatures, $a(T)$, is shown to be accurately determined by the modified Debye theory of lattice vibrations and first-principles total energy band calculations with the MNP procedure. (3) The existence of structural anomalies in hcp Zn and Cd has been shown from first-principles total-energy calculations using WIEN2k with the EBP procedure. Evaluation of the pressure dependence of various elastic quantities which are much more sensitive to the anomaly shows that the anomalies in hcp Zn and hcp Cd exist over a considerable range of pressure; several abrupt changes in the electron distribution are thereby indicated in that pressure range. (4) Calculations on the zone-center transverse optical phonon frequencies $\nu^{TO}(p)$ of hcp Zn, which found oscillatory behavior of $\nu^{TO}(p)$ in the pressure range of the anomalies, support the conclusions made in (3) on the structural anomalies. Based on this dissertation research four papers have been published in refereed journals.

Table of contents

List of tables

List of figures

Chapter 1

Introduction

1.1 Motivation

First-principles theory can now find metastable phases and structural anomalies of metals with good accuracy. Metastable phases are locally stable against small perturbations but are higher in Gibbs free energy G than the ground state. Sometimes metastable phases have very large barriers against transitions to the ground state and can be used and studied individually and at length. The classical example is diamond carbon that is unstable compared to graphite. Similarly white tin (tetragonal) is unstable with respect to gray tin (diamond), but white tin has practical uses. All phase transitions are between a metastable phase and the ground state phase or between two metastable phases. Metastable phases of a crystal are analogous to different molecules formed by the same atoms. Only one molecule has the lowest cohesive energy, but the others, although metastable, can have enough stability to persist and be useful.

Metastable phases of a material are essentially new materials that may have properties very different from the ground state phase. Much experimental effort has been made to find the metastable phases of a material by applying pressure, changing temperature, and

by varying constituent atoms [1-6]. These experimental procedures change the ground-state phase and suggest the existence at ambient conditions of metastable phases. Advanced thin film growth techniques have recently stimulated great interest in making crystalline structures that are metastable when isolated**.** The growing interest in finding such new materials makes theoretical studies of metastable phases particularly important, both to indicate where experimentalists should look and to verify any theoretically predicted phases.

Although the vast literature on phase transitions is full of calculations on metastable phases, there is still a large number of undiscovered stable and metastable phases when all symmetries are considered, when two or more atoms in the unit cell are allowed and when large ranges of pressure and temperature are studied.

Structural anomalies, i.e., abrupt changes in lattice vectors with pressure, have been observed in many metals under pressure [7-11]. The nature of these anomalies is the abrupt changes in the electron distribution over the pressure range in which anomalies occur. Structural anomalies have a large effect on the ratio of linear compressibilities, on the elastic constants and on the zone-center transverse optical phonon frequencies [7-11]. In some cases the structural anomalies are accompanied by phase transitions [7, 8]. Study of the structural anomalies under pressure, like the study of the metastable phases under pressure, has broad practical importance.

Based on our experiences and achievements we expect that our first-principles calculations will open up a vast realm of new metastable structures and structural anomalies, which will stimulate more experimental research for new materials. The

calculations will provide accurate quantitative values of the Gibbs free energy, structure and elastic constants of the stable and metastable phases. Their values will be a valuable guide to experimental pressure studies and the development of phase diagrams.

1.2 Gibbs free energy

At a given pressure p and temperature T the Gibbs free energy is defined as

$$G = E + pV + F\,, \tag{1.1}$$

where E is the total internal energy per atom, V is the volume per atom and F is the free energy of lattice vibrations per atom, which we will take from Debye theory [12] by

$$F(\theta_D, T) = \frac{9}{8}k_B\theta_D + \frac{9k_B\theta_D}{x^4}\int_0^x z^2 \ln\left(1-e^{-z}\right)dz, \quad x \equiv \frac{\theta_D}{T}\,, \tag{1.2}$$

where k_B is Boltzmann's constant, θ_D is the Debye temperature, and $\frac{9}{8}k_B\theta_D$ is the zero-point energy (ZPE).

In a crystal held at constant pressure and temperature, thermodynamic equilibrium corresponds to the state in which G is minimized with respect to the structure. The minimum of G corresponds to the ground state if all deformations of *any size* increase G and the state is called stable. However if we can only say *all small* deformations increase G, the equilibrium state may just be metastable. We include both stable and metastable phases by calling the equilibrium state locally stable. As p or T changes, phases can change between stable and metastable and can appear and disappear as minima appear and disappear.

It should be pointed out that the Gibbs free energy can be defined for systems in either equilibrium or non-equilibrium states. Landau and Lifshitz [13] state "... in a state of thermodynamic equilibrium the free energy [the Helmholtz free energy] and the thermodynamic potential [the Gibbs free energy] have minimum values, the former with respect to all changes of state with T and V constant, and the latter with respect to changes of state with T and p constant". In other words thermodynamics can be applied to systems not in equilibrium, such as crystals at constant p and T with any structure, and G has a value in non-equilibrium states. G is minimized when the system is in equilibrium.

1.3 EBP and MNP procedures

Two first-principles procedures for finding the minima of G have been used in this dissertation research: (1) the epitaxial Bain path (EBP) [8-11, 14-18], and (2) the minimum path program (MNP) [19, 20]. Both procedures are based on finding equilibrium structures from minimizing the Gibbs free energy G with respect to structure at a given hydrostatic pressure p and temperature T. The EBP procedure was described in detail in Hong Ma's dissertation [21] and also used in the early part of this dissertation research. We have recently developed a more efficient first-principles search tool called the minimum path program (MNP) [19, 20], which will be described in detail in Ch. 3.

The main differences between EBP and MNP procedures are as follows.

The EBP for tetragonal and hexagonal symmetries, which have just two lattice parameters a and c, is defined by the condition that the stress in the c direction is $-p$.

At each lattice constant a, one point is thereby found on the EBP, which is followed continuously by steps δa until minima of G on the EBP are found. At a minimum of G on the EBP, the first derivative of G vanishes in two directions (in the c direction and along the EBP), hence the derivative must vanish in all directions (in the a, c plane) at an ordinary quadratic minimum.

The MNP procedure has recently been developed and tested by comparison with our successful experience in finding metastable phases using the EBP procedure. In contrast to the point-by-point tracing of a path on the $a-c$ structure plane to find the minima of G in the EBP procedure, the MNP procedure starts at an arbitrary structure and approaches a minimum of G through a sequence of stages. Each stage corresponds to a jump to a new structure; the stages rapidly converge to the structure of the minimum.

In the EBP calculations, an initialization of WIEN2k [22] is required for each structure while in the MNP calculations only one initialization is needed - just for the initial structure. The EBP procedure finds the equilibrium structure, but does not directly find any elastic constants, which would require a series of band calculations at various strained structures. In contrast, the MNP procedure finds both the equilibrium structure and the elastic constants in the same calculation.

1.4 Objective

This dissertation research project intends to find the structural anomalies of Zn and Cd under pressure using the EBP procedure, and the stable and metastable phases of Fe

and Al under pressure and at temperatures ranging up to ambient values using the MNP procedure.

Experimental measurements of a variety of properties of hcp Zn and hcp Cd have indicated anomalous behavior around 100 kbar, including the Lamb-Mössbauer factor, the phonon linewidth of optical phonons etc. [23-25]. Our previous work demonstrates that the EBP procedure [8-11, 14-18] can be used to determine the lattice parameters and the elastic constants with good accuracy. It is interesting to see if the EBP procedure can find the small anomalies with the same magnitude and at the same pressure as observed in experimental measurements.

The major project in this dissertation research is to find the metastable phases of metals using the MNP procedure. The number of such phases, i.e., of periodic atomic bonding arrangements with local stability, grows substantially under stress. A finite fraction of them can be specified by limiting attention to Bravais phases, i.e., one-atom per unit cell of a crystal, at pressures under a specified maximum value of hydrostatic pressure for a rigid lattice. The one-atom equilibrium states of elements such as Fe and Al are particularly interesting because they must be new metastable phases. MNP calculations will be carried to high pressures on Fe and Al, where many phase transitions occur, to see what happens to the phases made metastable by the transitions.

The Debye form of free energy of lattice vibration (in Eqs. (1.1) and (1.2)) will be included in the Gibbs free energy to extend our search for stable and metastable phases from zero temperature to finite temperatures. Complete phonon spectra at each structure

would be too costly and also requires a pressure correction if the mode frequencies are calculated at constant volume V .

The energy calculations in both EBP and MNP procedures are performed using a modern first-principles band structure program, WIEN2k [22], which can calculate total energy for any crystalline structure with a very good accuracy. WIEN2k is an implementation of the full-potential augmented-plane-wave plus local orbital (APW+lo) method together with either the generalized-gradient-approximation (GGA) or the local-spin-density-approximation (LSDA). The APW+lo method expands the Kohn-Sham orbitals in atomiclike orbitals inside the atomic spheres and plane waves in the interstitial region.

- The detailed description of WIEN2k is given in Chapter 2.
- The detailed description of the MNP procedure is given in Chapter 3.
- In Chapter 4 we show the importance of the pressure correction to elastic constants.
- In Chapter 5 the MNP procedure for finding metastable phases is illustrated for four Bravais structures of Fe.
- In Chapter 6 the MNP procedure for finding metastable phases at finite temperature is illustrated for fcc Al by remedying the third defect of the Debye theory.
- In Chapter 7 the EBP procedure for finding the structural anomalies is illustrated for hcp Zn and hcp Cd.

- In Chapter 8 the EBP procedure for finding the oscillatory behavior of the zone-center transverse optical phonon frequencies is illustrated for hcp Zn.
- Summary and future work are given in Chapter 9.

1.5 Publications

During this dissertation research four papers have been published in refereed journals:

(1) S. L. Qiu, F. Apostol and P. M. Marcus, "Bravais phases of Fe under pressure from first principles", *J. Phys.: Condens. Matter* **20**, 345233 (2008).

(2) S. L. Qiu, F. Apostol and P. M. Marcus, "Low temperature properties of fcc Al from modified Debye theory", *J. Phys.: Condens. Matter* **19**, 136213 (2007).

(3) S. L. Qiu, F. Apostol and P. M. Marcus, "Pressure dependence of the TO phonon frequency in hcp Zn", *J. Phys.: Condens. Matter* **17**, 2121 (2005).

(4) S. L. Qiu, F. Apostol and P. M. Marcus, "Structural anomalies in hcp metals under pressure: Zn and Cd", *J. Phys.: Condens. Matter* **16**, 6405 (2004).

Chapter 2
WIEN2k package

WIEN2k [22] is an implementation of the full-potential augmented-plane-wave plus local orbital (APW+lo) method together with either the generalized-gradient-approximation (GGA) or the local-spin-density-approximation (LSDA). The APW+lo method expands the Kohn-Sham orbitals in atomiclike orbitals inside the atomic spheres and plane waves in the interstitial region. WIEN2k is one of the most reliable and accurate software packages for the first-principles band calculations.

2.1 Density functional theory

Density functional theory (DFT) is based on the Hohenberg-Kohn (HK) theorems [26]. Hohenberg and Kohn showed that the ground-state charge density $\rho(\vec{r})$ of a system of interacting electrons in an external potential (the Coulomb potential due to the nuclei in a solid) determines everything about the system, including the ground-state total energy E. They further proved that the total energy functional $E[\rho]$ reaches its minimal value (equal to the ground-state total energy) for the ground state charge density.

Kohn and Sham [27] developed a practical procedure to obtain the ground state density by reducing a many-body problem to a set of one-body problems coupled through

an effective potential, which takes into account the exchange-correlation energy as well as the classical electron-nucleus and electron-electron interactions. Then, $E[\rho]$ can be written as

$$E[\rho] = T_S[\rho] + E_{ei}[\rho] + E_H[\rho] + E_{XC}[\rho] \tag{2.1}$$

where T_S denotes the kinetic energy of non-interacting electrons, E_{ei} is the Coulomb interaction energy between the electrons and nuclei, E_H is the Hartree component of electron-electron energy and E_{XC} is the exchange-correlation energy. The correct density is given by the self-consistent solutions of a set of single particle Schrödinger-like equations known as Kohn-Sham (KS) equations,

$$(T + V_{ei}(\vec{r}) + V_H(\vec{r}) + V_{XC}(\vec{r}))\varphi_k(\vec{r}) = \varepsilon_k \varphi_k(\vec{r}) \tag{2.2}$$

with the density constructed as

$$\rho(\vec{r}) = \sum_k \chi_k \left|\varphi_k(\vec{r})\right|^2 . \tag{2.3}$$

Here the χ_k are occupation numbers, the φ_k are single particle orbitals, ε_k are the corresponding eigenvalues. T is the kinetic energy operator, V_{ei} is the Coulomb potential due to nuclei, V_H is the Hartree potential and V_{XC} is the exchange correlation potential [22].

Both V_H and V_{XC} depend on density, which in turn depends on the orbitals that are being search. Therefore, a density must be found such that it yields an effective potential that, when inserted into the Schrödinger-like equations, yields orbitals that reproduce it. Thus, the KS equations must be solved self-consistently in an iterative process.

The difficulty of the many-body problems is still present in the unknown exchange-correlation energy functional $E_{XC}[\rho]$. To overcome this, Kohn and Sham proposed a local-density approximation (LDA), which assume that exchange correlation energy E_{XC} can be calculated additively from each portion of a non-uniform gas as if it were locally uniform. Thus, the functional $E_{XC}[\rho]$ is given by

$$E_{XC}[\rho] = \int \rho(\vec{r}) \in_{XC} (\rho(\vec{r}))d^3\vec{r}. \tag{2.4}$$

The function $\in_{XC} (\rho)$ for the homogeneous but interacting electronic gas, is known only approximately. It can be calculated numerically to an accuracy, which results in different parameterizations [28, 29].

The widely used correction to the LDA is the generalized-gradient approximation (GGA) [30, 31]. In the GGA, an expression similar to (2.3) is used but with $\in_{XC} (\rho)$ replaced by a local function of the density and the magnitude of its gradient

$$E_{XC}[\rho] = \int f(\rho(\vec{r}), \nabla\rho(\vec{r}))d^3\vec{r}. \tag{2.5}$$

2.2 The APW+lo method

The full-potential augmented-plane-wave plus local orbital (APW+lo) method together with either the generalized-gradient-approximation (GGA) or the local-spin-density approximation (LSDA), as implemented in the WIEN2k program, is used for all total energy calculations in this work. The APW+lo method [22] is one of the most accurate methods for performing electronic structure calculations for crystals within density functional theory.

The APW+lo method is a procedure for solving Kohn-Sham equations for the ground state charge density, total energy, and energy bands of a crystal by introducing a basis set that is especially adapted to the problem: close to the nuclei the electrons behave quite as they are in a free atom, and they could be described more efficiently by atomic-like functions whereas in the region far away from the nuclei, the electrons are more or less 'free', and they could be described by plane waves. Therefore, space is divided into (I) non-overlapping atomic spheres (centered at the atomic sites) and (II) an interstitial region as shown in Fig. 2.1.

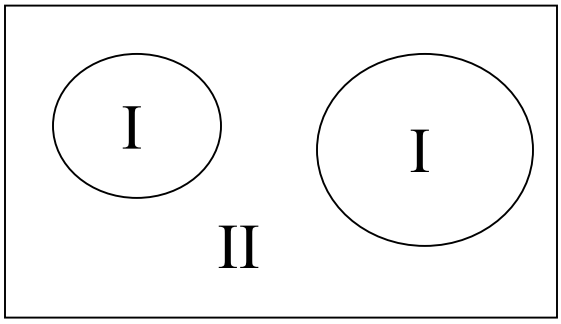

Figure 2.1. Partitioning of the unit cell into atomic spheres (I) and an interstitial region (II) for a case with two atoms.

Inside atomic sphere of radius R use

$$\phi_{\vec{k}_n} = \sum_{lm} A_{lm}(\vec{k}_n) u_l(r, E_l) Y_{lm}(\hat{r}) \tag{2.6}$$

where $\vec{k}_n = \vec{k} + \vec{K}_n$ ($\vec{k}$ is the wave vector inside the first Brillouin zone and $\vec{K}_n$ are the reciprocal lattice vectors), $u_l(r, E_l)$ is the (at the origin) regular solution of the radial

Schroedinger equation for energy E_l (chosen normally at the center of the corresponding band with l-like character) and $Y_{lm}(\hat{r})$ are spherical harmonics. In order to have enough variational flexibility in the radial basis functions local orbitals (*lo*) are added:

$$\phi_{lm}^{lo} = [A_{lm}^{lo} u_l(r, E_{1,l}) + B_{lm}^{lo} \dot{u}_l(r, E_{1,l})] Y_{lm}(\hat{r}) \tag{2.7}$$

Note that A_{lm}^{lo} and B_{lm}^{lo} do not depend on $\vec{k}_n$ and are determined by the requirement that the local orbital is zero at the sphere boundary and normalized.

In the interstitial region a plane wave expansion is used:

$$\phi_{\vec{k}_n} = \frac{1}{\sqrt{V}} e^{i\vec{k}_n \cdot \vec{r}} \tag{2.8}$$

where V is the volume of the unit cell. Each plane wave is augmented by an atomic-like function in every atomic sphere.

The Kohn-Sham orbitals are expanded in the combined basis set of the APW+lo method

$$\varphi_{\vec{k}}(\vec{r}) = \sum_n c_n \phi_{\vec{k}_n} \tag{2.9}$$

and the coefficients c_n are determined by the Rayleigh-Ritz variational principle. The convergence of this basis set is controlled by a cut-off parameter $R_{mt} K_{\max} = 6 - 9$, where R_{mt} is the smallest atomic sphere radius in the unit cell and $K_{\max}$ is the magnitude of the largest K vector in equation (2.9).

Chapter 3

MNP procedure

We have recently developed an efficient first-principles search tool called minimum path program (MNP) [19, 20] that is based on finding equilibrium structures from minimizing the Gibbs free energy G with respect to structure at a given hydrostatic pressure p and temperature T. The MNP procedure can find the structure and elastic properties of the stable and metastable phases of metals of arbitrary symmetry under arbitrary pressures and at 0 K (rigid lattice). The MNP procedure is completely automated. From the initial input parameters $a, b, c, \alpha, \beta, \gamma, p, z$ (structure, pressure and atomic number) the MNP creates all the strained and unstrained structure files and calls WIEN2k for energy evaluations, then calculates the slopes and curvatures of G at a point in structure space (axes are orthogonal components of the lattice vectors). Based on the local slope and curvature of G the MNP makes a jump to a new structure close to a minimum of G. The calculation rapidly approaches the minimum of G through a sequence of jumps in structure and simultaneously provides the values of G, the lattice parameters and the elastic constants c_{ij} at the equilibrium state. The MNP code is given in Appendix.

3.1 Computation of the minima of *G*

A small homogeneous deformation of a periodic crystal at an arbitrary structure can be specified by the 6 Eulerian strains, with rigid rotation removed. The strains are related to the components of the lattice vectors in orthogonal axes by [32,33]

$$\underline{\underline{R}}' = \left(\underline{\underline{I}} + \underline{\underline{\varepsilon}}\right)\underline{\underline{R}}$$

or
$$\begin{pmatrix} a_1' & b_1' & c_1' \\ a_2' & b_2' & c_2' \\ a_3' & b_3' & c_3' \end{pmatrix} = \begin{pmatrix} 1+\varepsilon_{11} & \varepsilon_{12} & \varepsilon_{13} \\ \varepsilon_{12} & 1+\varepsilon_{22} & \varepsilon_{23} \\ \varepsilon_{13} & \varepsilon_{23} & 1+\varepsilon_{33} \end{pmatrix} \begin{pmatrix} a_1 & b_1 & c_1 \\ a_2 & b_2 & c_2 \\ a_3 & b_3 & c_3 \end{pmatrix} \tag{3.1}$$

where $\underline{\underline{\varepsilon}} \equiv \begin{pmatrix} \varepsilon_{11} & \varepsilon_{12} & \varepsilon_{13} \\ \varepsilon_{12} & \varepsilon_{22} & \varepsilon_{23} \\ \varepsilon_{13} & \varepsilon_{23} & \varepsilon_{33} \end{pmatrix} = \begin{pmatrix} \varepsilon_1 & \varepsilon_6/2 & \varepsilon_5/2 \\ \varepsilon_6/2 & \varepsilon_2 & \varepsilon_4/2 \\ \varepsilon_5/2 & \varepsilon_4/2 & \varepsilon_3 \end{pmatrix}$ (in Voigt notation) is the first-order strain matrix which has 6 components, and $\underline{\underline{I}}$ is the identity matrix,

$\underline{\underline{R}} = \begin{pmatrix} a_1 & b_1 & c_1 \\ a_2 & b_2 & c_2 \\ a_3 & b_3 & c_3 \end{pmatrix}$ is the 3x3 matrix of components of the initial state and

$\underline{\underline{R}}' = \begin{pmatrix} a_1' & b_1' & c_1' \\ a_2' & b_2' & c_2' \\ a_3' & b_3' & c_3' \end{pmatrix}$ is the matrix of components of the strained state**.**

If we assume that there are no body torques on the crystal, so G is independent of rotations, the change in G around any given state can be expanded in a power series in the Eulerian strains ε_i

$$\frac{G-G_0}{V_0} = \frac{\delta G}{V_0} = \sum_{i=1}^{6} c_i \varepsilon_i + \frac{1}{2}\sum_{i,j=1}^{6} c_{ij}\varepsilon_i \varepsilon_j . \tag{3.2}$$

Then $c_i = \frac{1}{V_0}\frac{\partial G}{\partial \varepsilon_i}$, $c_{ij} = \frac{1}{V_0}\frac{\partial^2 G}{\partial \varepsilon_i \partial \varepsilon_j}$, (3.3)

where the derivatives in (3.3) are at the given state and G_0, V_0 are the values of G and V respectively at the given state.

If a state of the system is stationary, i.e., has no stress, the state will have $c_i = 0$, $i = \overline{1,6}$. For the stationary state to be a minimum the quadratic form $\frac{1}{2}\sum_{i,j} c_{ij}\varepsilon_i\varepsilon_j$ must be positive definite, i.e., positive for all values of the ε_i.

The positive definiteness of $\sum_{i,j} c_{ij}\varepsilon_i\varepsilon_j$ is tested even when the $c_i \neq 0$. Suppose it is positive definite - this is called CASE 1. Look for a minimum by putting

$$\frac{1}{V_0}\frac{\partial G}{\partial \varepsilon_i} = c_i + \sum_{j=1}^{6} c_{ij}\varepsilon_j = 0,\ i = \overline{1,6} \tag{3.4}$$

Then (3.4) is a set of six equations for values of the six ε_i. With these ε_i and (3.1) the new structure $\underline{\underline{R}}'$ can be found. If (3.2) held exactly, the c_i of $\underline{\underline{R}}'$ would vanish. But higher terms in the power series in the ε_i will interfere, and the process of finding new c_i, c_{ij} in the state $\underline{\underline{R}}'$ will usually have to be repeated; however convergence to the state with $c_i \cong 0$ will be quadratic, hence rapid.

To test the positive definiteness of $\sum_{i,j} c_{ij}\varepsilon_i\varepsilon_j$ it is useful to represent it by a matrix product

$$(\varepsilon_1 \quad \varepsilon_2 \quad . \quad . \quad . \quad \varepsilon_6)\begin{pmatrix} c_{11} & c_{12} & . & . & . & c_{16} \\ c_{21} & c_{22} & . & . & . & c_{26} \\ . & . & . & . & . & . \\ . & . & . & . & . & . \\ . & . & . & . & . & . \\ c_{61} & c_{62} & . & . & . & c_{66} \end{pmatrix}\begin{pmatrix} \varepsilon_1 \\ \varepsilon_2 \\ . \\ . \\ . \\ \varepsilon_6 \end{pmatrix}. \tag{3.5}$$

If $\begin{pmatrix} \bar{\varepsilon}_1 \\ . \\ . \\ \bar{\varepsilon}_6 \end{pmatrix}$ and λ are an eigenvalue and eigenvector respectively of the $\underline{\underline{c_{ij}}}$ matrix then

$$\begin{pmatrix} c_{11} & c_{12} & . & . \\ c_{21} & . & . & . \\ . & . & . & . \\ . & . & . & c_{66} \end{pmatrix}\begin{pmatrix} \bar{\varepsilon}_1 \\ . \\ . \\ \bar{\varepsilon}_6 \end{pmatrix} = \lambda \begin{pmatrix} \bar{\varepsilon}_1 \\ . \\ . \\ \bar{\varepsilon}_6 \end{pmatrix}. \tag{3.6}$$

Multiply (3.6) on the left by the row eigenvector $(\bar{\varepsilon}_1 \quad . \quad . \quad \bar{\varepsilon}_6)$ and get

$$\sum_{ij=1}^{6} c_{ij}\bar{\varepsilon}_i\bar{\varepsilon}_j = \lambda\left(\bar{\varepsilon}_1^2 + \bar{\varepsilon}_2^2 + ... + \bar{\varepsilon}_6^2\right). \tag{3.7}$$

Hence if $\lambda > 0, \sum_{ij=1}^{6} c_{ij}\bar{\varepsilon}_i\bar{\varepsilon}_j > 0$. Note that an arbitrary strain matrix can always be expanded in a linear combination of the eigenvectors, which form a complete orthogonal set. Therefore, $\sum_{i,j} c_{ij}\varepsilon_i\varepsilon_j$ is positive definite if all 6 $\lambda's$ are positive.

If some $\lambda's$ are negative, $\sum_{i,j} c_{ij}\varepsilon_i\varepsilon_j$ is not positive definite, and (3.7) shows that the eigenvector belonging to a negative λ will decrease the value of $\sum_{i,j} c_{ij}\varepsilon_i\varepsilon_j$ - this is called CASE 2. Hence the structure is modified taking steps in structure space along an

eigenvector with the most negative λ to decrease G until the minimum is reached. The state at the minimum will have at least one fewer negative eigenvalues. The process is repeated until all eigenvalues are positive. There must be a minimum because the system cannot go below the ground state. Then home in on the actual minimum by the procedure in CASE 1.

3.2 Computation of c_i and c_{ij}

Case 1: to calculate c_i and c_{ii} take the strain $\varepsilon_i = \pm\varepsilon$ $\varepsilon_j = 0$, $j \neq i$.

Example of calculations for c_1 and c_{11}:

Let $\varepsilon_1 = \varepsilon$, $\varepsilon_j = 0$, $j = \overline{2,6}$. Then (3.2) gives

$$\frac{G_{(\varepsilon\ 0\ \ldots\ 0)} - G_0}{V_0} = \frac{\delta G}{V_0} = c_1\varepsilon + c_{11}\varepsilon^2 . \tag{3.8}$$

Let $\varepsilon_1 = -\varepsilon$, $\varepsilon_j = 0$, $j = \overline{2,6}$. Then

$$\frac{G_{(-\varepsilon\ 0\ \ldots\ 0)} - G_0}{V_0} = \frac{\delta G}{V_0} = -c_1\varepsilon + c_{11}\varepsilon^2 . \tag{3.9}$$

The Eqs. (3.8) and (3.9) give c_1 and c_{11}:

$$c_1 = \frac{G_{(\varepsilon\ 0\ \ldots\ 0)} - G_{(-\varepsilon\ 0\ \ldots\ 0)}}{2\varepsilon V_0} , \tag{3.10}$$

$$c_{11} = \frac{G_{(\varepsilon\ 0\ \ldots\ 0)} + G_{(-\varepsilon\ 0\ \ldots\ 0)} - 2G_0}{2\varepsilon^2 V_0} . \tag{3.11}$$

Case 2: to calculate the fifteen c_{ij} ($j > i$) take the strain $\varepsilon_i = \varepsilon_j = \varepsilon$, $\varepsilon_k = 0, k \neq i \neq j$. Example of calculations for c_{12}:

Let $\varepsilon_1 = \varepsilon_2 = \varepsilon$, $\varepsilon_k = 0$, $k = \overline{3,6}$. Then

$$\frac{G_{(\varepsilon\ \varepsilon\ 0\ .\ .\ 0)}-G_0}{V_0}=\frac{\delta G}{V_0}=(c_1+c_2)\varepsilon+\left(\frac{c_{11}+c_{22}}{2}+c_{12}\right)\varepsilon^2 \tag{3.12}$$

and $c_{12}=\frac{G_{(\varepsilon\ \varepsilon\ 0\ .\ .\ 0)}-G_0}{\varepsilon^2 V_0}-\frac{c_1+c_2}{\varepsilon}-\frac{c_{11}+c_{22}}{2}$. (3.13)

For a better accuracy, the term from (3.13) that contains c_1 and c_2 is eliminated by using an additional strain: $\varepsilon_1=\varepsilon_2=-\varepsilon,\ \varepsilon_k=0,\ k=\overline{3,6}$. Then

$$\frac{G_{(-\varepsilon\ -\varepsilon\ 0\ .\ .\ 0)}-G_0}{V_0}=\frac{\delta G}{V_0}=-(c_1+c_2)\varepsilon+\left(\frac{c_{11}+c_{22}}{2}+c_{12}\right)\varepsilon^2 \ . \tag{3.14}$$

By combining (3.12) and (3.13) we finally get

$$c_{12}=\frac{G_{(\varepsilon\ \varepsilon\ .\ .\ 0)}+G_{(-\varepsilon\ -\varepsilon\ 0\ .\ 0)}-2G_0}{2\varepsilon^2 V_0}-\frac{c_{11}+c_{22}}{2}\ . \tag{3.15}$$

3.3 The logic of the MNP procedure

The current version of MNP is designed for one-atom unit cells at zero temperature. With only one initialization for the initial input parameters $a,b,c,\alpha,\beta,\gamma,p,z$ (structure, pressure and atomic number) MNP automatically approaches a minimum of $G(a,b,c,\alpha,\beta,\gamma,p)$ through a sequence of stages as follows.

- Creates all necessary structure files and finds c_i and c_{ij} of the initial input structure from 43 calculations of the free energy G (using WIEN2k).
- Finds the eigenvalues λ_i and the eigenvectors Ψ_i (column matrix with components ε_1 to ε_6) of the $\underline{\underline{c_{ij}}}$ matrix.

- Checks the signs of the λ_i; if all λ_i>0, $\sum_{i,j} c_{ij}\varepsilon_i\varepsilon_j$ is positive definite; call this CASE 1 and go to the CASE 1 branch.

- Tests the magnitudes of the c_i - if small enough, the minimum has been found and the program stops. If not, solves the 6 linear equations in (3.4) for the structure jump ε_i. The c_i will decrease in this strained state (they would vanish if (3.2) were exact).

- Finds the $\underline{\underline{R'}}$ produced by this strain (the solution of (3.4)); test the c_i values for this strained state and decide if a minimum has been found; if not, repeat the procedure.

- If some λ_i < 0, MNP finds the most negative (call it $\bar{\lambda}$) and its eigenfunction $\bar{\Psi}$; call this CASE 2 and go to the CASE 2 branch.

- Takes strains proportional to $\bar{\Psi}$ (in small steps) in the direction in which $\sum c_i\bar{\varepsilon}_i < 0$, and test that $G < G_0$.

- Continues taking steps of strains along $\bar{\Psi}$ until G increases, i.e., a minimum in the $\bar{\Psi}$ has been passed; find the state at the minimum by interpolation.

- Goes back to find new c_i and c_{ij} with the state at the minimum.

3.4 MNP script

MNP calls WIEN2k as a subroutine to carry out the first-principles band calculations. To make such a call a c-shell script called MNP.script is needed. The logic of the script is as follows.

1. MNP.script runs a sequence of three routines: MNP12N_optimize, MNP12N_optimize.job and MNP12N. MNP12N_optimize creates all necessary unstrained and strained structure files, MNP12N_optimize.job calculates the internal energies of all structures (using WIEN2k) and MNP12N computes the c_i and the c_{ij} from 43 calculations of the free energy G as well as the eigenvalues and eigenvectors of the matrix $\underline{\underline{c_{ij}}}$. Moroever, MNP12N establishes what case is: CASE 11 (all $\lambda_i > 0$ but some c_i are not convergent), CASE 12 (all $\lambda_i > 0$ and all c_i are convergent) and CASE 2 (some $\lambda_i < 0$). Note that both CASE 11 and CASE 12 are part of CASE 1, which is defined in Sect. 3.1.

2. MNP.script sets a separate branch for every case. Every case is analyzed independently by using the 'if' statement:

if (CASE X) then

commands

endif

The branches follow the order: CASE 11, CASE 12 and CASE 2.

CASE 11: The initial structure is strained with ε_i (the solution of (3.4)). A complete analysis of the strained structure is made using the same sequence of 3 routines as for the initial input structure. The procedure is repeated by using a "while" loop until the output of the MNP12N routine doesn't correspond to CASE 11 anymore (it must be CASE 12 or CASE 2). The maximum number of steps, e.g., structure jumps ε_i, is set at 40.

CASE 12: The script does stop, equilibrium state is found.

CASE 2: The script takes a series of steps in structure space along the eigenvector $\overline{\Psi}$ of the most negative eigenvalue $\bar{\lambda}$ to decrease G until a minimum is reached. This task is done with a main sequence of two routines, MNP12N_case2_optimize and MNP12N_case2_optimize.job. Briefly, MNP12N_case2_optimize creates a series of strained structure files whose strains are proportional to $\overline{\Psi}=(\bar{\varepsilon}_1 \ . \ . \ \bar{\varepsilon}_6)$. For instance, the strain of the N^{th} structure has the form: $\varepsilon_i^N = N\times e\times\bar{\varepsilon}_i$, where $N=\overline{1,19}$ and e=0.02. Then, MNP12N_case2_optimize.job calculates all necessarily free energies G of the strained structures until a minimum in the $\overline{\Psi}$ direction is reached. The structure parameters at the minimum $(a_{\min}^{CASE\,2}, b_{\min}^{CASE\,2}, c_{\min}^{CASE\,2}, \alpha_{\min}^{CASE\,2}, \beta_{\min}^{CASE\,2}, \gamma_{\min}^{CASE\,2}, p)$ will become the new input parameters $(a, b, c, \alpha, \beta, \gamma, p)$ by using a "goto" command.

There are several paths MNP.script can follow to reach the equilibrium as shown in Fig. 3.1. If the Hessian matrix $\underline{\underline{c_{ij}}}$ of initial structure is positive definite and all c_i are convergent, e.g., initial structure is at equilibrium, the script skips CASE 11 branch and goes directly to CASE 12 branch (route (3)). If $\underline{\underline{c_{ij}}}$ of initial structure is positive definite but some c_i are not convergent, the script goes to CASE 11 branch (route (1)); structure jumps ε_i (the solutions of (3.4)) are made to decrease the magnitudes of the c_i. Probably, after a few such jumps, the c_i become convergent and $\underline{\underline{c_{ij}}}$ remains positive definite; equilibrium has been found, and the script goes to CASE 12 branch (route (2)). If $\underline{\underline{c_{ij}}}$ is not positive definite anymore, the script goes to CASE 2 branch, regardless of the magnitude of the c_i (route (5)).

Let's assume that the $\underline{\underline{c_{ij}}}$ matrix of the initial structure is not positive definite. Then the script skips both CASE 11 and CASE 12 and goes to CASE 2 branch (route (4)). The script modifies the structure by taking steps in the $\overline{\Psi}$ direction to decrease *G* until a minimum is reached. The script goes back to its starting point and the structure at the minimum in the $\overline{\Psi}$ direction becomes the new input structure (route (6)). The procedure is repeated until an equilibrium structure is found.

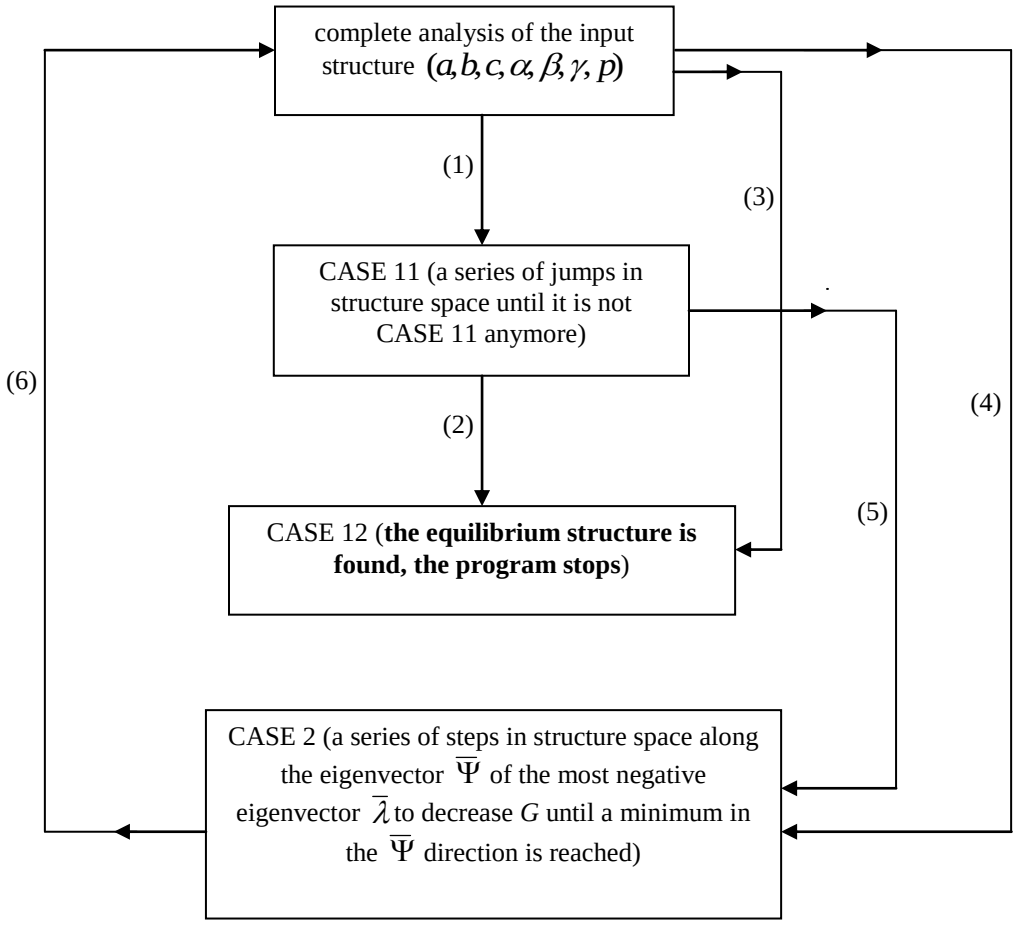

Figure 3.1. The logic of the MNP script.

3.5 Outstanding feature of MNP procedure

The MNP procedure has been tested on the ground states of several metallic elements at zero pressure and 0 K. In each case the procedure consists of choosing an arbitrary initial state and testing how close the final state found by MNP is to the known experimental data. The testing results on fcc Al and Cu are listed in Table 3.1. The agreement between the theoretical and experimental results listed in Table 3.1 would be considered quite good.

Table 3.1. Comparison of the MNP results with the experimental data of the lattice constant a, the elastic constants c_{11}, c_{12}, c_{44} of fcc Al and fcc Cu at $p=0$ and $T=0$. The experimental data are from [34] for the lattice constants (extrapolated to 0 K values), and from [35] for the elastic constants (0 K values).

Element	a (bohr)		c_{11} (Mbar)		c_{12} (Mbar)		c_{44} (Mbar)	
	MNP	Exp.	MNP	Exp.	MNP	Exp.	MNP	Exp.
Al (fcc)	7.646	7.620	1.114	1.143	0.601	0.619	0.329	0.316
Cu (fcc)	6.849	6.809	1.752	1.762	1.145	1.249	0.742	0.818

The outstanding feature of the MNP results is that the procedure succeeded in finding a minimum for all the assumed initial structures, which were chosen to cover several directions. Moreover, the greatest number of stages required in our preliminary tests was less than 10. The termination values (the lattice parameters at the equilibrium state) are functions of the convergence criteria, which are easily made smaller. As an example,

Fig.3.2 shows the paths to the minima of G of the fcc phase of Y starting from two arbitrary initial states as found with the MNP procedure (at $p=0, T=0$).

In general, different initial states can lead to different minima. We have performed another test on Y with another two arbitrary initial states, which are different than that shown in Fig. 3.2 and found the bct phase of Y (data are not shown). Therefore, with systematic variation of initial states, the MNP procedure should be able to locate all stable and metastable phases.

Notice that the ground state of Y is hcp. The fcc and bct phases found by the MNP procedure are at higher energies than the hcp phase, therefore, metastable. Thus far there are no experimental data available for the metastable fcc and bct phases of Y.

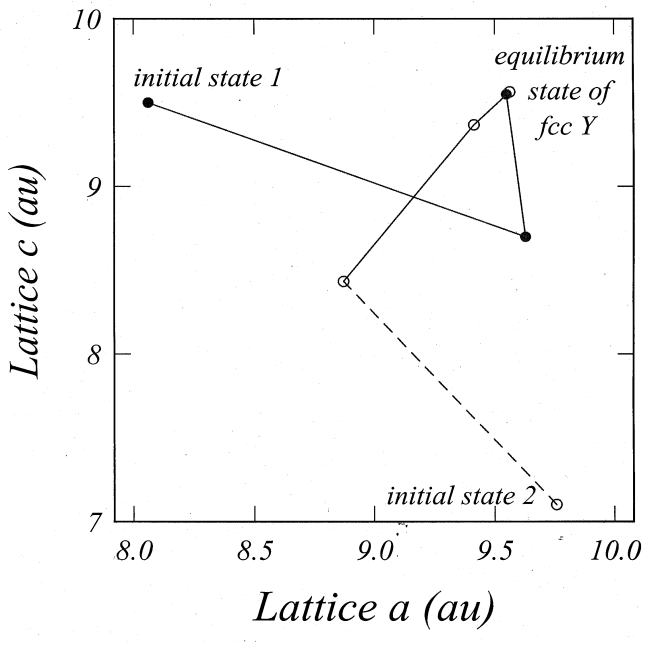

Figure 3.2. The paths to the minima of G of the fcc phase of Y starting from two arbitrary initial states as found with the MNP procedure. The solid (dashed) lines between the stage's points are CASE 1 (CASE 2) stages (see text).

The MNP procedure has also been successfully tested in finding the stability pressure p_s at which the shear constant $C' = (c_{11} - c_{12})/2$ vanishes for ferromagnetic (FM) bcc Fe. The MNP procedure gives the same value of p_s as that obtained from the EBP procedure [21].

It should be pointed out that although the current version of MNP is designed for one-atom unit cells, it can be used for two-atom unit cells, when the second atom in the two-atom unit cell is locked in place by symmetry, i.e., the second atom has no relaxation so that the position of the second atom relative to the first atom is unchanged when the unit cell is strained. The input file to WIEN2k includes the structure parameters $a, b, c, \alpha, \beta, \gamma$ of the unit cell and the positions of the two atoms in units of a, b, c, for example, (0, 0, 0) and $(2/3, 1/3, 1/2)$ for an hcp unit cell, which will be kept unchanged for the hcp cell because the second atom does not relax. As a result, the elastic constants of the equilibrium state found by MNP will be unrelaxed [9].

3.6 Comparison of the MNP procedure with other procedures

(a) Comparison of the MNP procedure with the MD procedure

It is interesting to compare MNP with the molecular dynamics (MD) technique extended to variable cell structure and finite pressures [36]. In this extension MD can be and has been applied to the phases of elements, but has different strengths and weaknesses versus MNP. MD calculates electronic structure and forces on the atoms quantum mechanically, but the atoms then follow classical orbits. Hence MD is not suitable for accurate descriptions of low-temperature equilibrium behavior. Quong and

Liu [37], who made a good first-principles calculation of thermal expansion in some cubic materials and rejected MD, remark: "First-principles molecular dynamics methods such as the Car-Parrinello method can be used to determine thermal properties expressed as statistical averages. However, since the ionic degrees of freedom are treated classically these simulations are not valid at temperatures comparable to or lower than the Debye temperature. A further drawback is that the entropy, and hence the free energy, cannot be expressed as an ensemble average." In contrast to MD, MNP is completely first-principles quantum-mechanical and could readily add the generalized Debye evaluation of the zero-point vibrational energy that is an intrinsic part of the crystal, but is not present in the MD calculation. MNP could also add the vibrational Helmholtz free energy at finite temperature (see Eqs. (1.1) and (1.2)) in the quasi-harmonic Debye approximation to give accurate low-temperature equilibrium structures. The MNP technique evaluates properties of the infinite lattice with the high accuracy of the WIEN2k band-structure program, whereas MD finds statistical averages over a finite number of atoms, which are subject to fluctuations.

The MD calculation appears to be more computationally intensive than the MNP calculation, since it approaches equilibrium through many small damped time-steps. At each time-step the self-consistent wave function and atomic forces must be computed. MNP makes a sequence of jumps in structure controlled by the local free energy curvature and slope as a function of strain. Rather few jumps are needed to find the minimum, and the final approach to such minima is second-order in the strains.

However we note that among the MD advantages is the ability to handle many atoms in a unit cell at finite temperatures and give plausible intermediate configurations between an initial and final structure. The MNP calculation will grow rapidly with addition of more atoms in the unit cell and the intermediate configurations apply just to a single cell, i.e., are homogeneous, and are not related to the path that an actual system would follow.

(b) Comparison of the MNP procedure with the procedure in the program CRYSTAL

It is also of interest to compare MNP with the procedure in the program CRYSTAL [38], which was adapted from programs to find equilibrium structures of molecules [39]. Both MNP and CRYSTAL are based on the well-known mathematical procedure that uses second derivatives of a function at an initial set of values of the variables to find a new set of values at which the first derivatives are smaller. If the function has positive curvature at the initial variable, a change in the variable can be found which reduces the first derivative. Iteration should then lead to variable values at which the first derivatives fall below a preset small value.

The most striking difference between MNP and CRYSTAL is that MNP, which is designed to solve a simpler structural problem than CRYSTAL, is much simpler in its operations and has much fewer operations. There are also many differences in detail. We note the following:

- CRYSTAL, at each stage *n*, finds a new direction along which to vary the structure from the structure at *n* to search for a minimum; MNP, at each stage *n*, finds a

new structure, which would be the minimum if the quadratic expansion of G in the variables were exact.

- CRYSTAL uses structural variables about which there is physical knowledge - bond lengths, bond angles, dihedral angles - which it orthogonalizes and tests for linear dependence; MNP uses the natural variables of crystal elasticity theory, the strains, so that all deformations are free of rotations.

- CRYSTAL calculates accurate analytic first derivatives in a Hartree-Fock formulation, which are used to update the matrix of second derivatives (the Hessian matrix) at each stage with elaborate formulas, hence accurate value of the first derivatives are needed; MNP calculates the first and second derivatives numerically in a density-functional formulation with about 1% uncertainty at each stage, hence does not need accurate values because the procedure is self-correcting.

- MNP has just two basic operations: 1) finding first and second derivatives numerically and applying the Hessian matrix to the vector of first derivatives to find a structure closer to the minimum energy; 2) if the Hessian matrix is not positive definite, steps are taken in the steepest descent direction to a one-dimensional minimum and the process is repeated. CRYSTAL adds operations on the coordinates, operations to update the Hessian matrix from an initial estimate based on a physical knowledge, and search operations for one-dimensional minima. Some of these more elaborate operations may be needed when MNP is modified to include more atoms in the unit cell and the atoms are allowed to relax. But MNP has been proven adequate for the interesting and important

question of the existence of stable and metastable phases of elements in several symmetrical common structures of metallic elements under pressure.

Chapter 4

Pressure corrections to elastic constants

When changes in internal energy due to strains introduced in a crystal in equilibrium at finite pressure are expanded to second order in the strains, the coefficients of the second-order terms have frequently been mistakenly assumed to be the elastic constants under pressure. However, to obtain the elastic constants from the coefficients requires correction dependent on the pressure, i.e., pressure correction is needed because measured elastic constants are at constant pressure, whereas the calculated coefficients are found from internal energy changes at constant volume. This correction is derived here simply from thermodynamic theory. It is shown that the second derivatives of Gibbs free energy G, but not of internal energy E, with respect to strains at the equilibrium structure give the elastic constants under pressure.

4.1 Elasticity under hydrostatic pressure

The pressure correction was well understood over forty years ago as described in the classic 1965 paper of Barron and Klein [40] before the era of quantitative first-principles calculations of elastic constants under pressure, but has been overlooked in a number of

modern papers, e.g., [41-45]. Here we give a simpler derivation of the pressure correction than in [40], based on introducing G to describe a crystal under pressure and on the thermodynamic minimization theorem about G at constant p and constant T, which may make the correction easier to understand.

Consider a small homogeneous deformation of a periodic crystal at an arbitrary structure at p. If we assume that there is no body torque on the crystal, so E and G are independent of rotations, the change in E and G can each be expanded in a power series in six Eulerian strains ε_i, which are linearly related to the changes in the lattice vectors $\vec{a}$, $\vec{b}$, $\vec{c}$. At an arbitrary structure, the expansions will have both first and second-order terms in ε_i. However if the expansion is around equilibrium, where G is a minimum, δG will not have first-order terms. Unlike δG, δE will have first-order terms because at equilibrium E is not a minimum for all structural changes, only for those which keep the volume V constant at least to first order in the ε_i, hence keep the crystal system closed.

The expansion of the Gibbs free energy $G = E + pV$ (at $T = 0$) in strain components around equilibrium for a periodic crystal at pressure p has the form (to second order in Eulerian strains)

$$\frac{\delta G}{V_0} = \frac{G - G_0}{V_0} = \frac{1}{2}\sum_{i,j=1}^{6} c_{ij}\varepsilon_i\varepsilon_j , \tag{4.1}$$

where V_0 is the equilibrium volume per atom, ε_i and ε_j are Eulerian strain components in Voigt notation. The coefficients c_{ij} of the second-order terms are in fact the elastic constants (also called elastic stiffness coefficients) and enter the stress-strain relations for

a crystal at p and the equation of motion of disturbances of equilibrium in the crystal at p; these properties of the c_{ij} are shown by Barron and Klein [40].

We relate (4.1) to the work of Barron and Klein by rearranging (4.1) as an equation for δE, the change in E for a homogeneous deformation ε_i, $i=\overline{1,6}$ at constant p,

$$\frac{\delta E}{V_0}=\frac{\delta G}{V_0}-p\frac{\delta V}{V_0}=-\frac{p}{V_0}\sum_{i=1}^{6}\left(\frac{\partial V}{\partial \varepsilon_i}\right)_0\varepsilon_i+\frac{1}{2}\sum_{i,j=1}^{6}\left(c_{ij}-\frac{p}{V_0}\left(\frac{\partial^2 V}{\partial\varepsilon_i\varepsilon_j}\right)_0\right)\varepsilon_i\varepsilon_j\,. \tag{4.2}$$

In (4.2) δV has been expanded in a power series around equilibrium to second order in ε_i. The strain derivatives of V can be calculated by expressing V as the determinant of the product of two matrices

$$V\left(\{\varepsilon_i\}\right)=\left|\begin{pmatrix}1+\varepsilon_1 & \frac{\varepsilon_6}{2} & \frac{\varepsilon_5}{2}\\ \frac{\varepsilon_6}{2} & 1+\varepsilon_2 & \frac{\varepsilon_4}{2}\\ \frac{\varepsilon_5}{2} & \frac{\varepsilon_4}{2} & 1+\varepsilon_3\end{pmatrix}\begin{pmatrix}a_1 & b_1 & c_1\\ a_2 & b_2 & c_2\\ a_3 & b_3 & c_3\end{pmatrix}\right|$$

$$=\left[1+\varepsilon_1+\varepsilon_2+\varepsilon_3+\varepsilon_1\varepsilon_2+\varepsilon_2\varepsilon_3+\varepsilon_3\varepsilon_1-\frac{1}{4}\left(\varepsilon_4^2+\varepsilon_5^2+\varepsilon_6^2\right)+\right.$$

$$\left.+\varepsilon_1\varepsilon_2\varepsilon_3+\frac{1}{4}\left(\varepsilon_4\varepsilon_5\varepsilon_6-\varepsilon_1\varepsilon_4^2-\varepsilon_2\varepsilon_5^2-\varepsilon_3\varepsilon_6^2\right)\right]V_0 \tag{4.3}$$

where the $\{\varepsilon_i\}$ means the six ε_i, a_i, b_i and c_i are the unstrained orthogonal components of the equilibrium lattice vectors that describe the unit cell and the matrix product gives the strained components. Differentiation of the polynomial in the ε_i in (4.3) shows that the only non-zero first and second strain derivatives of V are

$$\left(\frac{\partial V}{\partial \varepsilon_i}\right)_0 = V_0, i = \overline{1,3};\ \left(\frac{\partial^2 V}{\partial \varepsilon_i^2}\right)_0 = -\frac{V_0}{2}, i = \overline{4,6};\ \left(\frac{\partial^2 V}{\partial \varepsilon_i \partial \varepsilon_j}\right)_0 = V_0, i, j = \overline{1,3}; i \neq j \qquad (4.4)$$

Putting (4.4) into (4.2) gives for the expansion of δE around equilibrium

$$\frac{\delta E}{V_0} = -p(\varepsilon_1 + \varepsilon_2 + \varepsilon_3) + \frac{1}{2}\sum_{i,j=1}^{6} \overline{c}_{ij}\varepsilon_i\varepsilon_j \qquad (4.5)$$

where the $\overline{c}_{ij}$ contain pressure corrections defined by

$$\begin{aligned} c_{ij} &= \overline{c}_{ij} + p \quad ij = 12,13,23, \\ c_{ii} &= \overline{c}_{ii} - p/2 \quad i = 4,5,6, \\ c_{ij} &= \overline{c}_{ij} \text{ for all other } c_{ij}, \text{e.g., } c_{11}, c_{14}, c_{45}. \end{aligned} \qquad (4.6)$$

The relations in (4.3), (4.4), (4.5) and (4.6) hold for arbitrary symmetry.

Note that (4.6) is in fact identical with Eq. (5.4) of Barron and Klein [40] if you change the subscripts to simpler Voigt form, and drop the rotation dependence by restricting application to systems without body torques.

A volume-conserving strain procedure, which has been used for example in [46-49], is a source of confusion about the validity of (4.5) because the procedure finds the elastic constants c_{ij} in a system under pressure directly from the coefficients of second-order terms in δE without explicitly adding the pressure correction. However this procedure is made to work by modifying the strains used in δE (the strain components contain higher power of the ε_i) and does not demonstrate that (4.5) is invalid.

For example, Gülseren and Cohen [46, Eq. 3] use the strain elements

$$\varepsilon_1 = \varepsilon_2 = e,\ \varepsilon_3 = (1+e)^{-2} - 1,\ \varepsilon_4 = \varepsilon_5 = \varepsilon_6 = 0, \qquad (4.7)$$

which gives (using (4.5)) to second order in e (the first term vanishes) for cubic symmetry $\delta E/V_0 = 3(c_{11} - c_{12})e^2$, where $c_{11} - c_{12}$ is the pressure-corrected elastic constant.

Note that (4.7) contains second-order terms in e^2, where e is the magnitude of the Eulerian strains ε_1 and ε_2. Expansion of ε_3 in powers of e gives

$$\varepsilon_3 = -2e + 3e^2 + \text{ higher terms.} \tag{4.8}$$

The terms linear in e cancel in $-p(\varepsilon_1 + \varepsilon_2 + \varepsilon_3)$ in (4.5), but the e^2 term in ε_3 adds $-3pe^2$ to $\delta E/V_0$ which is the pressure correction in $3(\overline{c}_{11} - \overline{c}_{12}) - 3p \equiv 3(c_{11} - c_{12})$.

To calculate c_{44} for hcp structures ($c_{44} = c_{55}$) Steinle-Neumann et al [49, Eq. 9] use the isochoric strain

$$\varepsilon_1 = \varepsilon_3 = \varepsilon_4 = \varepsilon_6 = 0,\ \varepsilon_2 = \frac{e^2}{1 - e^2},\ \varepsilon_5 = 2e. \tag{4.9}$$

Expansion of ε_2 in powers of e gives

$$\varepsilon_2 = e^2(1 + e^2 + ...) = e^2 + \text{ higher terms} \tag{4.10}$$

To second order terms in e, (4.5) becomes

$$\delta E/V_0 = -pe^2 + 2\overline{c}_{44}e^2 = 2(\overline{c}_{44} - p/2)e^2 = 2c_{44}e^2 \tag{4.11}$$

We note that there are no linear terms in $-p(\varepsilon_1 + \varepsilon_2 + \varepsilon_3)$ in (4.5), but the e^2 term in ε_2 gives the pressure correction for c_{44}.

To find the elastic constants from calculations of E, one must first find equilibrium by minimizing E at a given V with respect to structure; for cubic symmetry V gives the

structure, for lesser symmetry changes of structure at constant V must be considered. To fix the pressure requires the equation of state $p(V)$ obtained from $p=-dE/dV$. The coefficients $\overline{c}_{ij}$ of $\varepsilon_i\varepsilon_j$ terms in (4.5) are then found from δE around equilibrium calculated for strains for which δV vanishes to first order in the ε_i, i.e., for which $\varepsilon_1+\varepsilon_2+\varepsilon_3=0$, but the strains are otherwise arbitrary (second-order strain terms in δV can be finite). Finally the $\overline{c}_{ij}$ must be corrected by the pressure correction in (4.6) to find the c_{ij}.

The procedure for calculating the c_{ij} from δG avoids the complications imposed by the requirement $\varepsilon_1+\varepsilon_2+\varepsilon_3=0$. The two cases required (for a crystal with no symmetry) are six choices $\varepsilon_i=e$, $i=\overline{1,6}$, other ε's are zero, and the fifteen choices of i, j in $\varepsilon_i=\varepsilon_j=e$, other ε's $=0$, $i\neq j$.

Thus using δG in (4.1)

Case 1: $\varepsilon_i=e$, $\varepsilon_j=0$, $j=\overline{2,6}$,

$$\frac{\delta G}{V_0}=\frac{1}{2}c_{11}e^2, \tag{4.12}$$

and five more permutations of (4.12)

Case 2: $\varepsilon_i=e$, $\varepsilon_2=e$, $\varepsilon_j=0$, $j=\overline{3,6}$,

$$\frac{\delta G}{V_0}=\left(\frac{c_{11}+c_{22}}{2}+c_{12}\right)e^2, \tag{4.13}$$

where c_{11} and c_{22} are known from *case 1*. The fourteen other permutations of (4.13) give the remaining c_{ij}. No simultaneous equations for the c_{ij} occur.

4.2 Discussion

It is easy to overlook the pressure correction because δE can be calculated at any V without knowing the pressure p that corresponds to that V. Then it is tempting to assume the coefficients of the second order terms $\varepsilon_i\varepsilon_j$ are the elastic constants at p by analogy with the calculation of elastic constants at $p=0$.

An example of the ease with which the pressure correction is overlooked is the paper on elastic constants of Fe under pressure by Söderlind et al [43], which uses the procedure in Fast et al [33] to find $c_{ij}(p)$ of hcp Fe. Fast et al find δE at volume V_0 by using various first-order Eulerian strains ε_i without stating that V_0 must be at $p=0$. They apply the procedure at the theoretical equilibrium V, hence no pressure correction is needed in their work, but Söderlind et al apply the same procedure at finite p without mentioning a pressure correction (also without always satisfying $\varepsilon_1+\varepsilon_2+\varepsilon_3=0$); their c_{12} is low by about the pressure correction $(+p)$ in (4.6) than c_{12} found by Qiu et al [9] based on δG, and their c_{44} is higher than c_{44} calculated in [9] with about the pressure correction $(-p/2)$ in (4.6).

Another example of how the pressure correction can be overlooked is in the more recent papers on bcc V and Nb by Landa et al [45], which calculate c_{44} and

$C' = (c_{11} - c_{12})/2$ using the procedure in Mehl et al [50]. Mehl et al expand δE in ε_i and assume that the coefficient of $\varepsilon_i \varepsilon_j$ is c_{ij} rather than $\overline{c}_{ij}$; Mehl et al apply their equation at the experimental V, hence p is approximately zero, and the pressure correction would be small, but Landa et al apply the equation at large finite p, and their c_{44} values are high. In fact applying the correction in (4.6) $(-p/2)$ would bring their value for the instability pressure of bcc V (1.9 Mbar) into better agreement with the experimental value found by Ding et al (0.65 Mbar) [51]. We have repeated the calculation of c_{44} for V with pressure corrections and find the instability in bcc V at about 0.6 Mbar, close to the observed value.

In conclusion, we note that the pressure correction exhibits the physical idea that the elastic response of a crystal is different when the boundary condition is the flexible one of constant pressure than when the boundary condition is the rigid one of constant volume.

Chapter 5

Bravais phases of Fe under pressure from first principles

The structure and stability of four Bravais phases of Fe under pressure are determined by a procedure which first looks for minima of the internal energy E at constant volume V and then tests the states at the minima for stability (or instability) by showing that the Gibbs free energy G at constant pressure p is a minimum (or not a minimum) with respect to all possible strains. The phases considered here are either body-centered tetragonal (bct), which includes bcc and fcc, or rhombohedral (*rh*). The results show that bcc Fe becomes unstable at 1500 kbar, that fcc Fe is stable at $p = 0$, that a phase transition from bcc to fcc is thermodynamically favored at 290 kbar, that a bct phase at $c/a = 0.89$ is unstable up to 2700 kbar and that a *rh* phase with angle $\alpha = 60.5^0$ is stable at $p = 0$ with slightly higher E than that of fcc Fe.

5.1 Introduction

First-principles theory can now find metastable phases of elements with good accuracy. The number of such phases, i.e., of periodic atomic bonding arrangements with

local stability, grows substantially under stress. A finite fraction of them can be specified by limiting attention to Bravais phases, i.e., one-atom per unit cell of a crystal, at pressures under a specified maximum value of hydrostatic pressure for a rigid lattice. In this work a systematic procedure for finding metastable phases is illustrated for four Bravais structures of Fe, which possibly could be extended to all the Bravais structures.

Our procedure for finding stable atomic bonding arrangements under pressure uses three basic theoretical tools:

1) The capability of first-principles band structure programs to calculate the total energy E of an arbitrary periodic structure with relative accuracy to $\cong 10^{-6}$ Ry, 2) the thermodynamic theorem that relates E to equilibrium states, 3) the thermodynamic theorem that relates the Gibbs free energy G to the stability of an equilibrium state at constant pressure.

The E theorem states that in the equilibrium state of a system (at zero temperature) constrained to constant volume, E is a minimum with respect to all strains satisfying the constraint [13]. However, the equilibrium state is not necessarily stable, and the G theorem is needed to establish stability.

The G theorem states that in a system held at constant applied pressure p, the Gibbs free energy $G \equiv E + pV$ (for the rigid lattice) is a minimum with respect to all strains [13]. Hence a state found as a minimum of E at some volume can be tested for stability by checking whether G is a minimum too at the pressure corresponding to the volume of the phase.

For finding and characterizing the phases of a two-parameter structure like bct (structural parameters a and c) it is convenient to look for minima of E at constant V as a function of one parameter, e.g. c/a; at each c/a no further minimization is needed since V and c/a fix the structure. Then p is found from the equilibrium E (of the minimum corresponding to a particular phase) at several adjacent V values and G calculated at that minimum is tested to see if G is also a minimum. The test involves the elastic constants, as will be shown in Section 5.2. If the structure has more than two parameters, the E values found at the minima of E as one parameter varies will have to be minimized with respect to additional parameters while continuing to constrain the volume.

We check the instability pressure for bcc Fe to be 1500 kbar as found in [52, 53], which differs from the instability pressure given in several recent papers [42-44, 54, 55]. We note that in some cases the difference appears to be due to neglect of a "pressure correction" discussed in Chapter 4.

We show that fcc ferromagnetic (FM) Fe at zero pressure is stable, which disagrees with several other calculations [56-58], and we show why we differ. We show that the bct phase found in [53] is unstable at all pressures up to 2700 kbar; the phase does not pass the absolute stability test, i.e., that no small strain exists that decreases G.

We find an unexpected stable rhombohedral (*rh*) phase at zero pressure (and above) with E close to but greater than that of fcc FM Fe, which would complicate the structure of Fe films on various substrates.

5.2 Procedure and results

The total-energy band calculations for each structure were performed using the full-potential augmented-plane-wave plus local orbital (APW+lo) method together with the Perdew-Burke-Ernzerhof generalized-gradient-approximation (PBE-GGA) as implemented in the WIEN2k package [22]. The computation parameters in all cases were: plane wave cutoff $R_{MT}K_{\max} = 7$, $R_{MT} = 1.6$ a.u., $G_{\max} = 14$ mixer $= 0.05$, 1000 k-points in the irreducible Brillouin zone, and convergence criterion on the energies $1\text{x}10^{-3}$ mRyd (10^{-6} Ryd). All calculations were spin polarized. All the four phases have pressure-dependent finite magnetic moments.

In the first stage (of three stages), a comprehensive set of functions $E(c/a)$ at $V = V_i,\ i = \overline{1,36}$ were calculated which cover a range of pressure from 0 to 2800 kbar. A selected set of $E(c/a)$ curves is shown in Fig. 5.1 to illustrate the presence of up to three minima corresponding to bct, bcc and fcc phases. Each of the minima corresponds to an equilibrium state of a phase at volume V_i, since E has been minimized at that V_i with respect to all structural parameters satisfying the constraints $V_i(a,c)$ constant - in the bct case only c/a since c/a and V fix the structure. However, the existence of a minimum does not mean stability. In fact in Fig. 5.1 there is a gap between the V_i at which the curvature of $E(c/a)$ vanishes and the smaller V_i (and higher pressure) at which each phase stabilizes, as will be illustrated later. In the gap all minima are equilibrium states that are unstable.

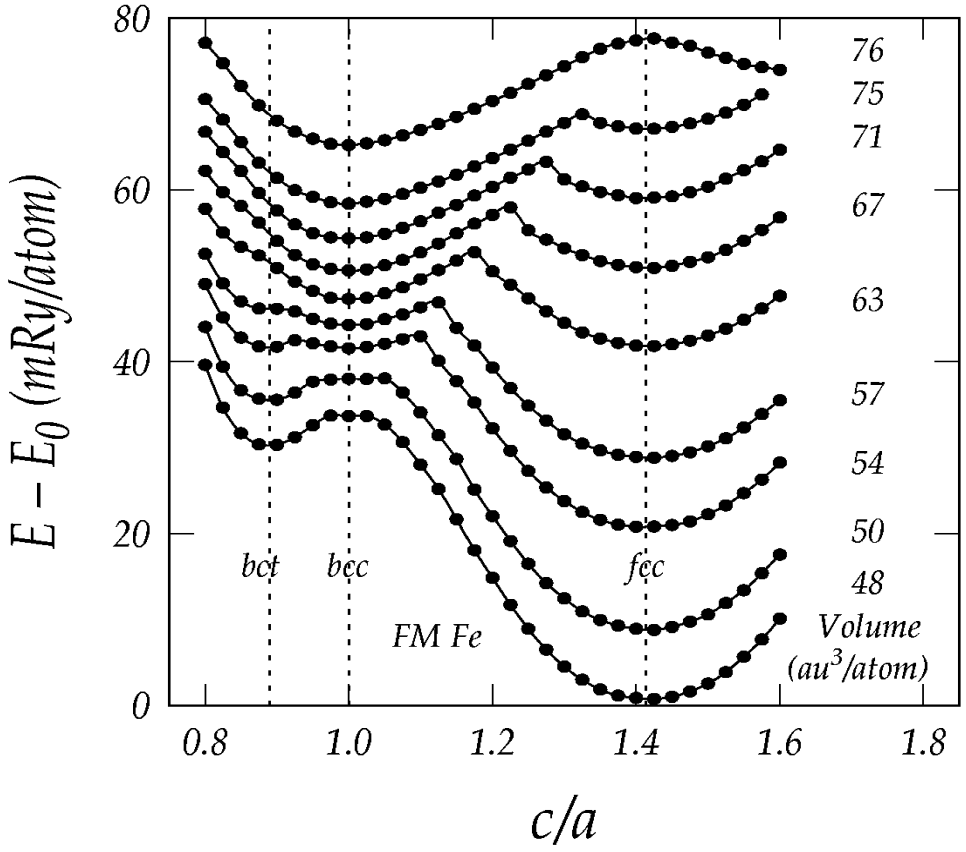

Figure 5.1. Total internal energy as a function of c/a (called $E_V(c/a)$ curves) of FM Fe at selected volumes; E_0 is the total energy of fcc Fe at V = 48 au^3/atom. For clarity the $E_V(c/a)$ curves at volumes from 50 to 76 au^3 are shifted toward E_0 by 36.20, 89.90, 120.0, 158.5, 175.2, 186.9, 194.7 and 201.9 mRy/atom, respectively. The vertical dashed lines indicate the bct, bcc and fcc phases at c/a 0.89, 1.00 and 1.414, respectively. The solid lines interpolate between the calculated points.

In the second stage, the separate minima, which determine the structure $(c/a)_m^{ph}$ and energy $E_m^{ph}(V)$ of the separate phases, are used to find the equation of state (EOS) of each phase from

$$p^{ph}(V) = -dE_m^{ph}(V)/dV\ , \tag{5.1}$$

where $ph =$ bct, bcc, fcc with different $(c/a)_m$ values. The separate EOS are plotted in Fig. 5.2.

The $p^{ph}(V)$ then determine the Gibbs free energies at each minimum from

$$G^{ph}(p) = E_m(V^{ph}(p)) + pV^{ph}(p)\ . \tag{5.2}$$

Differences of $G^{ph}(p)$ from the bcc phase are plotted in Fig. 5.3 to find the thermodynamic transition pressure from bcc $\rightarrow$ fcc at 290 kbar.

Finally the stability of each of the equilibrium states is determined by a calculation of the eigenvalues of the 6x6 $\underline{\underline{c_{ij}}}$ matrix whose elements are the elastic constants c_{ij} ($i, j = \overline{1,6}$). The minimum path program (MNP), which is described in detail in Chapter 3, converges on minima of G, finds the c_{ij}, and calculates the eigenvalues. A negative eigenvalue means the expansion in eq. (4.1) is not positive definite and indicates instability. In this way the X's used in Fig. 5.4 for instability were found including the instability of the bct phase at $c/a = 0.89$ found in [53], where the bct phase was incorrectly called stable above 1825 kbar.

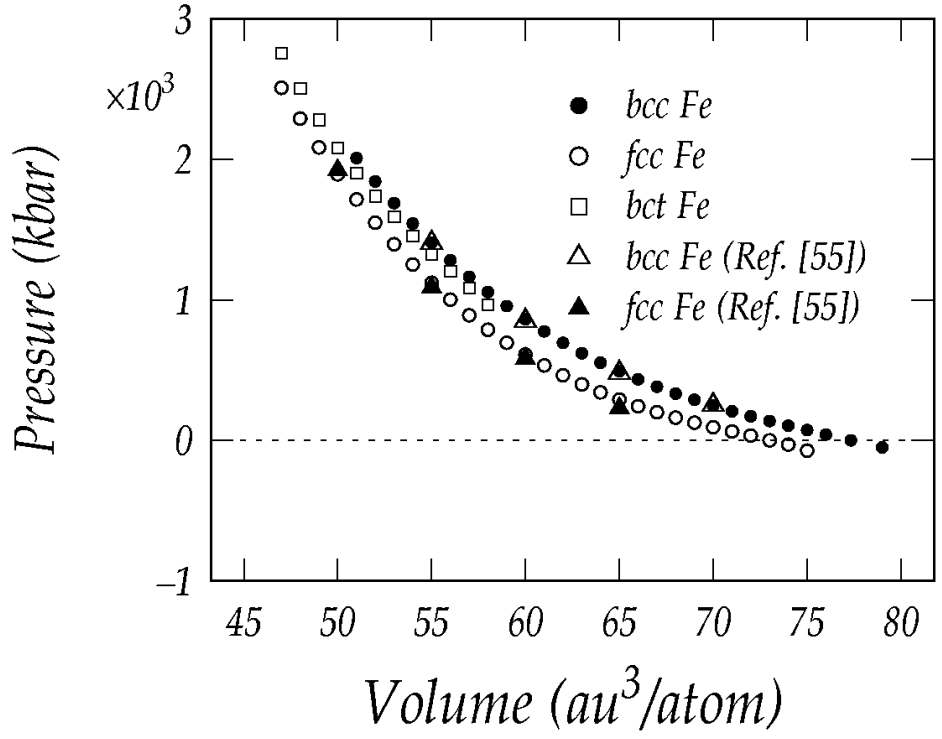

Figure 5.2. $p(V)$ curves for bcc phase (filled circles), bct phase (open squares) and fcc phase (open circles) of FM Fe. The crossing of the $p(V)$ curve and the dashed line (p = 0) gives the equilibrium volume: $V_0^{fcc} = 72.8$ au^3/atom, $V_0^{bcc} = 77.3$ au^3/atom. For comparison selected $p(V)$ data of bcc Fe (open triangles) and of fcc Fe (filled triangles) deduced from Fig. 2 of [55] are plotted.

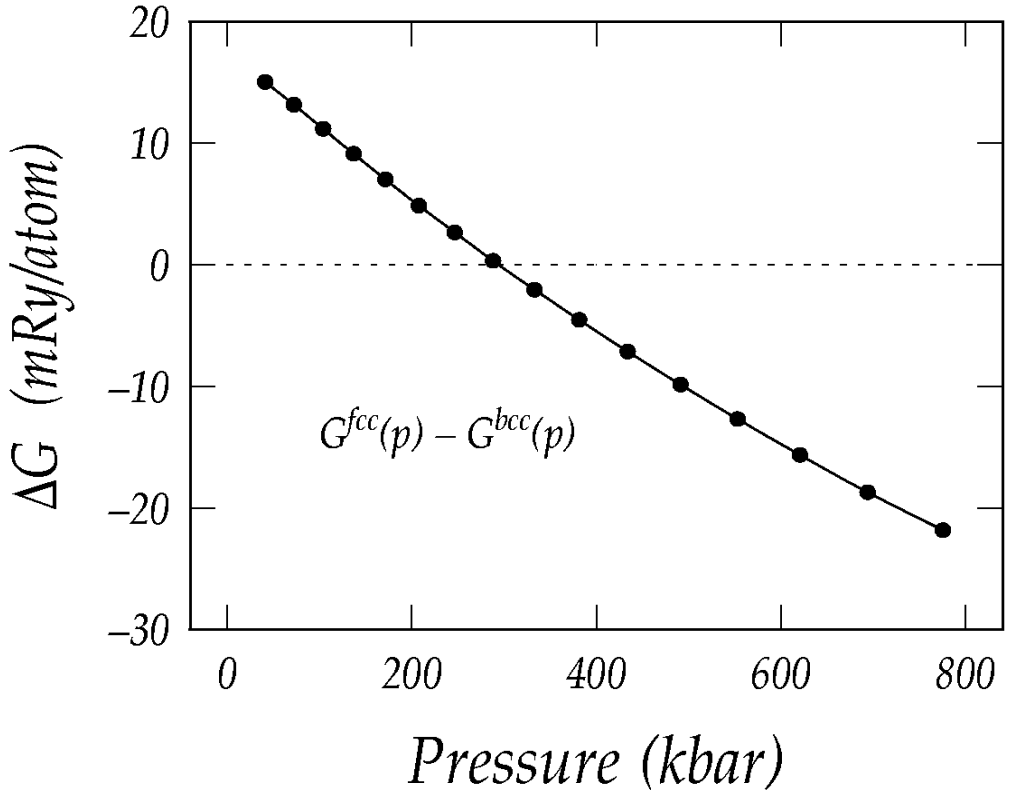

Figure 5.3. Free energy difference curve $G^{fcc}(p) - G^{bcc}(p)$ of FM Fe indicating the phase transition from bcc to fcc phase at 290 kbar. The solid line interpolates between the calculated points.

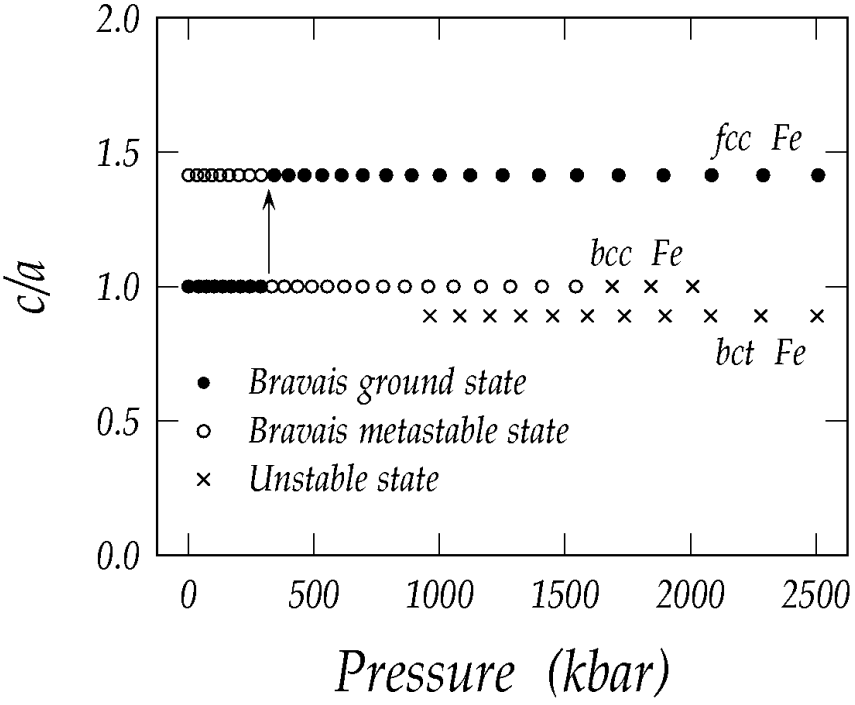

Figure 5.4. c/a versus pressure for bct, bcc and fcc phases of FM Fe. The meanings of the symbols are: filled circle – Bravais ground state, open circle – Bravais metastable state, cross -- unstable state. The phase transition from bcc to fcc at 290 kbar is indicated by an arrow.

In the previous chapter we derived the relations (Eq. (4.6)) between $\overline{c}_{ij}$, which are the coefficients of the second-order terms of the δE expansion in Eulerian strains (Eq. (4.5)), and the elastic constants c_{ij}. For cubic symmetry Eq. (4.6) gives

$$\begin{aligned} c_{11} &= \overline{c}_{11} \\ c_{12} &= \overline{c}_{12} + p \\ c_{44} &= \overline{c}_{44} - p/2 \\ C' &\equiv (c_{11} - c_{12})/2 = (\overline{c}_{11} - \overline{c}_{12})/2 - p/2 \equiv \overline{C}' - p/2. \end{aligned} \tag{5.3}$$

The elastic shear constant C' of a phase can be evaluated directly from minima of the function $E(c/a)$ at constant V from the curvature of $E(c/a)$ at the minimum [59]. From Eq. (4.5) by changing variables from $\varepsilon_1 = \varepsilon_2 = \delta a/a$, $\varepsilon_3 = \delta c/c$ to $\delta(c/a)$ and δV where $V = ca^2/2$, the quadratic term in δE for $[\delta(c/a)]^2$ gives (at the minimum corresponding to a particular cubic phase)

$$\frac{1}{V_0}\left(\frac{\partial^2 E}{\partial (c/a)^2}\right)_V = \frac{4}{3}\overline{C}' = \frac{4}{3}C' + \frac{2}{3}p\,. \tag{5.4}$$

The coefficient $\overline{C}'$ of the quadratic term $[\delta(c/a)]^2$ in δE requires the pressure correction $-p/2$ to give C', which vanishes when bcc Fe becomes unstable. Note that the vanishing of the curvature of $E(c/a)$ does not occur at the instability pressure, but at a higher pressure.

The formula corresponding to (5.4) for the more general case of a bct structure is

$$\frac{1}{V_0}\left(\frac{\partial^2 E}{\partial (c/a)^2}\right)_V = \frac{2}{9(c/a)^2}[\overline{c}_{11} + \overline{c}_{12} - 4\overline{c}_{13} + 2\overline{c}_{33}], \tag{5.5}$$

which reduces to (5.4) for bcc symmetry where $\overline{c}_{13} = \overline{c}_{12}$, $\overline{c}_{33} = \overline{c}_{11}$, $c/a = 1$.

In Fig. 5.5 $C'(p)$ obtained from eq. (5.4) is compared to $C'(p)$ obtained from the elastic constants $c_{11}(p)$ and $c_{12}(p)$, which are calculated with the MNP program. Both show instability around 1500 kbar, and an anomaly in $C'(p)$ below 500 kbar. The instability pressure 1500 kbar found here in two different calculations is substantially lower than some values found in recent first-principles calculations [42, 43, 54], generally due to neglect of the pressure correction. Table 5.1. lists various published values of the instability pressure.

Table 5.1 Instability pressure p_s of bcc FM Fe calculated from first-principles in recent papers.

References	Instability pressure p_s (kbar) of bcc FM Fe
This work and Ref. [52, 53]	1500
Ref. [42]	3200
Ref. [43]	2000
Ref. [44]	1600
Ref. [54][a]	1800
Ref. [55]	1000

[a] From a gap in the phonon dispersion curves of bcc Fe.

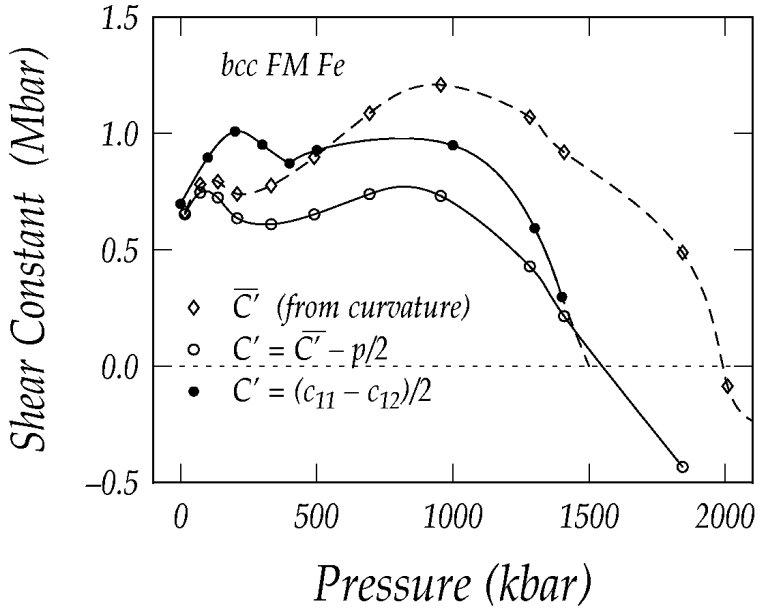

Figure 5.5. Shear elastic constants C' and $\bar{C}'$ of bcc FM Fe as functions of pressure. The data of C' are calculated in two ways: the filled circles are obtained from $C' = (c_{11} - c_{12})/2$ where c_{11} and c_{12} are calculated with MNP program; the open circles are obtained from $C' = \bar{C}' - p/2$, where the data of $\bar{C}'$ are calculated from the curvature of the $E(c/a)$ curves using (5.4). Both filled and open circles show that C' vanishes at the instability pressure of bcc Fe $p_s \approx$ 1500 kbar. In contrast, $\bar{C}'$, or the curvature at minima of $E(c/a)$ curves at constant V, does not vanish at p_s but at a higher pressure around 2000 kbar.

An important result of this detailed study, which refers to fcc Fe and phases near the fcc structure as $\gamma - Fe$ phases, is the conclusion that the fcc magnetic phase of Fe under ambient conditions is stable. This conclusion disagrees with previous first-principles studies of Fe [56-58]. From the EOS of the fcc Fe phase in Fig. 5.2, at $p^{fcc} = 0$, $V_0^{fcc} = 72.8$ au^3/atom. A stability test with the MNP program shows that the fcc phase is stable. Note that if we had wrongly used the bcc EOS which shows at $p^{bcc} = 0$ a value of 77.3 au^3/atom, then Fig. 5.1 would show a maximum at $c/a = 1.414$ and the fcc phase would be called unstable.

In [56] Peng and Jansen calculate $E(c/a)$ at $V = 79$ au^3/atom and find a maximum for the fcc structure, hence conclude that fcc Fe is unstable. But Fig. 5.2 shows that at $V = 79$ au^3/atom fcc is under negative pressure and the condition of instability found in [56] does not apply at $p = 0$.

In [57] Spišák and Hafner state that fcc Fe is unstable in agreement with [56], but give no details. In [58] they look for a stable monoclinic phase of Fe by minimizing E with respect to two structural parameters c/a and δ (which determines angle γ) and find a minimum at $V = 78$ au^3/atom. The state they find is unlikely to be an equilibrium state because a monoclinic crystal has four structural parameters (a, b, c, γ) hence one more minimization of E is needed. Even if the state is close to equilibrium, the pressure is unlikely to be zero, since the pressure has not been controlled, the value of V is large compared to fcc Fe at $p^{fcc} = 0$ and is in the range of instability for fcc Fe. To find a monoclinic stable phase at $p = 0$ the minimization of E at constant V must be made

with respect to three structural parameters and must be repeated over a range of V to obtain pressures from (5.1) to be searched for a zero value of p. In a calculation with the MNP program starting from the state in [58] and assuming $p = 0$ the result indicates that the state found in [56] is not a phase at $p = 0$, i.e., is not a minimum of the Gibbs free energy G. The MNP program is able to find a monoclinic equilibrium state near the state in [58] if the state in [58] approximates a phase, since the MNP program homes in on minima of G; however the MNP program starting from the monoclinic phase of [58] converges to the fcc phase at $V = 72.8$ au^3/atom.

Our procedures are also able to find phases of two-parameter structures like *rh* structures, parameters a and α. Fig. 5.6 (a), like Fig. 5.1, shows equilibrium states by the presence of minima of $E(\alpha)$ at constant V, which includes the fcc structure. Several *rh* minima appear, and we focus on the one at $\alpha \cong 60.5^0$. A plot of $E_m^{rh60.5^0}(V)$ values in Fig. 5.6 (b) shows the minimum and the equilibrium volume at $p^{rh} = 0$ to be 72.45 au^3/atom. The E value of *rh* FM Fe at the lowest data point ($V =$ 72.5 au^3/atom) in Fig. 5.6 (b) is -2545.539266 Ry/atom, which is slightly higher than -2545.539362 Ry/atom of fcc FM Fe at $p^{fcc} = 0$. A stability check with the MNP program shows the *rh* phase is stable.

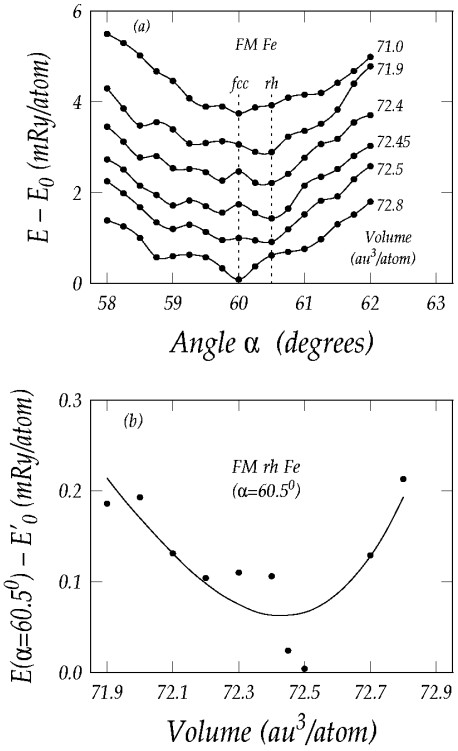

Figure 5.6. (*a*) Total internal energy as a function of angle α (called $E(\alpha)$ curves) of the 1-atom *rh* unit cell of FM Fe at selected volumes near $p^{fcc} = 0$; E_0 is the total energy of *fcc* FM Fe at $V = 72.8$ au^3/atom. For clarity the $E(\alpha)$ curves at volumes from 72.5 to 71.0 au^3/atom are shifted away from E_0 by 0.75, 1.25, 2.04, 2.55 and 3.15 mRy/atom, respectively. The solid lines interpolate between the calculated points. The vertical dashed line at $\alpha = 60^0$ denotes the *fcc* phase, while the vertical dashed line at $\alpha = 60.5^0$ denotes the *rh* phase. (b) Total internal energy at $\alpha = 60.5^0$ on the $E(\alpha)$ curve as a function of volume; E_0' is the total energy of *rh* FM Fe at V = 72.5 au^3/atom. The solid curve is the result of fitting the data points with a third-order polynomial, which shows that the equilibrium state of the *rh* phase of FM Fe is at $V = 72.45$ au^3/atom.

5.3. Discussion

The procedure used here to find and describe phases of Fe requires evaluation of both the internal energy E and the Gibbs free energy G. Equilibrium states at constant volume, which are possible phases, are located by searching for minima of E in a given structure as a function of one structure parameter at constant V. Advantages of this search are that the number of variables by which E needs to be minimized is reduced by one by the constraint to constant volume, and also that all phases with the given structure are treated together in the same way, which improves the accuracy of differences between phases. In the case of two-parameter systems like bct and *rh*, the value of a single parameter and the volume fix both the structure and E and no further minimization is required.

The equilibrium states found from E are not necessarily stable; establishing stability of a state under pressure requires evaluation of G and proving that G is a minimum with respect to all possible small deformations around the equilibrium state. Proving a minimum of G is equivalent to showing the positive definiteness of the quadratic form in the strains in the expression of δG in eq. (4.1), whose coefficients are the elastic constants c_{ij} $(i, j = \overline{1, 6})$. Positive values of all six eigenvalues of the 6x6 $\underline{\underline{c_{ij}}}$ matrix then prove stability.

The fact that some equilibrium states corresponding to minima of E at constant V are not stable gives meaning to the theoretical description of some states as "unstable phases". A critical pressure can be evaluated at which a minimum appears in $E(c/a)$ at constant V, which only becomes stable at a larger pressure. Each phase can be

characterized by the pressures of appearance and disappearance or by the pressures of the onset of stability and instability, and by the pressures at which transitions to and from other phases are thermodynamically permitted.

The geophysically interesting pressure at which bcc Fe becomes unstable has been found to be 1500 kbar in three separate calculations: 1) in Ref. [52,53] using the WIEN97 band structure program and evaluation of second strain derivatives of G, 2) by the WIEN2k program [22] and evaluation of δG using various strains; the data are shown in Fig. 5.5 with filled circles, 3) by the evaluation of the second derivatives of $E(c/a)$ at constant V from the curvatures at minima of E, from which the shear elastic constant C' is calculated using eq. (5.4) and plotted in Fig. 5.5 with open circles. A number of first-principles papers have found different values of the instability pressure, in some cases due to neglect of the pressure correction. Fig. 5.5 shows the important effect of the pressure correction in determining the instability pressure of bcc Fe.

In summary, in this work we show the effectiveness of procedures for finding stable phases based on calculating E at constant V and δG at constant p, e.g., the proof that bcc Fe is unstable at 1500 kbar, the proof that fcc Fe is stable at $p^{fcc} = 0$, the proof that bct Fe at $c/a = 0.89$ is unstable at all pressures up to 2700 kbar, the observation of a stable *rh* phase at $p^{rh} = 0$. Essential elements of the procedure are the use of separate EOS for different phases, and the capability of testing an equilibrium state for stability.

Chapter 6

Low temperature properties of fcc Al from modified Debye theory

The thermal expansion of the lattice parameter of fcc Al, $a(T)$, is shown to be accurately determined by the Debye theory of lattice vibrations and first-principles total energy band calculations. The Debye theory uses the well-known generalization to direction-dependent elastic mode frequencies and is further modified by introducing a parameter β_z, which gives the fraction of the full Debye zero-point energy that is possessed by the actual dispersive mode frequencies. The calculation of $a(T)$ is simplified by minimizing the Gibbs free energy of the vibrating lattice rather than the usual procedure of minimizing the total energy at constant volume. The parameter β_z is shown to affect the value of $a(T)$, but comparison of $a(T)$ with experiment cannot be used to evaluate β_z because of the inherent inaccuracy of the band calculations (GGA is 0.7% high, LSDA is 1.2% low for $a(T)$). By using experimental values of $a(T)$ and elastic constants $c_{ij}(T)$, $ij = 11, 12, 44$ as well as the modified Debye theory, β_z is

evaluated as 0.48 without band calculations. From β_z, the rigid lattice of a is shown to be 4.01 Å, midway between the GGA and LSDA values.

6.1 Introduction

In this chapter we show that the Debye theory of lattice vibrations combined with first-principles total-energy band calculations can find accurately the temperature dependence of the lattice parameter $a(T)$ of fcc Al from 0 to at least 300 K. Hence the Debye theory is an alternative procedure for calculating $a(T)$ at low temperatures that is simpler than the computationally intensive complete phonon spectra usually used to compute thermal expansion from first principles.

The Debye theory of lattice vibrations derives a one-parameter formula for the free energy of lattice vibrations as a function of temperature $F(\theta_D, T)$. The parameter θ_D depends on volume but in the quasi-harmonic approximation does not depend on T. The original form of the Debye theory [60] had three defects: 1) it assumed that the elastic waves that were used to describe the lattice vibration modes were isotropic, 2) it neglected dispersion of the actual lattice modes, which have frequencies that differ from the frequencies of elastic waves as functions of wavenumber, 3) it assumed the zero point energy (ZPE) was a sum of elastic wave contributions over the entire phonon spectrum, thereby neglecting the fact that dispersion would change the contributions of all the higher frequencies.

The first two defects were remedied for low-temperature applications in the 1930's and 1940's (for a review see [61]) by obtaining elastic wave velocities as functions of direction from solutions of the elastic equations of motion. This generalized Debye theory thus made the temperature dependence of $F(\theta_D, T)$ accurate at sufficiently low temperatures and exact approaching 0 K. Also, at temperatures sufficiently low that only elastic waves are excited, the second defect, neglect of dispersion, could be ignored. However the third defect, the wrong estimate of ZPE, is not remedied by using directionally correct elastic wave velocities at low temperatures because all modes enter the ZPE, including dispersive ones.

The third defect does not affect the application of the generalized Debye theory to specific heats, which were the physical measurements of initial interest [60]. However in application of the theory to the calculation of lattice dimensions, the ZPE is important. The present work attempts to remedy the third defect for low-temperature applications by introducing a parameter β_z that fractionally reduces the Debye values of the ZPE in $F(\theta_D, T)$.

In Section 6.2 we find the equilibrium lattice dimension $a(T)$ of fcc Al by minimizing with respect to structure the Gibbs free energy G at zero pressure obtained by adding the modified Debye free energy of lattice vibration $F_m(\theta_D, T)$ (modified by β_z) to the rigid-lattice band energy $E(a)$. The resulting theoretical equilibrium lattice dimensions can then be compared to measured lattice dimensions, which of course contain the vibrational effects. We establish some important results: that the Debye theory gives $a(T) - a(0)$

accurately up to at least 300 K; that the limiting T^4 term for $F_m(\theta_D, T)$ is not adequate to fit experiment; that the use of the Gibbs free energy at zero pressure is simpler than the usual procedure of calculating the internal energy at constant volume from complete phonon spectra at many volumes (to find the volume of zero pressure); that the band calculation with the GGA gives high values of a compared to experiment and the LSDA gives low values. Therefore, although β_z affects the value of a, the inaccuracies of the band energy calculations are too large to permit evaluation of β_z.

In Section 6.3 we avoid the inherent inaccuracies of GGA and LSDA by using experimental values of $a(T)$ and $c_{ij}(T)$, $ij = 11,\ 12,\ 44$ to find θ_D and $F_m(\theta_D, T)$; $F_m(\theta_D, T)$ is then fitted to the experimental change in $a(T)$ between 100 and 200 K to determine β_z and a_R, the rigid-lattice value of a, which can be compared directly with the results of rigid-lattice band calculations. The measured $a(T)$ and $c_{ij}(T)$ also give a value of a Grüneisen-type parameter γ_{DG} describing the volume dependence of the Debye parameter θ_D, which in the quasi-harmonic approximation does not depend on temperature. The values of β_z, γ_{DG} and a_R do not require band calculations and their accuracy rests on the accuracy of measured dimensions and elastic constants at several temperatures and on the accuracy of the generalized and modified Debye theory near 0 K.

6.2 Procedure and results of band calculations

First-principles band calculations of fcc Al were performed using the full-potential augmented-plane-wave plus local orbitals (APW+lo) method together with either the generalized-gradient-approximation (GGA) or the local-spin-density-approximation (LSDA) as implemented in the WIEN2k package [22]. A plane-wave cutoff $R_{MT}K_{\max}=7$, $R_{MT}=1.6$ a.u., $G_{\max}=14$, mixer = 0.05 and 1000 k-points in the irreducible Brillouin zone were used in all the band calculations. The k-space integration was done by the modified tetrahedron method. Tests with larger basis sets and different Brillouin-zone samplings yielded only very small changes in the results. The convergence criterion on the energies is set at $1\text{x}10^{-3}$ mRyd (10^{-6} Ryd) per atom.

Eqs. (1.1) and (1.2) are used to calculate Gibbs free energy G at a given temperature T and pressure p. Note that in Eq. (1.1) $E+pV$ is the rigid-lattice Gibbs free energy (Ryd/atom), which is calculated with the MNP program. A detailed description of the MNP program is given in Chapter 3. Briefly, MNP calls WIEN2k as a subroutine and simultaneously finds the Gibbs free energy, the lattice structure and the elastic constants at rigid-lattice equilibrium at a given pressure p.

The free energy of lattice vibrations $F(\theta_D,T)$ is given in the generalized Debye theory by Eq. (1.2) [12]. In the low-temperature limit, the first two terms of the expansion of $F(\theta_D,T)$ in powers of T [12] are

$$F(\theta_D,T)\cong\frac{9}{8}k_B\theta_D-\frac{\pi^4}{5}\frac{k_BT^4}{\theta_D^3}, \tag{6.1}$$

where k_B is Boltzmann's constant, θ_D is the Debye temperature, and $\frac{9}{8}k_B\theta_D$ is the full Debye zero-point energy (ZPE).

To determine the temperature dependence of the equilibrium lattice constant $a(T)$ we select three reference values of the lattice parameter a that bracket $a(T)$, the equilibrium value of a at T. We then evaluate $E(a)+pV$, $\theta_D(a)$ and $F(\theta_D,T)$ at each reference value of a using Eq. (1.2); hence we can calculate $G(a,T)$ using Eq. (1.1) (here we only consider the zero-pressure case). We evaluate $\theta_D(a)$ at the reference values of a using the $c_{ij}(a)$, $ij = 11$, 12, 44 determined from $(\partial^2 G/\partial\varepsilon_i\partial\varepsilon_j)/V$. Fitting of the G values at the three reference points at a given temperature T with a second-order polynomial gives the equilibrium lattice constant $a(T)$, e.g., the value of a that minimizes $G(a,T)$.

We make the calculated $a(T)$ depend on a factor β_z in the ZPE by using a modified free energy of vibration $F_m(\theta_D,T)$ in Eq. (1.1), namely

$$F_m(\theta_D,T) = \frac{9}{8}\beta_z k_B\theta_D + \frac{9k_B\theta_D}{x^4}\int_0^x z^2 \ln\left(1-e^{-z}\right)dz, \quad x \equiv \frac{\theta_D}{T} \tag{6.2}$$

Table 6.1 on page 64 lists the calculated values of the Debye temperature θ_D, the electronic energy E and the Gibbs free energy $G(a,T) = E + F_m(\theta_D,T)$ (at $p = 0$) of fcc Al at the three reference points a_1, a_2, a_3. The modified free energy of lattice vibrations $F_m(\theta_D,T)$ is calculated from (6.2) using GGA at $T = 0$, 50 and 100 K with both $\beta_z = 0$ and 1 for each case. Fittings of the values of the Gibbs free energies $G(a,T)$ at the three reference points with a second-order polynomial give at the minimum of G the

equilibrium lattice constants $a^{GGA}(T)$ with $\beta_z = 0$ and 1. The equilibrium lattice constants $a^{LSDA}(T)$ with $\beta_z = 0$ and 1 are found similarly.

Fig. 6.1 shows the comparison of calculated $a(T)$ with the experimental result for fcc Al. The solid diamonds are the experimental data from [34]. The open and solid circles are calculated from (6.2) using GGA with $\beta_z = 0$ and 1, respectively. The open and solid triangles are calculated from (6.2) using LSDA with $\beta_z = 0$ and 1, respectively. The open squares are the linear combination of the GGA and LSDA results with $a(T) = 0.57a^{GGA} + 0.43a^{LSDA}$ at $\beta_z = 1$ to fit the experimental data. The open diamonds are calculated from (6.1) using GGA with $\beta_z = 1$. At low temperatures ($T \leq 50$ K) the calculated $a(T)$ are the same from both (6.1) and (6.2). However, for temperatures larger than 50 K the term $\frac{\pi^4}{5}\frac{k_B T^4}{\theta_D^3}$ in (6.1) increases with increasing T much faster than the integral term in (6.2). As shown in Fig. 6.1 at $T = 150$ K the value of $a(T)$ calculated from (6.1) is much larger than that from (6.2) (the open diamond vs the solid circle). Calculations of $a(T)$ from (6.1) at $T > 150$ K would require more reference points with larger a.

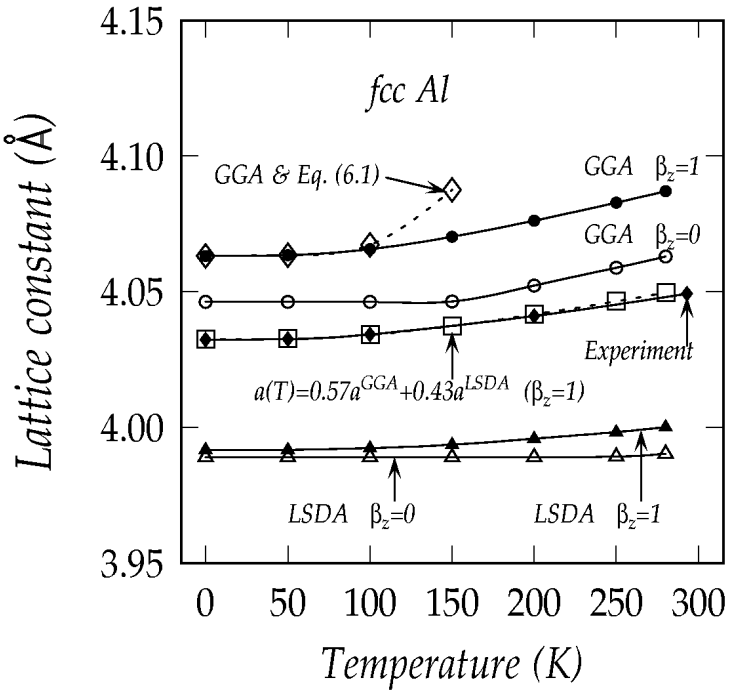

Figure 6.1. Temperature dependence of the equilibrium lattice constant of fcc Al. The solid diamonds are the experimental data from [34]. The open and solid circles are calculated from (6.2) using GGA with $\beta_z = 0$ and 1, respectively. The open and solid triangles are calculated from (6.2) using LSDA with $\beta_z = 0$ and 1, respectively. The open squares are linear combination of the GGA and LSDA results with $a(T) = 0.57a^{GGA} + 0.43a^{LSDA}$ at $\beta_z = 1$ to fit the experimental data. The open diamonds are calculated from (6.1) using GGA with $\beta_z = 1$. The solid and dashed lines interpolate between data points.

Table 6.1. Debye temperature θ_D, electronic energy E and Gibbs free energy $G(a,T) = E + F_m(\theta_D, T)$ (at $p = 0$) of fcc Al at the three reference points a_1, a_2, a_3. The modified free energy of lattice vibrations $F_m(\theta_D, T)$ in $G(a,T)$ is calculated from (6.2) using GGA with $\beta_z = 1$ and 0, respectively.

	a_1 = 4.046197 Å	a_2 = 4.070474 Å	a_3 = 4.094751 Å
θ_D (K)	433.91	409.13	385.23
E (Ryd/atom)	-485.638978	-485.638839	-485.638519
$G(T = 0K)$ (Ryd/atom) $\beta = 1$	-485.635887	-485.635924	-485.635774
$\beta = 0$	-485.638978	-485.638839	-485.638519
$G(T = 50K)$ (Ryd/atom) $\beta = 1$	-485.635896	-485.635935	-485.635788
$\beta = 0$	-485.638987	-485.638850	-485.638533
$G(T = 100K)$ (Ryd/atom) $\beta = 1$	-485.636011	-485.636067	-485.635938
$\beta = 0$	-485.639102	-485.638982	-485.638683

6.3 Vibrational parameters evaluated without band calculations

In Section 6.2 we showed two features of the Debye theory: 1) Debye theory can describe rather well the temperature dependence of the lattice parameter up to at least 300 K, 2) Debye theory does not find the lattice parameter at 0 *K* accurately because of the inherent inaccuracy of the band calculations, even when the full range of zero-point energy for $\beta_z = 0$ to 1 is considered.

To evaluate β_z we need a procedure that does not require band calculations.

We consider using the first feature of the Debye theory given above, namely the accurate evaluation of the thermal expansion, to evaluate β_z. We tried first a procedure that assumed that θ_D had an exponential dependence on volume with one parameter, $\theta_D \propto V^{-\gamma_{DG}}$, where γ_{DG} is a Grüneisen-type parameter that we shall call the Debye-Grüneisen parameter. If $\theta_D(V_0)$ is known from measurement, where V_0 is the volume at 0 K, then θ_D and $F_m(\theta_D, T)$, the modified (by factor β_z) Helmholtz free energy of vibration, would be known as functions of V and T. We expand E around $a(0)$ (the lattice parameter at $T = 0$ including the ZPE effect) as a function of a in terms of the known bulk modulus B_0 and minimize the Gibbs free energy (at $p = 0$) with respect to a at several T, where

$$G(a,T) = E(a) + F_m(\theta_D(a), T). \tag{6.3}$$

This procedure expresses the equilibrium a at T in terms of B_0, γ_{DG} and β_z. We tried to find β_z and γ_{DG} by fitting $a(T)$. It proved possible to fit measured $a(T)$ values [34]

at $T =$ 50, 100, 200 K with $\beta_z = 0$ to 1 over narrow non-overlapping ranges of γ_{DG} ($\gamma_{DG} = 2.30$ to 2.39 at 50 K, 2.62 to 2.70 at 100 K and 2.99 to 3.20 at 200 K), but no unique values of β_z and γ_{DG} would fit even two values of T. Hence a single γ_{DG} parameter would not represent $\theta_D(V)$ adequately.

To evaluate β_z we then added to the measured $a(T)$ values the measured values of $c_{11}(T)$, $c_{12}(T)$, $c_{44}(T)$ for fcc Al [35]. The values of $a(T)$ and $c_{ij}(T)$ give $\theta_D(T)$. We now use the Debye theory to develop an equation containing β_z for the thermal expansion between two temperatures T_1 and T_2 at which we have the measured lattice parameter values a_1, a_2 and values of θ_D. The numerical procedure is as follows. The results are in Table 6.2 on page 69.

At each T the equilibrium equation

$$\left(\frac{\partial G(a,T)}{\partial a}\right)_T = \frac{dE(a)}{da} + \left[\frac{\partial F_m(\theta_D(a),T)}{\partial a}\right]_T = 0 \tag{6.4}$$

relates dE/da to $(\partial F/\partial a)_T$. Then the difference in dE/da between T_1 and T_2 can be expressed in two ways

$$\left(\frac{dE}{da}\right)_2 - \left(\frac{dE}{da}\right)_1 = \overline{\frac{d^2E}{da^2}}(a_2 - a_1) = \left(\frac{\partial F}{\partial a}\right)_1 - \left(\frac{\partial F}{\partial a}\right)_2 . \tag{6.5}$$

In (6.5), $\overline{d^2E}/da^2$ is an average value over the range a_1 to a_2 which can be expressed in terms of the bulk modulus

$$\left(\frac{d^2E}{da^2}\right)_i = \frac{9}{4}a_i B_i + \frac{2}{a_i}\left(\frac{dE}{da}\right)_i, \quad i = 1, 2 \tag{6.6}$$

In (6.6) B is the bulk modulus Vd^2E/dV^2 at a_1 and a_2 and the second term is needed in transforming variables from $V = a^3/4$ to a when $dE/da \neq 0$.

To complete (6.5), we need the relations

$$\left(\frac{\partial F}{\partial a}\right)_T = \left(\frac{\partial F}{\partial \theta_D}\right)_T \frac{d\theta_D}{da}, \tag{6.7}$$

$$\left(\frac{\partial F}{\partial \theta_D}\right)_T = k_B\left(\frac{9}{8}\beta_z + J(x)\right), \quad x \equiv \frac{\theta_D}{T}, \tag{6.8}$$

$$J(x) \equiv I(x) + x\frac{dI(x)}{dx}, \tag{6.9}$$

$$I(x) \equiv \frac{9}{x^4}\int_0^x z^2 \ln\left(1 - e^{-z}\right) dz. \tag{6.10}$$

Putting (6.6) to (6.10) in (6.5) gives a linear equation for β_z

$$\frac{9}{8}(a_2 - a_1)(a_1B_1 + a_2B_2) - \frac{a_2}{a_1}\left(\frac{\partial F}{\partial a}\right)_1 + \frac{a_1}{a_2}\left(\frac{\partial F}{\partial a}\right)_2 = 0. \tag{6.11}$$

Equation (6.11) is now applied at $T_1 = 100$ K and $T_2 = 200$ K. The five values of $a(T)$ given in [34], plotted in Fig. 6.2 (a), are used to find the best-fit cubic, which gives da/dT at 100 and 200 K (Table 6.2). The measured $c_{11}(T)$, $c_{12}(T)$, $c_{44}(T)$, values in [35] and $a(T)$ values in [34] were used to find $\theta_D(T)$ (Fig. 6.2 (b)). The best-fit cubic to five consecutive values of $\theta_D(T)$ were then used to find $d\theta_D/dT$ at 100 and 200 K (Table 6.2). Then

$$\frac{d\theta_D}{da} = \frac{d\theta_D/dT}{da/dT} \tag{6.12}$$

was evaluated at 100 and 200 K (Table 6.2). At low temperature (50 K and below), both a and θ_D varied too slowly to give accurate derivatives, but the variations were reasonable at 100 and 200 K. Then $(\partial F/\partial a)_T$ was found from (6.7) and (6.8) at 100 and 200 K (Table 6.2) using interpolation in a large table of $J(x)$, and inserted in (6.11) to find $\beta_z = 0.48$. The bulk moduli B_1 and B_2 were found from the measured c_{11} and c_{12} at 100 and 200 K (Table 6.2).

The Debye-Grüneisen parameter γ_{DG}, which is defined by

$$\gamma_{DG} \equiv -\frac{\partial \ln \theta_D}{\partial \ln V} = -\frac{a}{3\theta_D}\frac{d\theta_D}{da}, \tag{6.13}$$

can be calculated from θ_D, $d\theta_D/da$ and a at 100 and 200 K (Table 6.2).

Finally a_R, the rigid-lattice value of a, can be estimated as the a value at which $dE/da = 0$, where

$$\left(\frac{dE}{da}\right)_R = \left(\frac{dE}{da}\right)_1 + (a_R - a_1)\left(\frac{d^2E}{da^2}\right)_1 = 0. \tag{6.14}$$

Then using (6.4), (6.6) to (6.10) in (6.14) gives $a_R = 4.01$ Å, which may be compared to the GGA value of 4.05 Å and LSDA value 3.98 Å (Fig. 6.1 at $\beta_z = 0,\ T = 0$).

Table 6.2. Parameter values for fcc Al at 100 K, 200 K and zero pressure leading to values of β_z, γ_{DG} and a_R.

T (K)	100	200
a (Å) [34]	4.034195	4.040980
c_{11} (Mbar) [35]	1.1333	1.1040
c_{12} (Mbar) [35]	0.6185	0.6130
c_{44} (Mbar) [35]	0.3104	0.2064
B (Mbar)	0.7901	0.7767
θ_D (K)	426.87	417.62
$d\theta_D / dT$ (no dimension)	-0.07823	-0.10223
da / dT (Bohr/K)	0.4790×10^{-4}	0.8305×10^{-4}
$d\theta_D / da$ (K/Bohr)	-1.6332×10^{3}	-1.2309×10^{3}
γ_{DG} (no dimension)	5.14	3.97
$\left(\partial F / \partial \theta_D\right)_T$ (Ryd/K)	0.4132×10^{-5}	0.7304×10^{-5}
$\left(\partial F / \partial a\right)_T$ (Ryd/Bohr)	0.3571×10^{-2}	0.4756×10^{-2}

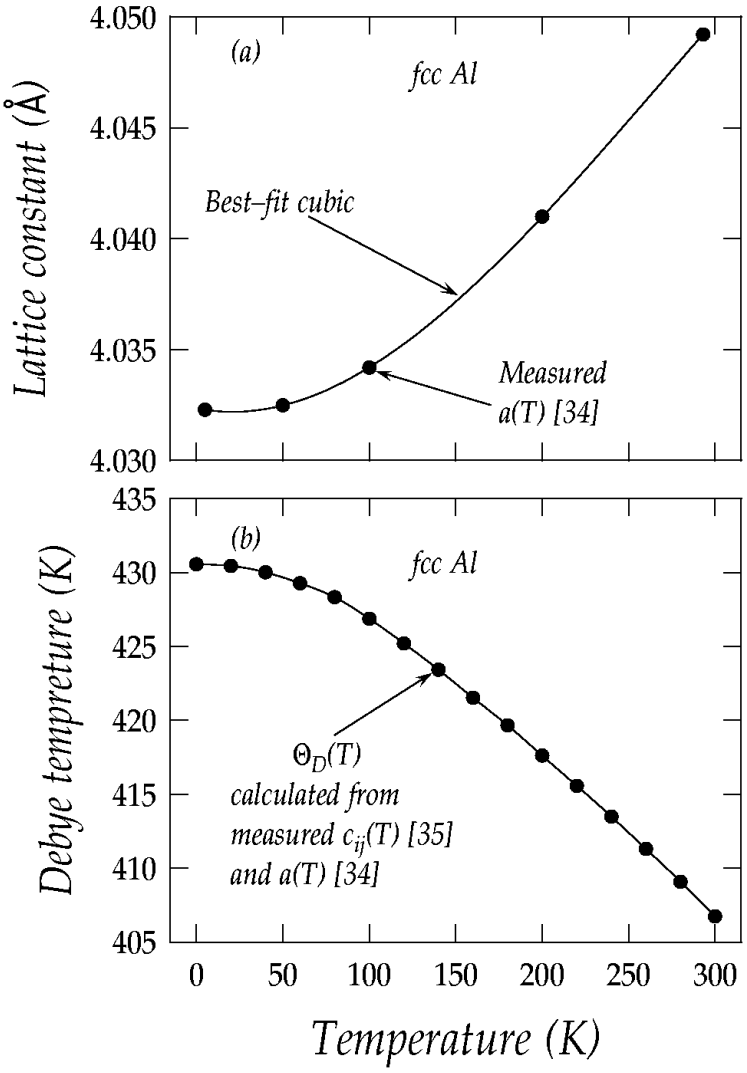

Figure 6.2. (*a*) Experimental lattice constant (solid circles, from [34]) and its best-fit cubic (solid line) as a function of temperature. (*b*) Debye temperature $\theta_D(T)$ (solid circles) calculated from the measured $c_{11}(T)$, $c_{12}(T)$, $c_{44}(T)$ [35] and $a(T)$ values [34] as a function of temperature. The solid line interpolates between the data points.

6.4 Discussion

Section 6.2 uses the Debye theory of lattice vibrations, generalized by direction-dependent elastic waves and modified by a fractional factor β_z in the ZPE combined with first-principles full potential total-energy band calculations. The combined theories are applied to calculation of the equilibrium lattice parameter $a(T)$ of fcc Al as a function of temperature (only $p = 0$ is considered).

The following features of this form of Debye theory are shown.

1) The calculated $a(T)$ differs from measured values over the full range of β_z for both GGA and LSDA, hence β_z cannot be evaluated. The GGA results are high by an average 0.7% and the LSDA results are low by 1.2%. These results on the band theory errors are similar to those found by Narasimhan and Gironcoli for thermal parameters of Cu [62].

2) The calculated thermal expansion from 0 to 300 K fits the measured thermal expansion rather well.

3) The frequently quoted lowest-order term in the low temperature expansion of $F(V,T)$, the T^4 term, is of little value. It is a poor approximation where the thermal expansion is large enough to be measured with good accuracy, and where both a and θ_D vary significantly to give accurate derivatives.

The procedure used to find $a(T)$ is an application of the thermodynamic theorem that equilibrium structure is found at a given p and T by minimizing the Gibbs free energy $G = E + pV + F$ (Eq. (1.1)). By use of G at reference structures, which are not in general in equilibrium states, the structure at the minimum can be found by fitting a smooth

function to the G values and finding the a of the minimum. Here we vary T at $p = 0$, but the procedure could be used at any p and T.

An alternative procedure finds equilibrium for cubic materials (which have only one structure parameter V or a) from $p = -d(E+F)/dV$ which is equivalent to $dG/dV = 0$. In the alternative procedure E is evaluated as a function of V, F as function of V and T, and $p(V,T)$ is found by differentiating with respect to V. It is then necessary to solve $p(V,T) = p_0$ to find $V(T)$ at p_0. This procedure was used for the thermal expansion of Ag by Xie et al. [63], who found complete phonon spectra calculated at constant V as a function of V, which gave $F(V,T)$ to high values of T. In the present work, we fix p and T first, evaluate E and F at a few reference values of V and interpolate $G(V)$ to find equilibrium at the minimum of G. The process is repeated at each T (and p if wanted) to find $a(T)$. Over a range of T the E values do not have to be recalculated, and θ_D in $F(\theta_D(V),T)$ also does not have to be recalculated; only T is varied. The expansion in $a(T)$ as T increases is driven by the decrease of θ_D due to the decrease of elastic constants as a increases (an anharmonic effect).

In Section 6.3 we evaluated β_z, the fraction by which the ZPE in the Debye theory should be reduced, and we found it to be about one half for fcc Al. A previous theoretical work [41] takes in account the ZPE effect on transition pressure but overestimates the transition from fcc Al to hcp Al by using the full Debye ZPE (at $\beta_z = 1$). In the present work, we used the value of β_z to estimate that purely theoretical quantity a_R, the rigid-

lattice value of a, which came out midway between the GGA and LSDA estimates. The evaluation of a_R directly from measurements provides a useful check on the accuracy of band calculations. In the evaluation of β_z from (6.11), the values of the bulk moduli B_1 at 100 K and B_2 at 200 K were taken from measurements. These values of B_1 and B_2 are given by $V\left(\partial^2(E+F)/\partial V^2\right)_T$, including a contribution from $V(\partial^2 F/\partial V^2)_T$ added to Vd^2E/dV^2, whereas (6.5) and (6.11) require just the contribution from E. However, the F contribution to B is only a few percent of the contribution from E and can be neglected. In [64] the contribution from F at 0 K, which is just the ZPE, is evaluated from the complete phonon spectra of fcc Al to be 1.8% of the total B.

The calculation of β_z from the complete phonon spectra has a complication because mode frequencies are calculated at constant volume, whereas experiment is at constant pressure. To use complete phonon spectra at constant volume the total energy must be calculated at enough volumes to find the volume and frequencies corresponding to the pressure of the experiment (here zero); moreover, the calculation must be repeated at each temperature, since the volume changes with temperature. The use of the Debye theory avoids this complication because the elastic constants that determine θ_D are at constant pressure.

Finally, we note that the values of the Debye-Grüneisen parameter γ_{DG}, 5.1 at 100 K and 4.0 at 200 K, are larger than the values for the standard Grüneisen parameter, e.g., γ_G = 2.2 at 100 and 200 K for fcc Al [12, page 57]; in addition γ_{DG} varies strongly with

T. The accuracy of γ_{DG} depends directly on the accuracy of measured $a(T)$ and $c_{ij}(T)$, and does not involve any thermodynamic or electronic theory.

CHAPTER 7

Structural anomalies in hcp Zn and hcp Cd under pressure

First-principles total energy calculations with WIEN2k, using the epitaxial Bain path (EBP) procedure modified for finite pressure, have found structural anomalies in hcp Zn and hcp Cd under pressure. The calculated small, but definite, anomaly in the pressure dependence of the structural parameters of hcp Zn contradicts a previous theoretical work that found that the anomaly disappears at a large number of k-points in the Brillouin zone. The calculation also shows that the uncertainty in locating equilibrium found in another recent paper is absent here. Reasons are given for computational differences from previous work. The pressure dependence of various elastic quantities, which are much more sensitive to the anomaly, shows the anomalies in hcp Zn and hcp Cd exist over a considerable range of pressure; several abrupt changes in the electron distribution are thereby indicated in the pressure range.

7.1 Introduction

In the present work, we revised the previous experimental and theoretical opinions that the existence of the structural anomaly in hcp Zn under pressure is doubtful. The calculated structural anomalies as a function of pressure were shown to fit the more recent data (2002) of Takemura *et al* [65-67] and both theory and experiment show a small but definite anomaly at about 100 kbar. Calculations at both low and high k-point density in the irreducible wedge of the Brillouin zone (IBZ) show that the anomaly is present at both densities without significant change. This conclusion contradicts the results of a recent first-principles calculation [68] that found the anomaly disappeared at high k-point density.

We provide additional information about the results on hcp Zn and give similar information for hcp Cd. The additional material includes the earlier structural data (1995) of Takemura [69] on hcp Zn, which has a poorer fit to the theory, includes an explicit comparison of structural parameters at low and high k-point density for both Zn and Cd, and extends the pressure range to give more perspective on the ranges of the large anomalies in elastic quantities. The same structural quantities are given for hcp Cd, where the theory does not fit the 1997 data of Takemura [23] for hcp Cd as well as the theory fitted the 2002 data on hcp Zn. The anomaly in Cd is shown to be larger and to have more structure than in Zn.

7.2 Calculation procedure and results

First-principles total energy calculations on hcp Zn and hcp Cd under hydrostatic pressure were performed using the full-potential augmented-plane-wave plus local orbital (APW+lo) method together with the Perdew-Burke-Ernzerhof generalized-gradient-approximation (PBE-GGA), as implemented in the WIEN2k package [22]. A plane-wave cutoff $R_{MT}K_{\max}=7$, $R_{MT}=1.6$ a.u., $G_{\max}=14$ and mixer$=0.05$ were used in all the calculations. We used 5300 k-points in the IBZ in both the free energy and the elastic constants calculations for Zn in order to check the negative results in [68] and, for comparison, we also carried out the free energy calculations using 550 k-points in the IBZ. A similar comparison was also made for hcp Cd. The k-space integration was done by the modified tetrahedron method [22]. Tests with larger basis sets and different Brillouin-zone samplings yielded only very small changes in the results. The convergence criterion on the energies was set at 1×10^{-3} mRyd / atom.

We used the epitaxial Bain path (EBP) procedure [8-11, 14-18] to find the equilibrium states and the elastic constants of the hcp lattice. Briefly, the equilibrium structure is found from the thermodynamic result that at a given pressure p the Gibbs free energy (at zero temperature) $G(a,c;p)\equiv E(a,c)+pV(a,c)$ is a minimum with respect to both the hcp structure parameters a and c, where E is the energy/atom and V the volume/atom. The elastic constants are then found as second strain derivatives of G in the equilibrium state at p, while p remains constant. This procedure finds the structural parameters and elastic constants directly as functions of p.

Figures 7.1(a) (c) show, respectively, the lattice constants a, c and the ratio c/a of hcp Zn as functions of pressure p in the range from 0 to 140 kbar. The open diamonds are the experimental data of Takemura [69] in 1995 showing a large structural anomaly in the vicinity of 120 kbar. The solid diamonds are the experimental results of Takemura *et al* [65-67] in 1999 and 2002 using a better pressure medium showing a smaller anomaly around 100 kbar. The open circles and crosses (using 5300 and 550 k-points in the IBZ, respectively) are the theoretical results of this work, which show that the anomaly has a small but definite effect on the lattice constants and occurs in the same pressure range and has the same magnitude as the latest experimental measurement.

Figure 7.2(a) shows that the anomaly has a large effect on the ratio of linear compressibilities k_c/k_a, where $k_c/k_a=(c_{11}+c_{12}-2c_{13})/(c_{33}-c_{13})$ [70]. Figure 7.2(b) shows that the anomaly also has a large effect on the elastic constant c_{66} in the vicinity of 100 kbar. Figure 7.2(c) shows the value of $G-G_0$ of hcp Zn at its minimum as a function of pressure, where G_0 is the value for hcp Zn at 0 kbar.

According to [68], the anomaly in lattice parameters of hcp Zn under compression exists at 732 k-points, but disappears at 5208 k-points in the IBZ. To check these results we have performed EBP calculations with 5300 (open circles) and 550 k-points (crosses) in the IBZ, which are shown in Fig. 7.1(a) (c). The comparison shows no significant change in $a(p)$, $c(p)$ and $(c/a)(p)$ in the pressure range of the anomaly of hcp Zn with the change in number of k-points in the IBZ.

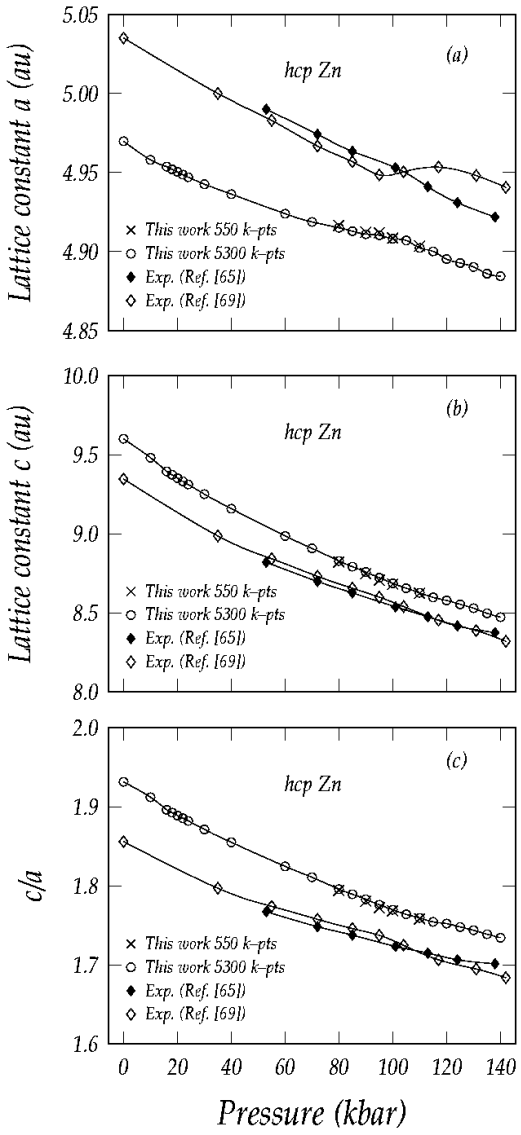

Figure 7.1. (a) The lattice constant a, (b) the lattice constant c and (c) the ratio c/a of hcp Zn as functions of pressure p. The solid and open diamonds are the experimental data from [65] and [69], the open circles and crosses (using 5300 and 550 k-points in the IBZ, respectively) are the theoretical results of this work. The solid curves interpolate between the data points.

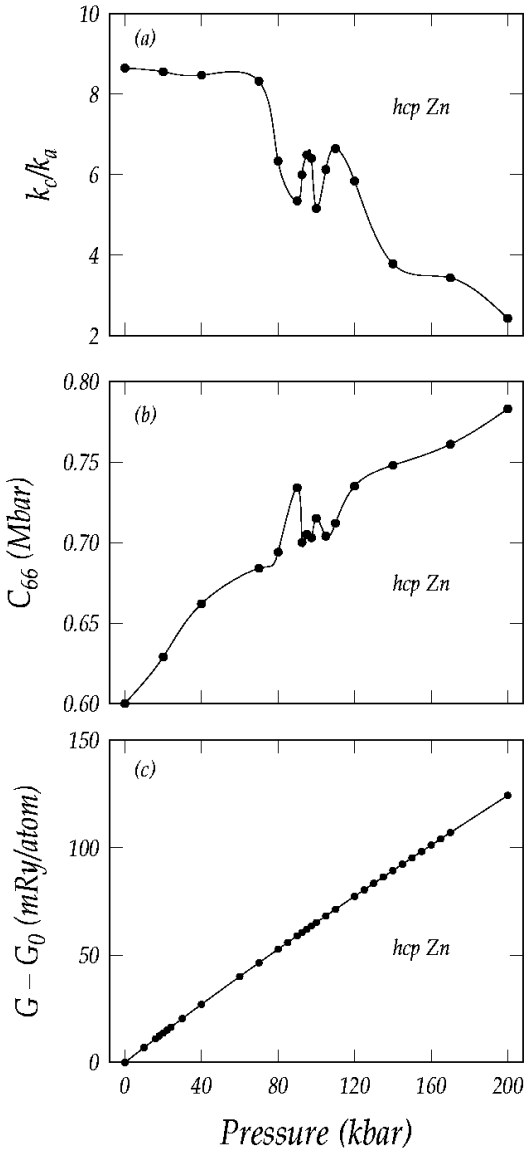

Figure 7.2. (a) The linear compressibility ratio k_c/k_a and (b) the elastic constant c_{66} of hcp Zn as functions of pressure. (c) Free energy difference $G-G_0$ of hcp Zn as a function of pressure, where G_0 is the free energy of hcp Zn at 0 kbar. The solid curves interpolate between the data points.

Figures 7.3(a) (c) show, respectively, the lattice constants a, c and the ratio c/a of hcp Cd as functions of pressure *p* in the range from 0 to 240 kbar. The open diamonds are the experimental data of Takemura [23] showing the slope changes in the vicinity of 60 and 120 kbar. The open circles and crosses (using 550 and 5300 k-points in the IBZ, respectively) are the theoretical results from the present work showing that the theoretical anomaly occurs in the same pressure range as the experimental measurement. The comparison between 550 and 5300 k-points in the IBZ shows no significant change with k-point density in $a(p)$, $c(p)$ and $(c/a)(p)$ in the pressure range of the anomaly of hcp Cd.

Figures 7.4 (a) and (b) show that the anomaly has a large effect for hcp Cd on the ratio of linear compressibilities k_c/k_a and a moderate effect on the elastic constant c_{66} in the same pressure range as the structural anomalies. Figure 7.4(c) shows the value of $G-G_0$ of hcp Cd at its minimum as a function of pressure, where G_0 is the value for hcp Cd at 0 kbar.

Figure 7.5 shows the comparison of the structural anomalies between hcp Zn (open circles) and hcp Cd (solid circles) in (a) the lattice constants a, (b) the lattice constant c and (c) the ratio c/a as functions of pressure p. The insets show the anomaly in hcp Zn on expanded scales.

Figure 7.6 shows that the minima of G along the EBP at pressures that include the range of the anomaly have well-defined minima in contrast to the results in [71, Fig. 10].

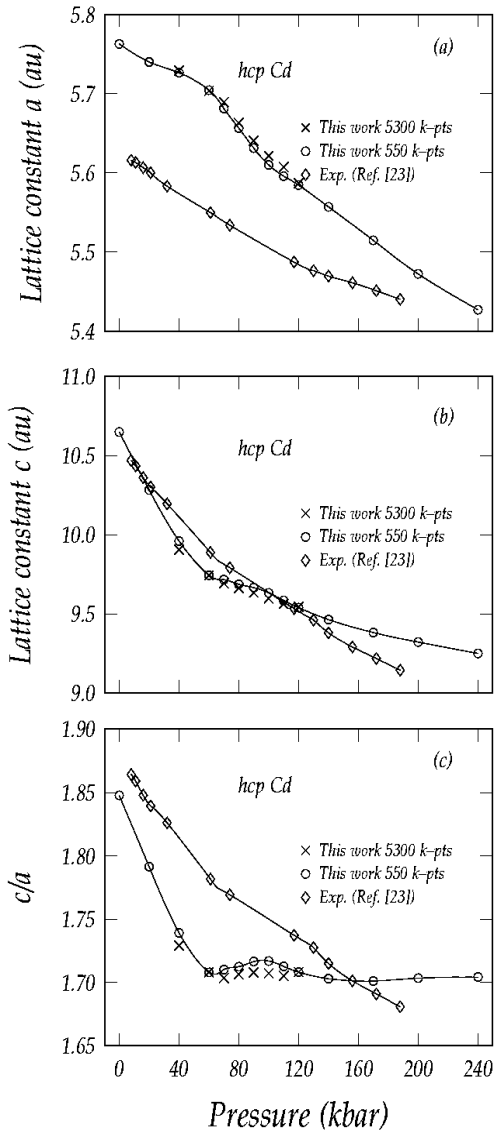

Figure 7.3. (a) The lattice constant a, (b) the lattice constant c and (c) the ratio c/a of hcp Cd as functions of pressure p. The open diamonds are the experimental data from [23], the open circles and crosses (using 550 and 5300 k-points in the IBZ, respectively) are the theoretical results of this work. The solid curves interpolate between the data points.

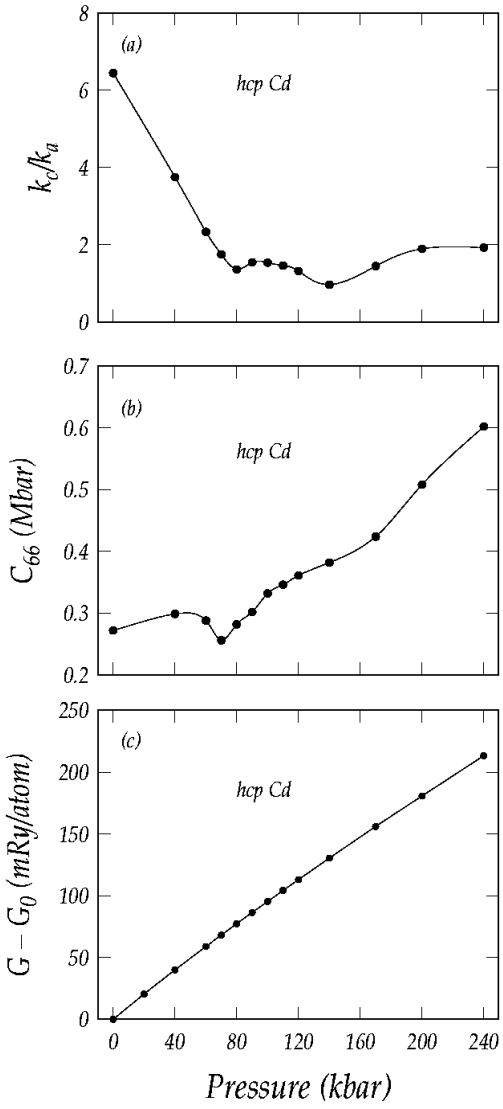

Figure 7.4. (a) The linear compressibility ratio k_c/k_a, (b) the elastic constant c_{66} and (c) free energy difference $G-G_0$ of hcp Cd as functions of pressure, where G_0 is the free energy of hcp Cd at $p = 0$. The solid and dashed lines interpolate between the data points.

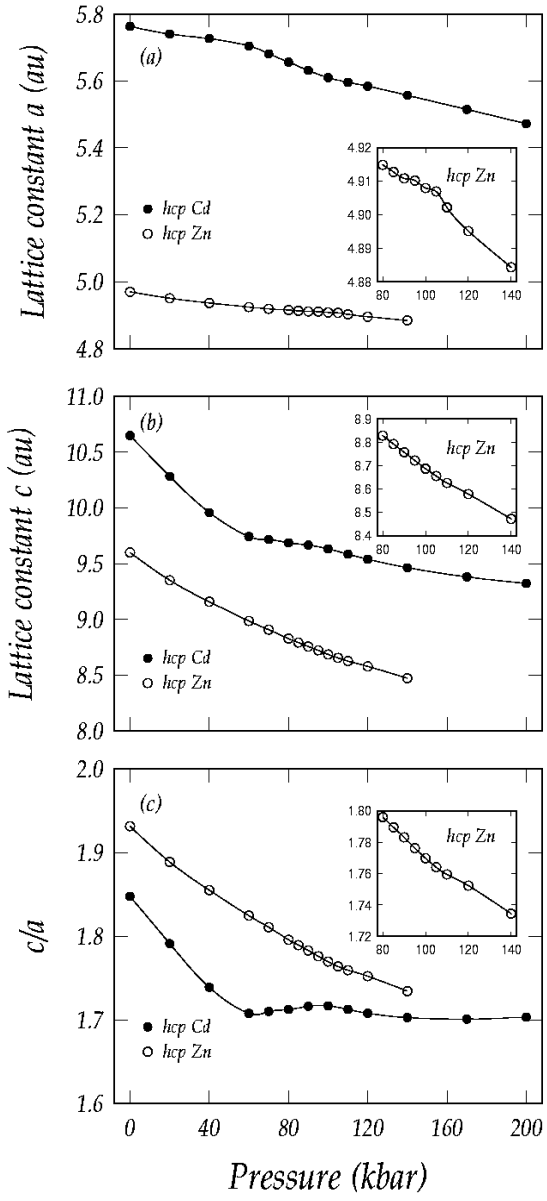

Figure 7.5. Comparison of the structure anomalies between hcp Zn (open circles) and hcp Cd (solid circles) in (a) the lattice constants a, (b) the lattice constant c and (c) the ratio c/a as functions of pressure p. The insets show the anomaly of hcp Zn on expanded scales.

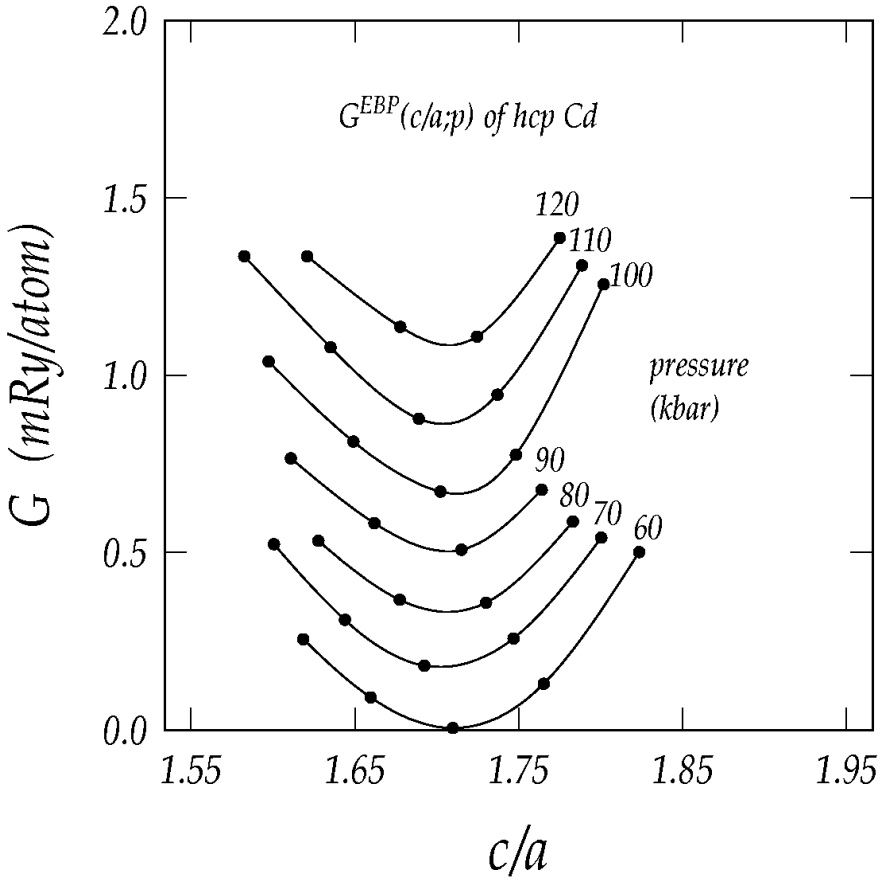

Figure 7.6. Gibbs free energy $G(c/a)$ of hcp Cd along the EBP at a series of pressures covering the anomalous range. For compact presentation, the minimum energy of the $G(c/a)$ curve at $p = 60$ kbar is set to zero and the $G(c/a)$ curves at pressures from 70 to 120 kbar are shifted toward zero by 9, 18, 27, 36, 45 and 53 mRy/atom, respectively.

7.3 Discussion

The initial linear decrease of calculated c/a as a function of pressure up to 40 kbar for hcp Zn is in good agreement with experimental data as shown in Fig. 7.1(c) and provides strong evidence of the reliability of our calculation. We note that the initial decrease in anisotropy under pressure is a basic feature of the structure, separate from the small anomalies.

The first evidence for the anomaly in hcp Zn is the rise and fall of the theoretical lattice parameter $a(p)$ forming an upward jog as p increases in the vicinity of 100 kbar (Fig. 7.1(a) and the inset in Fig. 7.5(a)). The jog is small but definite, and corresponds well in pressure range and magnitude to the small jog in the helium data in [65], whereas the theoretical jog clearly does not fit the earlier data in [69].

The comparison of theory and experiment in Fig. 7.1 is facilitated by the fact that pressure is the primary variable at which lattice constants are measured, and the theory gives the lattice constants directly as functions of pressure. When the theory gives lattice parameters as functions of volume, as in previous calculations [68, 70-72], the comparison of theory and experiment requires use of the equation of state $p(V)$ and incorporates the uncertainties in that function obtained by differentiating $E(V)$. The combination of theory in the present work and the helium data [65-67] provide a strong case for the existence of the anomaly.

The existence of the anomaly in hcp Zn is established without doubt by the remarkably large magnitudes and extended pressure range of the oscillations in elastic quantities plotted in Fig. 7.2, i.e. the linear compressibility ratio k_c/k_a and the elastic

constant c_{66}. Apparently four to six abrupt electronic transitions take place over a range of at least 60 kbar.

The effect of increasing the k-point density in the IBZ from 550 to 5300, shown in Fig. 7.1 for hcp Zn and Fig. 7.3 for hcp Cd, is small and the anomaly is clearly seen in both calculations. We note that [68] states (page 2, left) that at the k-point density of 5208 k-points in the 'the anomaly in c/a has disappeared'.

Refs. [68] and [71] suggest the occurrence of minima in $a(p)$ or $a(V)$ as pressure increases or volume decreases. Thus Fig. 7 of [71] shows that $a(V)$ has two minima and Fig. 5 of [68] shows that $a(V)$ has a minimum for Zn at 762 k-points in the IBZ, which is not present at 5208 k-points. Our calculations and the experimental data do not show any minima in $a(p)$. Note that [68] uses a muffin-tin radius R_{MT} of 2.0 a.u. for Zn and [71] uses $R_{MT} = 2.45$ a.u. for Zn and 2.75 a.u. for Cd. At these values of R_{MT} we found 'ghost bands' i.e. spurious energy bands produced by using over too great a range the approximation, which linearizes the energy dependence of the matrix elements of the Kohn Sham Hamiltonian. Filling these bands with electrons would produce errors in the total energy. To remove the ghost bands we reduced R_{MT} to 1.6 au for both Zn and Cd at the cost of greater computation time. Warnings about ghost bands are given in [22] but [68] and [71] do not mention ghost bands.

The pressure dependences of a, c and c/a of hcp Cd in Fig. 7.3 show distinct anomalies that match the trend and pressure values of the experimental data [23], but the theoretical anomalies are larger in magnitude. We note that the observed linear decrease

in anisotropy up to 60 kbar shown by c/a in figure 7.3(c) is in reasonable agreement with the theoretical values, although not as good as the agreement for Zn in figure 7.1(c); the theory levels more rapidly than experiment for Cd. This agreement for the initial linear decrease is evidence for the validity of the theory apart from the details of the anomaly.

In both [68] and [71] the procedure for finding equilibrium states is to obtain the minimum of $E(c/a)$ at constant V; the pressure corresponding to V is found from the equation of state $p(V)$. In the Cd calculations in [71] a difficulty with this procedure appeared which makes the theoretical results for $(c/a)(p)$ uncertain. Ref. [71] finds that $E(c/a)$ in the range of the anomaly has a flat bottom or a double-well bottom (their Fig. 10) so that c/a of equilibrium cannot be accurately determined. The uncertainty ranges for Cd shown in their Fig. 8 could contain the $(c/a)(p)$ curve in our figure 7.3(c) with its shallow minimum. The procedure used in the present work for Cd from the minima of G with respect to both a and c at constant p gives a well-defined equilibrium state. Figure 7.6 shows the well-defined minimum at each *p* for Cd, in contrast with Fig. 10 of [71].

The elastic quantities of hcp Cd in Fig. 7.4, k_c/k_a and c_{66}, show strong anomalous behavior at about the same pressure values in a plot from 40 to 200 kbar. The k_c/k_a values show linear decrease of anisotropy from a large value of 6.4 at 0 kbar to isotropy with $k_c/k_a \cong 1$ at about 80 kbar.

The numerous oscillations in $k_c/k_a(p)$ and $c_{66}(p)$ in hcp Zn and hcp Cd suggest that several abrupt changes take place in the electron distribution over the pressure range in which anomalies occur. Examining closely the electron distributions in this restricted range should reveal the nature of these changes; these distributions are implicit in the calculation.

Chapter 8

Pressure dependence of the TO phonon frequency in hcp Zn

Zone-centre transverse optical phonon frequencies $\nu^{TO}(p)$ of hcp Zn as a function of hydrostatic pressure p have been calculated using the full-potential augmented-plane-wave plus local orbitals first-principles method with the generalized gradient approximation and compared with Raman measurements of frequencies under pressure. The oscillatory behavior of $\nu^{TO}(p)$ found in the pressure range of the anomalies of hcp Zn supports our previous work on Zn, where such effects were shown both in the structural parameters and strongly in the elastic constant $c_{44}(p)$. By integrating the equation of motion using the exact potential and the zero-point and temperature excitations of the Raman active modes we show substantial anharmonic effects which make the frequency of one TO mode about 5% lower the frequency of the other mode; this split is a large part of the observed linewidths.

8.1 Introduction

The combination of the diamond anvil cell, intense laser light sources and highly sensitive radiation detectors has in recent years made possible Raman line measurements in reflected radiation from a specimen under pressure that provide information about lattice vibrations in crystals under high pressure. Crystals with more than one atom in the primitive unit cell, such as hexagonal close-packed (hcp) and diamond structures, have optical-mode vibrations in which atoms in the cell move strongly relative to each other and are Raman active. Such activity depends on variation of the polarizability of the unit cell as the electron distribution changes at the vibrational frequency of a particular mode. In a one-phonon scattering event in the bulk of the crystal, conservation of energy and momentum require that the phonon wavevector be very small, i.e., only zone-centre phonons contribute to the Raman measurement. The symmetry of the hcp structure then restricts Raman activity to the doubly degenerate zone-centre vibration in which alternate hexagonal layers slide on adjacent layers. The energy change in this motion is the energy of an internal strain. Olijnyk and Jephcoat, in a review of Raman measurements on hcp metals under pressure [73], list a dozen hcp metals in which Raman measurements have been made since 1992.

The Raman-active Brillouin zone-centre (Γ point) transverse optical (TO) mode frequency as a function of pressure ($\nu^{TO}(p)$) has been evaluated in previous theoretical work only for a few metals, including Zn, Mg and Zr. In most cases the calculated frequency follows the experimental values as a function of pressure, but is 5–10% less than experiment and possibly as much as 20% lower when the increase in frequency in

going from room temperature measurements to zero temperature values is taken into account.

In this chapter we recalculate the TO mode frequency of hcp Zn as a function of pressure at the Γ point to take advantage of the greater accuracy of the EBP method [8-11, 14-18],. Briefly, EBP finds equilibrium structural parameters a and c directly as functions of pressure p from the minima of the Gibbs free energy $G = E + pV$ (at 0 K) at constant p, whereas the usual procedure [68, 71] finds equilibrium from minima of $E(c/a)$ at constant volume V and calculates p by differentiating $E_{\min}(V)$ with respect to V. Then, we use the equilibrium state at each p to calculate $\nu^{TO}(p)$ of hcp Zn in the pressure range of the structural anomalies [10]. Contrary to the previous discussion of theory and experiment in [25], we find definite oscillations in $\nu^{TO}(p)$ in the pressure range of the anomalies. In addition we use our values of $c_{44}(p)$ to make a quantitative test of an empirical formula relating $\nu^{TO}(p)$ and c_{44} [25, 74] and show that it is rather poor for hcp Zn.

We also study the anharmonic content of the Raman-active mode by integrating the equation of motion of the transverse optic mode in the exact potential controlling the motion. The potential contains all anharmonic contributions, which are shown to be large (at 300 K) for one direction of vibration and negligible for the orthogonal direction. The split in the two frequencies due to the anharmonic part of the potential is shown to be a substantial part of the observed linewidth as a function of p.

8.2 Calculation details

First-principles band calculations of hcp Zn were performed using the full-potential augmented-plane-wave plus local orbital (APW+lo) method together with the Perdew-Burke-Ernzerhof generalized-gradient-approximation (PBE-GGA) as implemented in the WIEN2k package [22]. A plane-wave cutoff $R_{MT}K_{\max} = 7$, $R_{MT} = 1.6$ a.u., $G_{\max} = 14$ and $\text{mixer} = 0.05$ were used in all the calculations; 5300 k-points in the irreducible Brillouin zone were used in EBP calculations and in the calculation of the elastic constants. The k-space integration was done by the modified tetrahedron method. Tests with larger basis sets and different Brillouin zone samplings yielded only very small changes in the results. The convergence criterion on the energies was set at 1×10^{-3} mRyd per atom.

The procedures for calculating the pressure dependence of $\nu^{TO}(p)$ are as follows.

(1) Use the EBP method to find the equilibrium lattice parameters directly as functions of pressure.

(2) Calculate the vibrational potential δE versus displacements δd of the second atom in the unit cell from the equilibrium structure at given pressures. Figure 8.1 shows the projected hcp unit cell used for δE versus δd calculations. In a conventional two-atom hcp unit cell $\alpha = \beta = 90^\circ$, $\gamma = 120^\circ$, $a = b$ and the two atoms are located at $(0, 0, 0)$ and $(2/3, 1/3, 1/2)$ respectively with vector components along and in units of the lengths of the lattice vectors $(\vec{a}, \vec{b}, \vec{c})$.

To calculate δE versus δd it is more convenient to use an unconventional two-atom hcp unit cell with $\gamma = 60^\circ$ and to rotate the unit cell by 15° about the $c\,(x_3)$ axis, so as to

have the basal rhombus symmetrically oriented with respect to the orthogonal axes x_1 and x_2, as shown in Fig. 8.1. Then the position of the second atom in the equilibrium state is $(1/3, 1/3, 1/2)$. This orientation makes the internal relaxation (for the relaxed elastic constant calculation [8]) one dimensional for strains that preserve the reflection symmetry of the bisecting plane. We note that the elastic constants are independent of the orientation of x_1 and x_2 axes due to sixfold symmetry. Two directions of δd designated δd^{in} and δd^{p} are considered, as shown in Fig. 8.1. The position of the second atom with δd^{in} is $\left(\frac{1}{3}+\frac{\delta d^{in}}{\sqrt{3}a}, \frac{1}{3}+\frac{\delta d^{in}}{\sqrt{3}a}, \frac{1}{2}\right)$ while with δd^{p} the position is $\left(\frac{1}{3}+\frac{\delta d^{p}}{\sqrt{3}a}, \frac{1}{3}-\frac{\delta d^{p}}{\sqrt{3}a}, \frac{1}{2}\right)$. Both δd^{in} and δd^{p} are perpendicular to the c-axis corresponding to the displacements in the TO mode. The value of $a =$ 4.91 au shown in Fig. 8.1 is the equilibrium lattice parameter of the base of the unit cell at $p = 100$ kbar obtained from the EBP calculations. The values of δd^{in} and δd^{p} in Fig. 8.1 are the magnitudes of the vibrations corresponding to $\delta E = k_B T$ with $T = 300$ K at $p = 100$ kbar.

Figures 8.2(a) and (b) show δE versus δd^{in} and δE versus δd^{p} curves respectively at $p = 100$ kbar. The solid curves represent the full potential, the dashed curves represent the harmonic part of the potential and the horizontal dotted lines correspond to $\delta E = k_B T$ with $T = 300$ K at $p = 100$ kbar. Such calculations are repeated at different pressures from 0 to 200 kbar to obtain the pressure dependence of $\nu^{TO}(p)$.

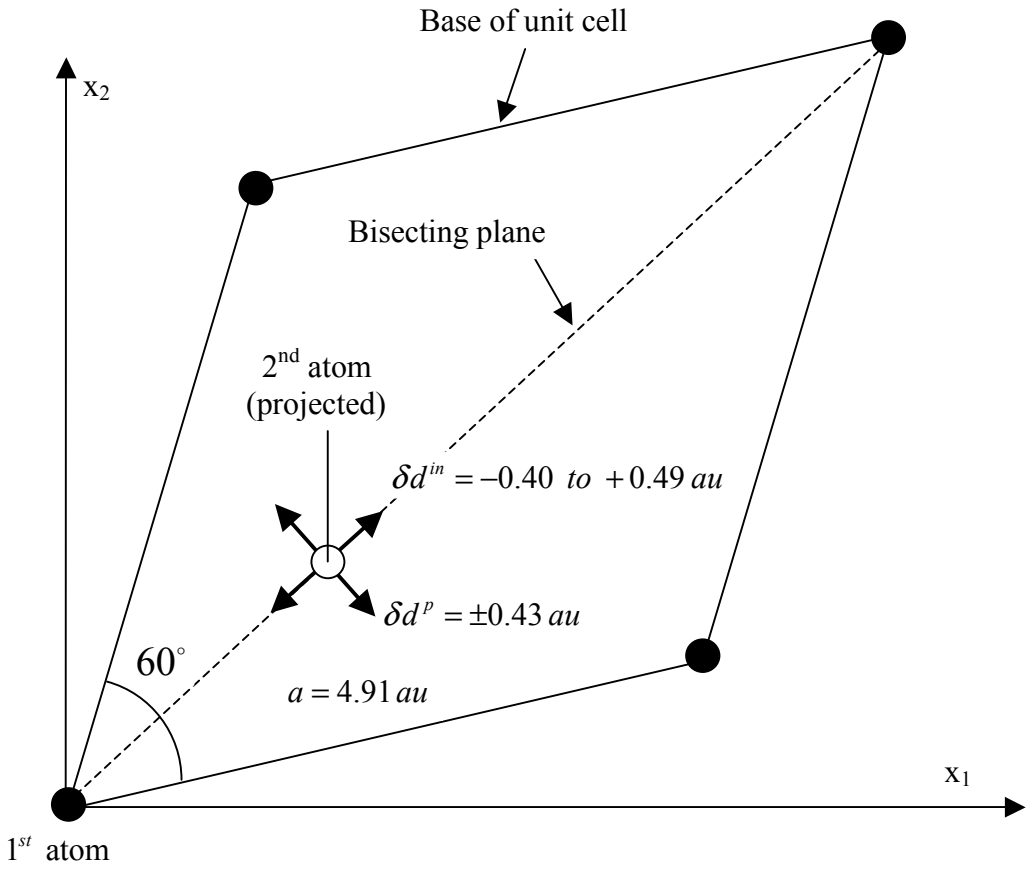

Figure 8.1. The base of an hcp unit cell with $\gamma = 60^{\circ}$ rotated 15° about c (or x_3) axis so that the basal rhombus is oriented symmetrically with respect to the orthogonal axes x_1 and x_2. The equilibrium position of the second atom in the unit cell is projected on the base.

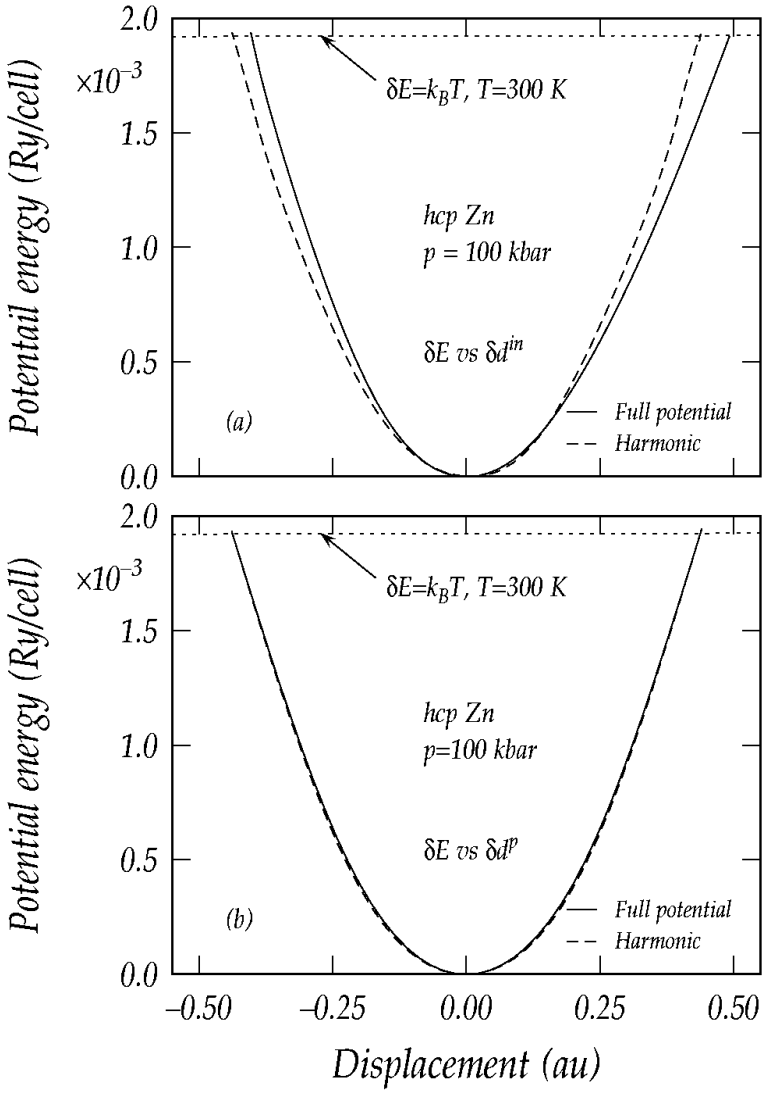

Figure 8.2. (*a*) δE versus δd^{in} and (*b*) δE versus δd^{p} curves at $p = 100$ kbar. The solid curves denote the full potential, the dashed curves denote the harmonic part of the potential and the horizontal dotted lines correspond to $\delta E = k_B T$ with $T = 300$ K at $p = 100$ kbar.

(3) Calculate $\nu^{TO}(p)$ from the full δE versus δd^{in} curves by integration over the full potential (Simpson's rule with 999 points). For convenience, in writing equations, let E and x represent δE and δd respectively. The equation of motion of the vibration is

$$\ddot{x} = -\frac{1}{m}\frac{\partial E}{\partial x}, \tag{8.1}$$

where $m = M_{Zn}/2$ is the reduced mass of the atom and M_{Zn} is the atomic mass of Zn. Equation (8.1) can be integrated and the solution over the full orbit gives the period of the vibration as

$$T = 2\int_{x_{\max 1}}^{x_{\max 2}} \frac{dx}{\left[\frac{2}{m}\left(E\left(x_{\max}\right) - E\left(x\right)\right)\right]^{1/2}}, \tag{8.2}$$

where $E(x_{\max}) = E(x_{\max 1}) = E(x_{\max 2}) = k_B T$ with $T = 300$ K, and $x_{\max 1}$ is negative while $x_{\max 2}$ is positive.

The integral is singular but integrable: expand the function $E(x)$ around $x_{\max}$ (which represents either $x_{\max 1}$ or $x_{\max 2}$),

$$E(x) = E(x_{\max}) + A\left(x - x_{\max}\right) + f(x), \tag{8.3}$$

where $|x| < |x_{\max}|$ and $f(x)$ has higher power of $(x - x_{\max})$. Then the singularity can be substracted out and integrated analytically:

$$\int_{x}^{x_{\max}} \frac{dx}{\left[\left(E\left(x_{\max}\right) - E\left(x\right)\right)\right]^{1/2}} = \int_{x}^{x_{\max}} g(x)dx + 2\left(\frac{x_{\max} - x}{A}\right)^{1/2} \tag{8.4}$$

where

$$g(x) \equiv \frac{1}{\left[E(x_{\max}) - E(x)\right]^{1/2}} - \frac{1}{\left[A(x_{\max} - x)\right]^{1/2}}, \tag{8.5}$$

and $g(x)$ can be integrated numerically. This procedure is used just for small intervals near $x_{\max}$.

(4) Calculate $\nu^{TO}(p)$ from c_{44} using the empirical relation (8.6) given in [73,74]:

$$\nu^{TO} = \frac{1}{\pi}\sqrt{\frac{\sqrt{3}a^2 c_{44}}{Mc}} \tag{8.6}$$

where a and c are the lattice constants, and M is the atomic mass. The elastic constant c_{44} of hcp Zn as a function of pressure has been calculated in this work as second strain derivative of G [8, 10].

8.3 Results and discussion

Figure 8.3 shows the zone-centre TO mode frequency $\nu^{TO}(p)$ as a function of pressure. The open diamonds in Figs. 8.3 (a) and (b) are the experimental data measured by Raman spectroscopy at room temperature from [25]. The open circles in Figs. 8.3 (a) and (b) are the calculated frequency-pressure data at zero temperature using the 'frozen-phonon' method, also from [25]. The solid circles and solid squares in Fig. 8.3 (a) are calculated from the numerical integration of δE versus δd^{in} curves of the full and harmonic potentials respectively. The solid triangles in Fig. 8.3 (b) are obtained from the integration of the δE versus δd^{p} curves. For the vibration perpendicular to the bisecting plane both the full and harmonic potentials give the same frequency at each given

pressure up to δE at 300 K. All the data (except the δd^{in} harmonic data) shown in Fig. 8.3 are replotted in Fig. 8.4 with expanded scales along with the data (open triangles) calculated from the relaxed c_{44} using (8.6). The oscillatory behavior of $\nu^{TO}(p)$, as shown in Figs. 8.3 and 8.4, occurs in the pressure range of the anomalies of hcp Zn, which are discussed in Chapter 7. The oscillation in $\nu^{TO}(p)$ demonstrates that the EBP procedure used in this work for finding equilibrium at a given p is more accurate than the usual procedure based on minima of $E(c/a)$ at constant V. The previous theoretical result in [25] was interpreted as a smooth curve in Fig. 2 of [25], although some irregularity is shown in Fig. 4 of [25]. The calculated data in this work show clearly visible oscillations of ν^{TO} at 145, 125, 105 and 95 kbar, which are present in both the full potential and harmonic part of the potential for the in-plane displacement δd^{in}. Somewhat different oscillations appear at 140, 120 and 110 kbar for the out-of-plane displacement δd^{p}, which is entirely harmonic. The experimental data show some anomalies at 140 kbar, and possibly at 110 and 95 kbar.

The comparison of calculated $\nu^{TO}(p)$ with values calculated with the empirical formula (8.6) using $c_{44}(p)$ in Fig. 8.4 shows poor correspondence. The formula (8.6) values are high by $\sim 30\%$ and the anomalous oscillations are much stronger than in the first-principles $\nu^{TO}(p)$. The comparison uses relaxed values of c_{44} [8]; use of unrelaxed values, which are larger, would increase the discrepancy.

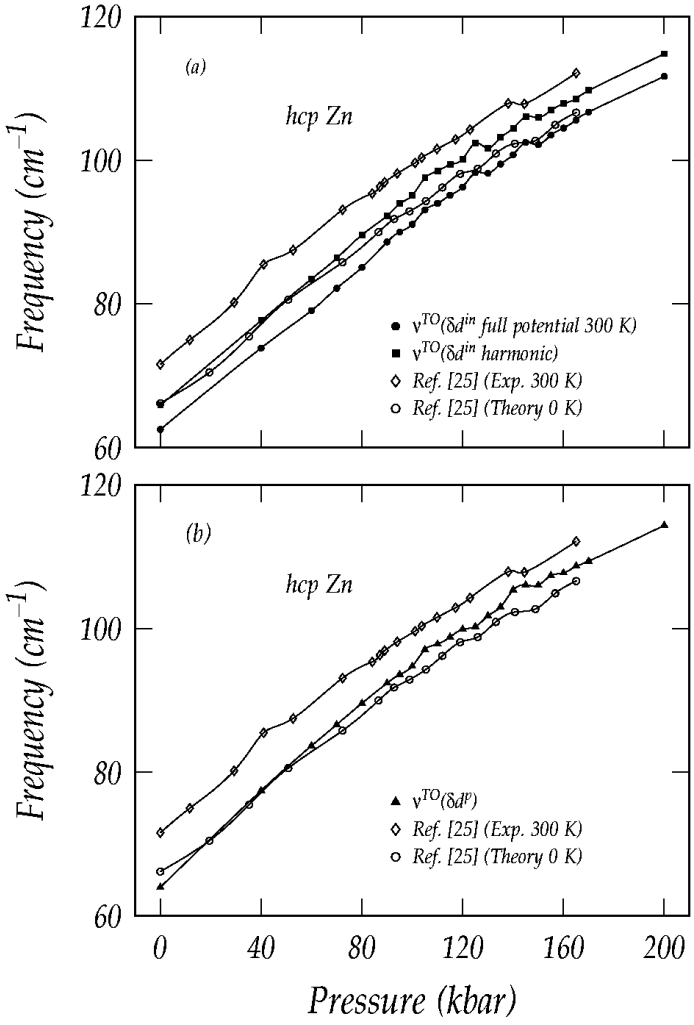

Figure 8.3. Zone-centre TO mode frequency as a function of pressure. The open diamonds and open circles in (*a*) and (*b*) are the experimental and theoretical data from [25]. The solid circles and solid squares in (*a*) are calculated from the δE versus δd^{in} curves of the full and harmonic potentials respectively. The solid triangles in (*b*) are obtained from the δE versus δd^{p} curves. In both (*a*) and (*b*) the solid curves interpolate between the data points.

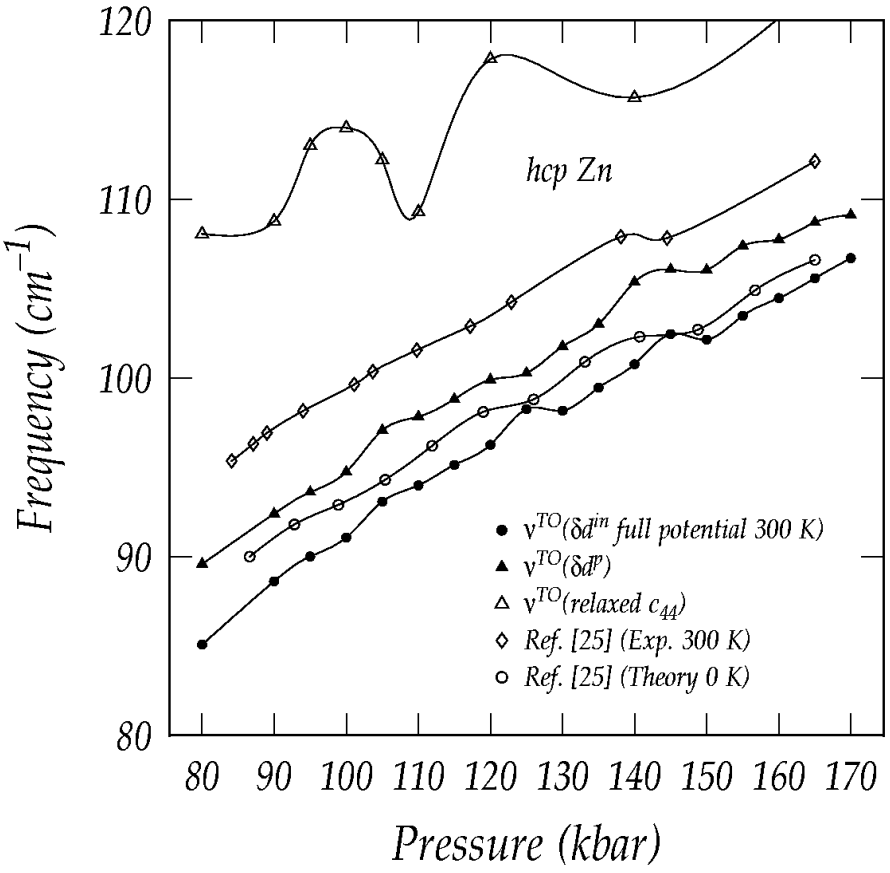

Figure 8.4. Oscillatory behavior of the TO mode frequencies in the pressure range of the anomalies of hcp Zn. The open triangles are calculated from the relaxed c_{44} using (8.6). All other data are the same as in Fig. 8.3 but with a smaller pressure range. The solid curves interpolate between the data points.

The open circles in Fig. 8.5 are the experimental linewidths of the Raman spectra of the TO mode of hcp Zn as a function of pressure [25]. The solid dels denote the frequency difference between the solid circles and the solid squares in Fig. 8.3 (a), which are calculated from the δE versus δd^{in} curves of the full and harmonic potentials.

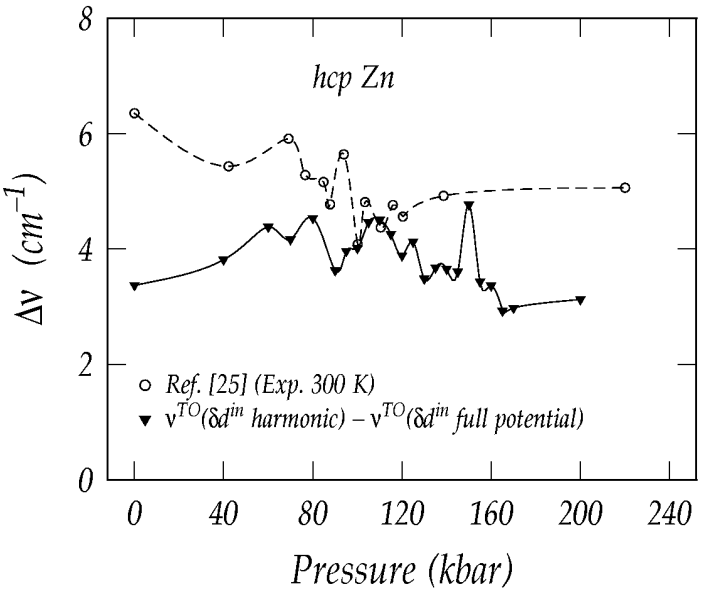

Figure 8.5. The open circles are the experimental linewidths of the Raman spectra versus pressure from [25]. The solid dels are the frequency differences between ν^{TO} (δd^{in} *harmonic*) and ν^{TO} (δd^{in} *full potential* 300 K) as a function of pressure. The solid and dashed curves interpolate between the data points.

The full potential for δd^{in} shows a substantial asymmetry, which is due to dependence of the full potential on $(\delta d^{in})^3$ terms in the expansion around equilibrium. Such terms are forbidden in the potential for δd^{p} since the plane bisecting the 60° vertex angle in Fig. 8.1 is a plane of reflection symmetry for δd^{p}; the fourth-order terms in δd^{p} are negligible at $\delta E = 2$ mRyd corresponding to the phonon energy at 300 K.

The anharmonic content of $E(\delta d^{in})$, which lowers the full-potential frequencies by 5%, produces a spread of frequencies from ν^{TO} obtained with δd^{p} to ν^{TO} obtained with δd^{in}. The spread of frequencies is shown in Fig. 8.5 to be a substantial part of the observed line widths plotted in Fig. 8.5. The downward trend of the calculated frequency spread from 60 to 140 kbar also seems to correspond to the experimental line-width values.

Chapter 9

Summary and future work

9.1 Summary

In this dissertation research EBP and MNP procedures have been successfully applied to find the stable and metastable phases of Fe and Al and the structural anomalies of Zn and Cd. Especially, the effectiveness of the MNP procedure has been illustrated in finding the stable and metastable phases of metals based on finding equilibrium structures from minimizing the Gibbs free energy G with respect to structure at a given hydrostatic pressure p and temperature T.

- The structure and stability of four Bravais phases of Fe under pressure are determined by the MNP procedure. The four Bravais phases are body-centered tetragonal (bct), body centered cubic (bcc), face centered cubic (fcc), and rhombohedral (*rh*). The results show that bcc Fe becomes unstable at 1500 kbar, that fcc Fe is stable at $p = 0$, that a phase transition from bcc to fcc is thermodynamically favored at 290 kbar, that a bct phase at $c/a = 0.89$ is unstable up to 2700 kbar and that a *rh* phase with angle $\alpha = 60.5^0$ is stable at $p = 0$ with slightly higher E than that of fcc Fe.
- The thermal expansion of the lattice parameter of fcc Al, $a(T)$, is shown to be accurately determined by the Debye theory of lattice vibrations and first-principles total

energy band calculations with the MNP procedure. The Debye theory uses the well-known generalization to direction-dependent elastic mode frequencies and is further modified by introducing a parameter β_z, which gives the fraction of the full Debye zero-point energy possessed by the actual dispersive mode frequencies. The calculation of $a(T)$ is simplified by minimizing the Gibbs free energy of the vibrating lattice rather than the usual procedure of minimizing the total energy at constant volume. The parameter β_z is shown to affect the value of $a(T)$.

- First-principles total-energy calculations with WIEN2k using the EBP procedure, which determine the equilibrium states of hcp structures under pressure from minima of the Gibbs free energy, have found a structural anomaly in hcp Zn and in hcp Cd under pressure. The calculated small but definite anomaly in the pressure dependences of the structural parameters of hcp Zn allows a reinterpretation of the data to show the anomaly. We find a similar but stronger anomaly in Cd than in Zn. Evaluation of the pressure dependence of various elastic quantities which are much more sensitive to the anomaly shows the anomalies in hcp Zn and hcp Cd exist over a considerable range of pressure; several abrupt changes in the electron distribution are thereby indicated in that pressure range.

- Zone-center transverse optical phonon frequencies $\nu^{TO}(p)$ of hcp Zn as a function of hydrostatic pressure p have been calculated using the EBP procedure and compared with Raman measurements of frequencies under pressure. The oscillatory behavior of $\nu^{TO}(p)$ found in the pressure range of the anomalies of hcp Zn supports our

previous work on Zn, where such effects were shown both in the structural parameters and strongly in the elastic constant $c_{44}(p)$. By integrating the equation of motion using the exact potential and the zero-point and temperature excitations of the Raman active modes we show substantial anharmonic effects which make the frequency of one TO mode about 5% lower than the frequency of the other mode; this split is a large part of the observed linewidths.

9.2 Future work

Based on the MNP procedure we are currently developing a new and more efficient procedure called the E & G procedure, more explicitly, the E at constant volume and G at constant pressure procedure, where E is the total internal energy and G is the Gibbs free energy. From the minima of E as a function of structure at constant V, the existence and vanishing of phases can be found as minima appear and disappear as V changes. From the minimum E values separate equations of state can be determined and used to find separate $G(p)$ functions for each phase. Then the crossings of $G(p)$ curves determine phase transition pressures. The vanishing of eigenvalues of the $\underline{\underline{c_{ij}}}$ matrix determines instability pressures.

It appears entirely practical to find the phases of 11 Bravais structures – 3 cubic, 2 tetragonal, rombohedral, hexagonal and 4 orthorhombic. (Monoclinic phases will need an extension of the current program). We are headed toward a new point of view on stable and metastable phases of

the elements – there are many of them associated with different symmetries. We are going to use this new E & G procedure to search for all Bravais one-atom stable and metastable phases.

- The calculation on Ca will be the first to exhibit 7 Bravais symmetries, with all phases tested for stability and characterized by the δG to the lowest barrier against other phases.
- A study of In, which is believed to have orthorhombic phases, would bring in 4 more Bravais symmetries, This study will provide a good test of the procedure to determine the equilibrium line in the structural space.

Appendix

MNP code

A.1 MNP12N_optimize routine

```
! MNP12N_optimize.f
! MNP12N_optimize makes all 42 strained structure files and the script
! MNP12N_optimize_job; it calculates pV term for all structures
      CHARACTER*79      rows
      CHARACTER*11      STATUS, FORM
      CHARACTER*80      TITLE
      CHARACTER*80      FNAME, master
      CHARACTER*80       orname
      CHARACTER*1        backslash
      common  /name/ orname

        FNAME= 'MNP12N_optimize.def'
! ‘.def ’ file contains the names of all input and output files; it is automatically created
! when the program is run by x_lapw script (from WIEN2k package)
! ‘.def ’  has the form:
!                     20, ‘ case_initial.struct',      'unknown',    'formatted', 0     (output)
!                     18, 'MNP12N.prmt',      'old',    'formatted', 0                 (input)
!                     19, 'MNP12N.pv',  'unknown',  'formatted', 0                    (output)
!                     16, 'MNP12N_optimize.job', 'unknown',' formatted', 0     (output)
```

```
!                    17, 'case.struct',     'old',    'formatted', 0                    (input)
! ‘case’ = ‘name_of_current_directory’
      OPEN (1, FILE=FNAME, STATUS='OLD', ERR=8000)
8003 READ(1,*,END=8001) IUNIT, FNAME, STATUS, FORM
      OPEN (IUNIT, FILE=FNAME, STATUS=STATUS, FORM=FORM, iostat=ist &
            , ERR=8002)
      if (iunit.eq.20) master=FNAME
      GOTO 8003
8000 WRITE(*,*) ' ERROR IN OPENING MNP12N_optimize.def !!!!'
      STOP 'MNP12N_optimize.def'
8002 WRITE(*,*) ' ERROR IN OPENING UNIT:',IUNIT
     WRITE(*,*) '    FILENAME: ',FNAME,'  STATUS: ',STATUS,'  FORM:',FORM, ist
     STOP 'OPEN FAILED'
8001 CONTINUE
      do 8004 i=80,1,-1
8004   if (FNAME(i:i).eq.'.') goto 8005
8005  continue
      orname(1:i-1)=FNAME(1:i-1)

! Test if case_initial.struct exists, use it or create it
    read (20,'(a)', END=10, ERR=10) status
    close (17)
    close (20)
    OPEN (17,FILE=master, STATUS='old', FORM=FORM, ERR=8002)
    goto 11
10   continue
    close (20)
    OPEN(20, FILE=master, STATUS='unknown', FORM=FORM, ERR=8002)
12    read (17,245,end=13,err=13) rows
```

```
245   FORMAT (A79)
       write(20,245) rows
      goto 12
13    rewind (17)
11    continue
!-------------------------------------------------------------------------------------------------------
     call abc(i-1)
      end
!-------------------------------------------------------------------------------------------------------
! subroutine abc creates all structure files , '.job' and '.pV' files
     subroutine abc(ileng)
     common /name/ orname
     double precision  a, b, c,alpha, beta, gamma, E1, EP(43,6)      &
                       ap, bp, cp, alphap, betap, gammap              &
                       ,AX(3,3), AXP(3,3), EPC(6), V(43)          &
                        ,PC, P, PX, PV(43)
     character*79         rows
     character*80         orname
     character*2          zwname
      chracter*7          ext
     character*80         finame, f2name, joname(100)
     character*12         opname
     character*1           backslash
     integer               i, j, ii, iii, numb, va_ry(80), IE(6,43)
     data numb /43/
     data E1 /0.04D0/
     data PC /0.6798D-5/
     data ext / '.struct'/
```

```
      data IE / 0,0,0,0,0,0  ,1,0,0,0,0,0  ,2,0,0,0,0,0  ,0,1,0,0,0,0  ,0,2,0,0,0,0  ,0,0,1,0,0,0
     & ,0,0,2,0,0,0  ,0,0,0,1,0,0  ,0,0,0,2,0,0  ,0,0,0,0,1,0  ,0,0,0,0,2,0  ,0,0,0,0,0,1 &
     ,0,0,0,0,0,2  ,1,1,0,0,0,0  ,2,2,0,0,0,0  ,1,0,1,0,0,0  ,2,0,2,0,0,0  ,1,0,0,1,0,0 &
     ,2,0,0,2,0,0  ,1,0,0,0,1,0  ,2,0,0,0,2,0  ,1,0,0,0,0,1  ,2,0,0,0,0,2  ,0,1,1,0,0,0 &
     ,0,2,2,0,0,0  ,0,1,0,1,0,0  ,0,2,0,2,0,0  ,0,1,0,0,1,0  ,0,2,0,0,2,0 ,0,1,0,0,0,1 &
     ,0,2,0,0,0,2  ,0,0,1,1,0,0  ,0,0,2,2,0,0  ,0,0,1,0,1,0  ,0,0,2,0,2,0  ,0,0,1,0,0,1 &
     ,0,0,2,0,0,2  ,0,0,0,1,1,0  ,0,0,0,2,2,0  ,0,0,0,1,0,1  ,0,0,0,2,0,2  ,0,0,0,0,1,1 &
     ,0,0,0,0,2,2 /

     ! a, b, c, alpha, beta, gamma are input structure parameters

     ! ap, bp, cp, alphap, betap, gammap are parameters of  the strained structures

     ! E1= the magnitude of the strain

! AX(3,3) is the matrix of the orthogonal components of a, b, c vectors (see eq.(3.1))
! AXP(3,3) is the matrix of the orthogonal components af ap, bp, cp vectors (see eq.(3.1))

! V (PV) are the volume (pV term) matrices

! P (PX) is the pressure in kbar ( Ryd/bohr**3)

! PC is the conversion factor from kbar to Ry/bohr**3


! find EP(43,6); every line is a strain vectors EP(6), which will be applied to initial
! structure in order to obtain one particular strained structure
! EP(43,6) will have the form :  0    0    0    0    0    0 (unstrained state)
!                                 E1  0    0    0    0    0
!                                -E1  0    0    0    0    0
!                                 ……..
!                                 0    0    0    0 -E1 -E1
      do i=1,43
       do j=1,6
         EP(i,j)=0.D0
```

```
          if (IE(j,i).eq.1) EP(i,j)=E1
          if (IE(j,i).eq.2) EP(i,j)=-E1
         enddo
       enddo
! read input parameters from MNP12N.prmt
       read (18,2046) a, b, c, alpha, beta, gamma, P
       rewind(18)
! convert pressure from kbar to Ryd/bohr**3
     PX=P*PC
! find the orthogonal components of a, b, c vectors
call CONV1 (a,b,c,alpha,beta,gamma,AX)

! make ".struct" files for all 42 strained states and the unstrained state
! the structure file names have the form: case__1.struct ( unstrained state), case__2.struct
! …case_43.struct
     va_ry(1)=0
      DO i = 1, numb
        va_ry(i+1)=1+va_ry(i)
        write (zwname,'(I2)') va_ry(i+1)
        finame = orname(1:ileng) // '  '// zwname
          do iii = 1,ileng+3
              if (finame(iii:iii).ne.'  ') then
              f2name (iii:iii) = finame(iii:iii)
             else
              f2name (iii:iii) = '_'
              endif
            enddo
          joname(i+1) = f2name (1:ileng+3)
          f2name= f2name(1:ileng+3) // ext
```

```
! ‘f2name’ is the strained structure file (case__i.stuct); it has the same format as
! case.struct; only line 4 (that contain lattice parameters a, b, c, alpha, beta,  gamma)
! should be replaced.
          OPEN (21, file=f2name)
            do ii = 1,3
              read (17,245) rows
              write(21,245) rows
             enddo
! find the strain vector EPC for every single strained state
           do j=1,6
             EPC(j)=EP(i,j)
             enddo
! find the orthogonal components of ap, bp cp vectors of the strained unit cell
         call STRAIN1 (AX, EPC, AXP)
! find the volume (and pV term) of the strained unit cell
        V(i)=AXP(1,1)*(AXP(2,2)*AXP(3,3)-AXP(3,2)*AXP(2,3))  &
              +AXP(2,1)*(AXP(3,2)*AXP(1,3)-AXP(1,2)*AXP(3,3))  &
             +AXP(3,1)*(AXP(1,2)*AXP(2,3)-AXP(2,2)*AXP(1,3))
         PV(i)=PX*V(i)
! write the pV term in MNP12N.pv
       write(19,191) PV(i)
! find the lattice parameters  ap, bp, cp, alphap, betap, gammap of the strained  structure
       call CONV2(AXP,ap, bp, cp, alphap, betap, gammap)
          write (21,246)  ap, bp, cp, alphap, betap, gammap
         read (17,*) rows
         do ii=1,10000
             read (17, 245, END=244) rows
             write (21, 245) rows
         enddo
```

```
244      CONTINUE
         CLOSE (21)
         rewind (17)
         rewind (18)
     ENDDO
245    FORMAT (A79)
191    FORMAT (F10.6)
246    FORMAT (6F10.6)
2046   FORMAT (6F10.6, F10.2)
!-------------------------------------------------------------------------------------------------------
! Make the MNP12N_optimize.job script; see more details about '_optimize.job' in A.2
       write (16,'(a)') '#!/bin/csh -f'
!       backslash=1H\
       backslash=achar(92)
       write (16,'("foreach i ( ",a1)') backslash
       do i=1, numb
       write (16,'(7x,a50,a1,a1)') joname(i+1)(1:ileng+11),' ',backslash
       enddo
       write (16,*) ')'
       write (16,*) '    cp  $i', ext,' ', orname(1:ileng),ext
       write (16,*) ' '
       write (16,*) '   runsp_lapw -p -ec 0.00001 -i 200'
       write (16,*) '#   run_lapw -p -ec 0.000001 -i 200'
       write (16,*) '  '
       write (16,*) '    set stat = $status'
       write (16,*) '    if ($stat) then'
       write (16,*) '       echo "ERROR status in" $i>>MNP12N.status'
       write (16,*) '       exit 1'
       write (16,*) '    endif'
```

```
      write (16,*) '    save_lapw  $i'
      write (16,*) '    grepline1 :ENE "$i.scf" 1>>MNP12N.ene'
      write (16,*) '    clean_lapw -s'
      write (16,*) 'end'
      write (16,*) '   '
     close (16)
     return
     end
!-----------------------------------------------------------------------------------------------------
! subroutine CONV1 converts sides a, b, c in bohrs and angle alpha, beta, gamma in
! degrees to orthogonal components in bohrs
    SUBROUTINE CONV1 (a, b, c, alpha, beta, gamma, AX)
    REAL*8 a, b, c, alpha, beta, gamma, alrad, berad, garad &
              ,CGA, SGA, CBE, C0, DEGRAD,  AX(3,3)
    DATA C0, DEGRAD /0.D0, 0.017453293D0/
! DEGRAD is the conversion factor for degrees into radians
    alrad=alpha*DEGRAD
    berad=beta*DEGRAD
    garad=gamma*DEGRAD
    CGA=DCOS(GARAD)
    SGA=DSIN(GARAD)
    CBE=DCOS(BERAD)
    AX(1,1)=a
    AX(2,1)=C0
    AX(3,1)=C0
    AX(1,2)=b*CGA
    AX(2,2)=b*SGA
    AX(3,2)=C0
    AX(1,3)=c*CBE
```

```
      AX(2,3)=c*(DCOS(alrad)-CBE*CGA)/SGA
      AX(3,3)=DSQRT(c**2-AX(1,3)**2-AX(2,3)**2)
      return
      end
!-----------------------------------------------------------------------------------------------------
! subroutine CONV2 converts structure in orthogonal components in bohrs into a, b, c
! in bohrs and alpha, beta, gamma in degrees
      SUBROUTINE CONV2 (AX, a, b, c, alpha, beta, gamma)
      REAL*8 AX(3,3) , a, b, c, alpha, beta, gamma, DEGRAD
      DATA DEGRAD /0.017453293D0/
      a=DSQRT(AX(1,1)**2+AX(2,1)**2+AX(3,1)**2)
      b=DSQRT(AX(1,2)**2+AX(2,2)**2+AX(3,2)**2)
      c=DSQRT(AX(1,3)**2+AX(2,3)**2+AX(3,3)**2)
      alpha=DACOS((AX(1,2)*AX(1,3)+AX(2,2)*AX(2,3)+AX(3,2)*AX(3,3))
            /(b*c))/DEGRAD
      beta=DACOS((AX(1,3)*AX(1,1)+AX(2,3)*AX(2,1)+AX(3,3)*AX(3,1)) &
            /(c*a))/DEGRAD
      gamma=DACOS((AX(1,1)*AX(1,2)+AX(2,1)*AX(2,2)+AX(3,1)*AX(3,2)) &
            /(a*b))/DEGRAD
      return
      end
!-----------------------------------------------------------------------------------------------------
! subroutine STRAIN1 finds strained orthogonal components of the lattice vectors from
! the strain matrix and the unstrained structure (See eq. (3.1))
      SUBROUTINE STRAIN1 (AX, EPC, AXP)
      REAL*8 AX(3,3), AXP(3,3), EM(3,3), EPC(6), C1, C2
      DATA C1, C2 /1.D0, 2.D0/
! generate the strain matrix (see Eq. (3.1)) from the single-index strains; only the top
! half plus diagonal is needed
```

```
! The magnitude of the strains e1, e2 and e3 (Voigt notation in Eq. (3.1) is either 0 or E1;
! the magnitude of the strains e4, e5 and e6 (Voigt notation in Eq. (3.1) is either0 or 2*E1
      EM(1,1)=EPC(1)+C1
      EM(1,2)=2.D0*EPC(6)/C2
      EM(1,3)=2.D0*EPC(5)/C2
      EM(2,2)=EPC(2)+C1
      EM(2,3)=2.D0*EPC(4)/C2
      EM(3,3)=EPC(3)+C1
! apply the strain matrix to initial structure for strained structure
      AXP(1,1)=EM(1,1)*AX(1,1)+EM(1,2)*AX(2,1)+EM(1,3)*AX(3,1)
      AXP(1,2)=EM(1,1)*AX(1,2)+EM(1,2)*AX(2,2)+EM(1,3)*AX(3,2)
      AXP(1,3)=EM(1,1)*AX(1,3)+EM(1,2)*AX(2,3)+EM(1,3)*AX(3,3)
      AXP(2,1)=EM(1,2)*AX(1,1)+EM(2,2)*AX(2,1)+EM(2,3)*AX(3,1)
      AXP(2,2)=EM(1,2)*AX(1,2)+EM(2,2)*AX(2,2)+EM(2,3)*AX(3,2)
      AXP(2,3)=EM(1,2)*AX(1,3)+EM(2,2)*AX(2,3)+EM(2,3)*AX(3,3)
      AXP(3,1)=EM(1,3)*AX(1,1)+EM(2,3)*AX(2,1)+EM(3,3)*AX(3,1)
      AXP(3,2)=EM(1,3)*AX(1,2)+EM(2,3)*AX(2,2)+EM(3,3)*AX(3,2)
      AXP(3,3)=EM(1,3)*AX(1,3)+EM(2,3)*AX(2,3)+EM(3,3)*AX(3,3)
      return
      end
```

A.2 MNP12N_optimize.job script

```
! MNP12N_optimize.job calculates the energies of the unstrained and all 42 strained
! structures; the energies are stored in MNP12N.ene file.

#!/bin/csh –f
# ‘case’= ‘name of current directory’
        foreach i  (        case__1        \
                            case__2        \
```

```
                    ..............    \
                    case_43         )
        cp  $i.struct  case.struct

#  calculate the energy of  each structure by calling  the WIEN2k script, run(sp)_lapw
#  (non-spin or spin  polarized SCF calculations) ; the energy values are stored in case.scf
#  use the flags: -p=parallel calculation; -ec LIMIT =energy convergence LIMIT
# ( 0.000001 Ry);  -i NUMBER = maximum NUMBER (200) of iterations
# in this example spin polarized case is considered
        runsp_lapw -p -ec 0.000001 -i 200
 #      run_lapw -p -ec 0.000001 -i 200

# stop the calculation if an error occurs
        set stat = $status
        if ($stat) then
           echo "ERROR status in" $i >> MNP12N.status
           exit 1
        endif
# move case.scf (.clmsum, .dmat, vorb.) to  $i.scf, (.clmsum, .dmat, vorb.) e.g.,
# case__1.scf , by calling the WIEN2k script save_lapw after self-consistency has been
# reached
        save_lapw  $i
 # store the energy value in MNP12N.ene after self-consistency has been reached
# grepline1 script fetches from a file the last line that contains the specified string,
# e.g., ":ENE" ; it has a similar format with WIEN2k  script, grepline_lapw
        grepline1 :ENE "$i.scf" 1>>MNP12N.ene
# clean unnecessary files by calling WIEN2k script clean_lapw
        clean_lapw -s
        end
```

A.3 MNP12N routine

```
! MNP12N.f
! for a given structure,  MNP12N calculates Ci, Cij and eigenvalues and eigenvectors of
! the Cij matrix and decides what CASE it is

! input files: MNP12N.prmt, MNP12N.ene, MNP12N.pv
! output files: MNP12N.output1 and MNP12N.JSS if CASE11 or CASE 12; an additional
! output file,  MNP12N_case2.eignv,  if CASE 2

    REAL*8 a, b, c, alpha, beta, gamma,V0, P, E1, E2, PC1, AX(3,3), Ci(6), Cij(6,6) &
                , D(6), F(6), EV(6,6), CX1, CX2, CijMB(6,6), EPC(6), AXP(3,3) &
                , ap, bp, cp, alphap, betap, gammap, LM, PSI(6), XM, SPSI, &
                , E(100), G(100), PV(100)
    INTEGER i, ndata, j, JSS1, JSS2
    DATA E1, E2, PC1/ 0.04D0, 1.D-5, 147.1020888D0/
! a, b, c, alpha, beta, gamma are unit cell vector lengths (bohr) and angles (degree)
! of the input structure;
! V0 is the volume of the input unit cell.
! P is the pressure in kbar
! PC1 is the conversion factor from Ry/bohr**3 to Mbar
! ap, bp, cp, alphap, betap, gammap, are the lattice parameters of the new structure if
! CASE 11
! Ci is the matrix of the linear coefficients (in Ry/bohr**3) from Eq. (3.2)
! Cij is the matrix of the second order coefficients (in Ry/bohr**3) from Eq. (3.2)
! CijMB is the matrix of the second order coefficients (in Mbar) from Eq. (3.2)
! E1 is the strain value used to calculate the Cij
! E2 is the upper bound for the Ci that determine convergence
```

```
! E, G and PV matrices contain the energies , Gibbs free energies and PV terms (per unit
! cell) for the input structure and all 42 strained structures
! AX(3,3) is the matrix of the orthogonal components of a, b, c (see Eq.(3.1))
! AXP(3,3) is the matrix of the orthogonal components of ap, bp, cp, if  CASE 11
! EPC is the strain vector used to find the new structure, if CASE 11
! D is the eigenvalue matrix
! EV is the eigenvector matrix
! LM is the the lowest eigenvalue
! PSI is the eigenvector corresponding to LM
! JSS1=1 & JSS2= 1 if CASE 11
! JSS1=1 & JSS2= 2 if CASE 12
! JSS1=2 if CASE 2

! Read the input structure parameters from MNP12N.prmt
     OPEN (10, file='MNP12N.prmt', status='old')
     READ (10, 101) a, b, c, alpha, beta, gamma, P
101 FORMAT (6F10.6, F10.2)
      REWIND (10)
! Calculate the orthogonal components of a, b, c
     call CONV1(a, b, c, alpha, beta, gamma, AX)
! Calculate the volume of the input unit cell:
     V0=AX(1,1)*(AX(2,2)*AX(3,3)-AX(3,2)*AX(2,3)) &
          +AX(2,1)*(AX(3,2)*AX(1,3)-AX(1,2)*AX(3,3)) &
          +AX(3,1)*(AX(1,2)*AX(2,3)-AX(2,2)*AX(1,3))

     OPEN(15, file='MNP12N.output1', status='unknown')
     WRITE(15, *) ' '
     WRITE(15, 150)
150   FORMAT('     ENERGY      GIBBS FREE ENERGY   PV TERM')
```

```
! Read the energies of input and 42 strained structures from MNP12N.ene file, which is
! created by the MNP12N_optimize.job script
     OPEN (4, file='MNP12N.ene', status='old')
          i=1
410   READ (4, 41, end=411) E(i)
         i=i+1
        GO TO 410
411    ndata=i-1
41     FORMAT( 39X, F20.6)
! READ pV terms of input and 42 strained structures from MNP12N.pv file, which is
! created by MNP12N_optimize routine
     OPEN (5, file='MNP12N.pv', status='old')
          i=1
510   READ (5,51,end=511) PV(i)
         i=i+1
         GO TO 510
511    ndata=i-1
51    FORMAT (F10.6)
! Calclulate G
     DO i=1,ndata
           G(i)=E(i)+PV(i)
! write E, G, and pV terms in MNP12N.ouput1
      WRITE (15,151) E(i), G(i), PV(i)
151   FORMAT (3F15.6)
     ENDDO

! Calculate Ci and Cij (j>=i) from G(1) of the input (unstrained) structure and G(2)-G(43)
! of the strained structures
     CX1=2.D0*E1*V0
```

```
      CX2=V0*E1**2
! evaluate Ci(i), and Cij(i,i) from G(1) to G(12); see Eqs. (3.10) and (3.11)
! G(2) corresponds to the strain: e11=e1=E1 ( other e's=0);
! G(3) corresponds to the strain: e11=e1=-E1 ( other e's=0);
! use G(2) and G(3) to calculate Ci(1)=C1 (eq. (3.10)) and Cij(11)=C11 (Eq. (3.11))
! repeat the procedure to calculate C2 & C22, and C3 & C33
      do i=1,3
         j=2*i
         Ci(i)=(G(j)-G(j+1))/CX1
         Cij(i,i)=(G(j)+G(j+1)-2.D0*G(1))/CX2
      enddo
! calculate C4 & C44 using the procedure for C1 & C11; the magnitude of the strain
! e4=2* E1
! repeat the procedure to calculate  C5 & C55 and C6 & C66
      do i=4,6
         j=2*i
         Ci(i)=(G(j)-G(j+1))/(2.D0*CX1)
         Cij(i,i)=(G(j)+G(j+1)-2.D0*G(1))/(4.D0*CX2)
      enddo
! calculate the 15 off-diagonal elements of the Cij(i,j) matrix (see. Eq. (3.15))
! G(14) corresponds to the strain e1=E1; e2=E1 ( other e's=0);
! G(15) corresponds to the strain e1=-E1; e2=-E1 ( other e's=0);
! use G(14) and G(15) to calculate Cij(12)=C12 (eq. (3.15))
! repeat the procedure to calculate C13 and C23
      Cij(1,2)=(G(14)+G(15)-2.D0*G(1))/(2.D0*CX2)-(Cij(1,1)+Cij(2,2))/2.D0
      Cij(1,3)=(G(16)+G(17)-2.D0*G(1))/(2.D0*CX2)-(Cij(1,1)+Cij(3,3))/2.D0
      Cij(2,3)=(G(24)+G(25)-2.D0*G(1))/(2.D0*CX2)-(Cij(2,2)+Cij(3,3))/2.D0
! repeat the procedure to calculate the remaining Cij (j>=i) ; the magnitudes of
! the  strains are: ei=E1 for i=1, 2, 3 and ej=2*E1 for j=4, 5, 6
```

```
      Cij(1,4)=(G(18)+G(19)-2.D0*G(1))/(4.D0*CX2)-(Cij(1,1)+4.D0*Cij(4,4))/4.D0
     Cij(1,5)=(G(20)+G(21)-2.D0*G(1))/(4.D0*CX2)-(Cij(1,1)+4.D0*Cij(5,5))/4.D0
     Cij(1,6)=(G(22)+G(23)-2.D0*G(1))/(4.D0*CX2)-(Cij(1,1)+4.D0*Cij(6,6))/4.D0
     Cij(2,4)=(G(26)+G(27)-2.D0*G(1))/(4.D0*CX2)-(Cij(2,2)+4.D0*Cij(4,4))/4.D0
     Cij(2,5)=(G(28)+G(29)-2.D0*G(1))/(4.D0*CX2)-(Cij(2,2)+4.D0*Cij(5,5))/4.D0
     Cij(2,6)=(G(30)+G(31)-2.D0*G(1))/(4.D0*CX2)-(Cij(2,2)+4.D0*Cij(6,6))/4.D0
     Cij(3,4)=(G(32)+G(33)-2.D0*G(1))/(4.D0*CX2)-(Cij(3,3)+4.D0*Cij(4,4))/4.D0
     Cij(3,5)=(G(34)+G(35)-2.D0*G(1))/(4.D0*CX2)-(Cij(3,3)+4.D0*Cij(5,5))/4.D0
     Cij(3,6)=(G(36)+G(37)-2.D0*G(1))/(4.D0*CX2)-(Cij(3,3)+4.D0*Cij(6,6))/4.D0

     Cij(4,5)=(G(38)+G(39)-2.D0*G(1))/(8.D0*CX2)-(Cij(4,4)+Cij(5,5))/2.D0
     Cij(4,6)=(G(40)+G(41)-2.D0*G(1))/(8.D0*CX2)-(Cij(4,4)+Cij(6,6))/2.D0
     Cij(5,6)=(G(42)+G(43)-2.D0*G(1))/(8.D0*CX2)-(Cij(5,5)+Cij(6,6))/2.D0
! calculate Cji (j>=i); Cij matrix is symmetrical, e.g. Cji=Cij
     do i=1,6
       do  j=1,6
          Cij(j,i)=Cij(i,j)
        enddo
     enddo
! calculate CijMB from Cij by converting Ry/au**3 to Mbar
     do i=1,6
       do  j=1,6
         CijMB(j,i)=PC1*Cij(i,j)
       enddo
     enddo

! write the results in MNP12N.output1
      WRITE (15, 152) a, b, c, alpha, beta, gamma, P, Ci, Cij, CijMB
152   FORMAT (/ 'from MNP12N after Ci, Cij and CijMB are found' &
```

```
                / 'a ,b, c, alpha, beta, gamma, P(kbar)' / 6F10.6, F10.2 &
               / ' Ci(i)'/ 6F12.7 &
                / 'Cij(i,j)' / 6F12.7, 5 (/ 6F12.7) &
                / 'CijMB(i,j)' / 6F12.5, 5 (/6F12.5))

! calculate the eigenvalues and eigenvectors of  the Cij matrix
      do i=1,6
         do  j=1,6
          EV(i,j)=Cij(i,j)
        enddo
       enddo
     CALL DTRED2 (EV, 6, 6, D, F)
     CALL DTQLI (D, F, 6, 6, EV)
     WRITE (15,153) D
153   FORMAT(/ 'from MNP12N after eigenvalues and eigenvectors are found' &
                / 'D(6)'/ 6F10.6 &
                / 'EV(6,6)')
! write the vector components in columns
      do i=1,6
        WRITE (15,154) EV(i, 1), EV(i, 2), EV(i, 3), EV(i, 4), EV(i, 5), EV(i, 6)
       enddo
154   FORMAT (5X, 6F10.6)
! find the lowest eigenvalue
      LM=min (D(1), D(2), D(3), D(4), D(5), D(6))
! If LM is negative go to CASE 2 branch
      IF (LM .lt. 0.D0) GO TO 9
! set a branch for  CASE 1
      JSS1=1
      GO TO 91
```

```
! CASE 2 branch
9       do i=1,6
! find PSI vector
           if (LM .eq. D(i)) then
             PSI(1)=EV(1,i)
             PSI(2)=EV(2,i)
             PSI(3)=EV(3,i)
             PSI(4)=EV(4,i)
             PSI(5)=EV(5,i)
             PSI(6)=EV(6,i)
           endif
         enddo
! find the direction of steps that makes linear part of G (the first term on the right side
! in Eq. (3.2)) decrease
    XM=1.D0
    SPSI=0.D0
    do i=1,6
      SPSI=SPSI+Ci(i)*PSI(i)
    enddo
    if (SPSI.GT.0.D0) XM=-1.D0
! change the sign of PSI(i) if the linear part of G (SPSI) does not decrease.
       do i=1,6
          PSI(i)= XM*PSI(i)
        enddo
    JSS1=2
! MNP12N.JSS file is used by MNP12N.script to decide what case it is
    OPEN (20, file='MNP12N.JSS', status='unknown')
    WRITE (20,201) JSS1
```

```
201   FORMAT ('JSS1=', I1)
        WRITE (15,1501)
1501  FORMAT (/ 'CASE2')
        WRITE (15,1511) LM, PSI
1511  FORMAT (LM=',F10.6 &
                    / 'PSI', 6F10.6)
! MNP12N_case2.egnv is used as input file by MNP12N_case2 code
     OPEN (22, file='MNP12N_case2.egnv', status='unknown')
     WRITE(22,221)  PSI
221 FORMAT (6F10.6)
     STOP

! CASE 1 branch (includes CASE 11 and CASE 12)
! test if Ci  are convergent
91   do i=1,6
       if (DABS (Ci(i)) .GT. E2) GO TO 93
      enddo
!  convergence is reached, CASE 12 branch
       JSS2=2
       OPEN (20, file='MNP12N.JSS', status='unknown')
      WRITE (20,202) JSS1, JSS2
202   FORMAT( 'JSS1=', I1, 2X, 'JSS2=',I1)
       WRITE(15,1502) Cij, CijMB
1502  FORMAT (/ 'CASE12' &
                     / 'MINIMUM FOUND' &
                    / 'Cij(i,j)' / 6F12.7, 5 (/6F12.7) &
                   / 'CijMB(i,j)' /6F12.5, 5 (/6F12.5)/ )
      STOP
```

```
! Ci are not convergent, CASE 11 branch
93    JSS2=1
      OPEN (20, file='MNP12N.JSS', status='unknown')
      WRITE (20, 200) JSS1, JSS2
200   FORMAT ( 'JSS1=', I1, 2X, 'JSS2=', I1)
!  solve a set of 6 linear equations (Eq. (3.4)) to find the strains that reduce Ci (EPC strain
! matrix)
     do i=1,6
       EPC(i)=-Ci(i)
     enddo
     CALL DLUDCMP (Cij, 6, 6, INDX,D)
     CALL DLUBKSB (Cij, 6, 6, INDX, EPC)
! find the orthogonal components (AXP) of  the unit cell vectors of the new structure
   CALL STRAIN (AX, EPC, AXP)
! find the lattice parameters (ap, bp, cp, alphap, betap, gammap) of the new structure
     CALL CONV2 (AXP, ap, bp, cp, alphap, betap, gammap)
! write in MNP12N.output the EPC strain and the parameters of the new structure
     WRITE (15,1513) EPC, a, b, c, alpha, beta, gamma, &
                              ap, bp, cp, alphap, betap, gammap
1513  FORMAT (/ 'CASE11' &
                       / 'EPC(6)' / ,2X, 6F10.6 &
                      / 'a, b, c, alpha, beta, gamma'/ ,2X, 6F10.6 &
                      / 'ap, bp, cp, alphap, betap, gammap'/ ,2X, 6F10.6/ )
! replace (in MNP12N.prmt) the parameters of the input structure with the parameters of
! the new structure
     WRITE (10,103) ap, bp, cp, alphap, betap, gammap, P
103   FORMAT (6F10.6, F10.2)


     END
```

```
! ------------------------------------------------------------------------------------------------
! subroutines CONV1 and CONV2 are presented in A.1
!------------------------------------------------------------------------------------------------
! subroutine STRAIN finds strained orthogonal components of the lattice vectors from
! the strain matrix and the unstrained structure (See eq. (3.1))
      SUBROUTINE STRAIN (AX, EPC, AXP)
      REAL*8 AX(3,3), AXP(3,3), EM(3,3), EPC(6), C1, C2
      DATA C1, C2 /1.D0, 2.D0/
! generate the strain matrix (see Eq. (3.1)) from the single-index strains; only the top
! half plus diagonal is needed
! EPC(i) are the 6 Eulerian strains ei (in Voigt notation) calculated from Eq. (3.4)
      EM(1,1)=EPC(1)+C1
      EM(1,2)=2.D0*EPC(6)/C2
      EM(1,3)=2.D0*EPC(5)/C2
      EM(2,2)=EPC(2)+C1
      EM(2,3)=2.D0*EPC(4)/C2
      EM(3,3)=EPC(3)+C1
! apply the strain matrix to initial structure for strained structure
      AXP(1,1)=EM(1,1)*AX(1,1)+EM(1,2)*AX(2,1)+EM(1,3)*AX(3,1)
      AXP(1,2)=EM(1,1)*AX(1,2)+EM(1,2)*AX(2,2)+EM(1,3)*AX(3,2)
      AXP(1,3)=EM(1,1)*AX(1,3)+EM(1,2)*AX(2,3)+EM(1,3)*AX(3,3)
      AXP(2,1)=EM(1,2)*AX(1,1)+EM(2,2)*AX(2,1)+EM(2,3)*AX(3,1)
      AXP(2,2)=EM(1,2)*AX(1,2)+EM(2,2)*AX(2,2)+EM(2,3)*AX(3,2)
      AXP(2,3)=EM(1,2)*AX(1,3)+EM(2,2)*AX(2,3)+EM(2,3)*AX(3,3)
      AXP(3,1)=EM(1,3)*AX(1,1)+EM(2,3)*AX(2,1)+EM(3,3)*AX(3,1)
      AXP(3,2)=EM(1,3)*AX(1,2)+EM(2,3)*AX(2,2)+EM(3,3)*AX(3,2)
      AXP(3,3)=EM(1,3)*AX(1,3)+EM(2,3)*AX(2,3)+EM(3,3)*AX(3,3)
      return
```

```
      end
!-----------------------------------------------------------------------------------------------------
! subroutine DTRED2 converts a matrix A to tridiagonal form stored in D and E
      SUBROUTINE DTRED2 (A, N, NP, D, E)
      REAL*8 A(NP,NP), D(NP), E(NP), SCALE, H, F, G, HH
      INTEGER N, NP, I, K, L, J
      IF (N.GT.1) THEN
       DO 18 I=N, 2, -1
        L=I-1
        H=0.D0
        SCALE=0.D0
        IF (L.GT.1) THEN
         DO 11 K=1,L
          SCALE=SCALE+DABS(A(I,K))
11        CONTINUE
         IF (SCALE.EQ.0.D0) THEN
          E(I)=A(I,L)
           ELSE
          DO 12 K=1, L
           A(I,K)=A(I,K)/SCALE
           H=H+A(I,K)**2
12         CONTINUE
          F=A(I,L)
          G=-DSIGN(DSQRT(H),F)
          E(I)=SCALE*G
          H=H-F*G
          A(I,L)=F-G
          F=0.D0
          DO 15 J=1,L
```

```
            A(J,I)=A(I,J)/H
            G=0.D0
            DO 13 K=1,J
              G=G+A(J,K)*A(I,K)
13            CONTINUE
            IF(L.GT.J)THEN
              DO 14 K=J+1,L
                G=G+A(K,J)*A(I,K)
14              CONTINUE
            ENDIF
            E(J)=G/H
            F=F+E(J)*A(I,J)
15          CONTINUE
           HH=F/(H+H)
           DO 17 J=1,L
            F=A(I,J)
            G=E(J)-HH*F
            E(J)=G
            DO 16 K=1, J
              A(J,K)=A(J,K)-F*E(K)-G*A(I,K)
16            CONTINUE
17          CONTINUE
          ENDIF
        ELSE
          E(I)=A(I,L)
        ENDIF
        D(I)=H
18      CONTINUE
      ENDIF
```

```
      D(1)=0.D0
      E(1)=0.D0
      DO 23 I=1,N
       L=I-1
       IF (D(I).NE.0.D0) THEN
        DO 21 J=1,L
         G=0.D0
         DO 19 K=1,L
          G=G+A(I,K)*A(K,J)
19       CONTINUE
         DO 20 K=1,L
          A(K,J)=A(K,J)-G*A(K,I)
20       CONTINUE
21      CONTINUE
       ENDIF
       D(I)=A(I,I)
       A(I,I)=1.D0
       IF (L.GE.1) THEN
        DO 22 J=1,L
         A(I,J)=0.D0
         A(J,I)=0.D0
22      CONTINUE
       ENDIF
23    CONTINUE
      RETURN
      END
!-------------------------------------------------------------------------------------------
! subroutine DTQLI converts tridiagonal form to diagonal and puts eigenvectors in Z
      SUBROUTINE DTQLI (D, E, N, NP, Z)
```

```
      REAL*8 D(NP), E(NP),  Z(NP,NP), G, R, S, C, P, F, B,  DD
      INTEGER N, NP, I, ITER, L, M, K
      IF (N.GT.1) THEN
       DO 11 I=2,N
        E(I-1)=E(I)
11     CONTINUE
       E(N)=0.D0
       DO 15 L=1,N
        ITER=0
1       DO 12 M=L,N-1
         DD=DABS(D(M))+DABS(D(M+1))
         IF (DABS(E(M))+DD.EQ.DD) GO TO 2
12       CONTINUE
        M=N
2       IF (M.NE.L) THEN
         IF (ITER.EQ.30) PAUSE 'too many iterations'
         ITER=ITER+1
         G=(D(L+1)-D(L))/(2.D0*E(L))
         R=DSQRT(G**2+1.D0)
         G=D(M)-D(L)+E(L)/(G+DSIGN(R,G))
         S=1.D0
         C=1.D0
         P=0.D0
         DO 14 I=M-1,L,-1
          F=S*E(I)
          B=C*E(I)
          IF (DABS(F).GE.DABS(G)) THEN
           C=G/F
           R=DSQRT(C**2+1.D0)
```

```
            E(I+1)=F*R
            S=1.D0/R
            C=C*S
          ELSE
            S=F/G
            R=DSQRT(S**2+1.D0)
            E(I+1)=G*R
            C=1.D0/R
            S=S*C
          ENDIF
          G=D(I+1)-P
          R=(D(I)-G)*S+2.D0*C*B
          P=S*R
          D(I+1)=G+P
          G=C*R-B
          DO 13 K=1,N
            F=Z(K,I+1)
            Z(K,I+1)=S*Z(K,I)+C*F
            Z(K,I)=C*Z(K,I)-S*F
13          CONTINUE
14        CONTINUE
        D(L)=D(L)-P
        E(L)=G
        E(M)=0.D0
        GO TO 1
      ENDIF
15     CONTINUE
    ENDIF
    RETURN
```

```
      END
!-------------------------------------------------------------------------------------------------------
! subroutine DLUDCMP converts a matrix A to LU form
      SUBROUTINE DLUDCMP (A, N, NP, INDX, D)
      PARAMETER (NMAX=100, TINY=1.0D-20)
      REAL*8 A(NP,NP), VV(NMAX), D, AAMAX, SUM, DUM
      INTEGER N, NP, I, J, K, INDX(N), NMAX
      D=1.D0
      DO 12 I=1,N
       AAMAX=0.D0
       DO 11 J=1,N
        IF (DABS(A(I,J)).GT.AAMAX) AAMAX=DABS(A(I,J))
11     CONTINUE
       IF (AAMAX.EQ.0.D0) PAUSE 'Singular matrix.'
       VV(I)=1.D0/AAMAX
12    CONTINUE
      DO 19 J=1,N
       IF (J.GT.1) THEN
        DO 14 I=1,J-1
         SUM=A(I,J)
         IF (I.GT.1) THEN
          DO 13 K=1,I-1
           SUM=SUM-A(I,K)*A(K,J)
13         CONTINUE
          A(I,J)=SUM
         ENDIF
14      CONTINUE
       ENDIF
       AAMAX=0.D0
```

```
      DO 16 I=J,N
       SUM=A(I,J)
       IF (J.GT.1) THEN
        DO 15 K=1,J-1
         SUM=SUM-A(I,K)*A(K,J)
15       CONTINUE
        A(I,J)=SUM
       ENDIF
       DUM=VV(I)*DABS(SUM)
       IF (DUM.GE.AAMAX) THEN
        IMAX=I
        AAMAX=DUM
       ENDIF
16     CONTINUE
      IF (J.NE.IMAX) THEN
       DO 17 K=1,N
        DUM=A(IMAX,K)
        A(IMAX,K)=A(J,K)
        A(J,K)=DUM
17      CONTINUE
       D=-D
       VV(IMAX)=VV(J)
      ENDIF
      INDX(J)=IMAX
      IF (J.NE.N) THEN
       IF (A(J,J).EQ.0.D0) A(J,J)=TINY
       DUM=1.D0/A(J,J)
       DO 18 I=J+1,N
        A(I,J)=A(I,J)*DUM
```

```
18       CONTINUE
       ENDIF
19    CONTINUE
      IF (A(N,N).EQ.0.D0) A(N,N)=TINY
      RETURN
      END
!-----------------------------------------------------------------------------------------------------
! subroutine DLUBKSB finds solution of linear equations AX=B; puts solution in B
      SUBROUTINE DLUBKSB (A, N, NP, INDX, B)
      REAL*8 A(NP,NP), B(N), SUM
      INTEGER N, NP, I, J, II, INDX(N)
      II=0
      DO 12 I=1,N
       LL=INDX(I)
       SUM=B(LL)
       B(LL)=B(I)
       IF (II.NE.0)THEN
         DO 11 J=II,I-1
           SUM=SUM-A(I,J)*B(J)
11         CONTINUE
       ELSE IF (SUM.NE.0.D0) THEN
         II=I
       ENDIF
       B(I)=SUM
12    CONTINUE
      DO 14 I=N,1,-1
       SUM=B(I)
       IF(I.LT.N)THEN
         DO 13 J=I+1,N
```

```
          SUM=SUM-A(I,J)*B(J)
13        CONTINUE
        ENDIF
        B(I)=SUM/A(I,I)
14      CONTINUE
      RETURN
      END
```

Bibliography

[1] R. C. DeVries, *Ann. Rev. Matter. Sci.* **17**, 161 (1987).

[2] Z. C. Li, X. Q. Cheng and B. X. Liu, *J. Alloys Comp.* **327**, L1 (2001).

[3] P. F. Mcmillan, *Nature Materials* **1**, 19 (2002).

[4] S. H. Lu, J. Quinn, D. Tian, F. Jona, and P. M. Marcus, *Surf. Sci.* **209,** 364 **(**1989).

[5] D. Tian, F. Jona and P. M. Marcus, *Phys. Rev. B* **45,** 11216 (1992).

[6] H. Wormeester, E. Huger and E. Bauer, *Phys. Rev. Lett.* **77**, 1540 (1996).

[7] F. Jona and P. M. Marcus, *J. Phys.: Condens. Matter* **15,** 5009 (2003).

[8] S. L. Qiu and P. M. Marcus, *J. Phys.: Condens. Matter* **15,** L755 (2003).

[9] S. L. Qiu and P. M. Marcus, *Phys. Rev. B* **68** 054103 (2003).

[10] S. L. Qiu, F. Apostol and P. M. Marcus, *J. Phys.: Condens. Matter* **16**, 6405 (2004).

[11] S. L. Qiu, F. Apostol and P. M. Marcus, *J. Phys.: Condens. Matter* **17**, 2121 (2005).

[12] D. C. Wallance, *Thermodynamics of Crystals,* (John Wiley and Sons Inc. 1972).

[13] L. D. Landau and E. M. Lifshitz , *Statistical Physics*, 3rd ed. Part 1 (Pergamon, 1980).

[14] S. L. Qiu, P. M. Marcus, and H. Ma, *Phys. Rev. B* **62***,* 3292 (2000).

[15] S. L. Qiu, P.M. Marcus and H. Ma, *Phys. Rev. B* **64,** 104431(2001).

[16] P. M. Marcus, F. Jona and S. L. Qiu, *Phys. Rev. B* **66**, 064111 (2002).

[17] P. Alippi, P. M. Marcus, and M. Scheffler, *Phys. Rev. Lett.* **78**, 3892 (1997).

[18] E. C. Bain, *Trans. Am. Inst. Min. Metall. Eng*. **70**, 25 (1924).

[19] P. M. Marcus and F. Jona, *Eur. Phys. J. B* **45,** 39 (2005).

[20] S. L. Qiu, F. Apostol and P. M. Marcus, *J. Phys.: Condens. Matter* **19**, 136213 (2007).

[21] H. Ma, *"Epitaxial Bain paths and metastable phases of tetragonal Fe and Mn", Dissertation*, Physics Department, Florida Atlantic University, Boca Raton, 2002.

[22] P. Blaha, K. Schwarz, G. K. H Madsen, D. Kvasnicka and J. Luitz, *WIEN2k, An Augmented Plane Wave + Local Orbitals Program for Calculating Crystal Properties (*Karlheinz Schwarz, Techn. Universität Wien, Austria*,* 2001). ISBN 3-9501031-1-2; P. Blaha, K. Schwarz, P. Sorantin, *Comput. Phys. Commun.* **59** 399 (1990).

[23] K. Takemura, *Phys. Rev. B* **56** 5170 (1997).

[24] W. Potzel, M. Steiner, H. Karzel, W. Schiessl, M. Kofferlein, G. M. Kalvius and P. Blaha, *Phys. Rev. Lett.* **74**, 1139 (1995).

[25] H. Olijnyk, A. P. Jephcoat, D. L. Novikov and N. E. Christensen, *Phys. Rev. B* **62** 5508 (2000).

[26] P. Hohenberg and W. Kohn, *Phys. Rev.* **136,** B864 (1964).

[27] W. Kohn and L. J. Sham, *Phys. Rev.* **140**, A1133 (1965).

[28] V. L. Moruzzi, J. F. Janak, and A. R. Williams, *Calculated Electronic Properties of Metals*, (Pergamon Press, New York, 1978).

[29] J. P. Perdew and Y. Wang, *Phys. Rev. B* **45**, 13244 (1992).

[30] D. C. Langreth and M. J. Mehl, *Phys. Rev. B* **28** 1809 (1983).

[31] J. P. Perdew, K. Burke and M. Ernzerhof, *Phys. Rev. Lett.* **77,** 3865 (1996).

[32] J. F. Nye, *Physical Properties of Crystals*, (Clarendon Press, Oxford 1989).

[33] L. Fast, J.M. Wills, B. Johansson, and O. Eriksson, *Phys. Rev. B* **51**, 17431 (1995).

[34] Y. S. Touloukian, R. K. Kirby, R. E. Taylor and P. D. Desai, "*Thermal Expansion metallic Elements and Alloys*" *Thermophysical Properties of Matter* vol. **12** (IFI / Plenum, New York, 1979); W.B. Pearson, *A handbook of lattice spacing and structures of metals and alloys*, (Pergamon, Oxford, 1967).

[35] G. Simmons and H. Wang, *Single crystal elastic constants and calculated aggregate properties: a handbook*, (M.I.T. Press, Cambridge, Massachusettes, 1971).

[36] R. M. Wentzcovitch, J. L. Martins and G. D. Price, *Phys. Rev. Lett.* **70**, 3947 (1993).

[37] Andrew A. Quong and Amy Y. Liu, *Phys. Rev. B* **56,** 7767 (1997).

[38] B. Civalleri, Ph. D'Arco, R. Orlando, V. R. Saunders and R. Dovesi, *Chem. Phys. Lett.* **348,** 131 (2001).

[39] H. Bernhard Schlegel, *J. Comput. Chem.* **3,** 214 (1982).

[40] T. H. K. Barron and M. L. Klein, *Proc. Phys. Soc.* **85** 523 (1965).

[41] G. V. Sin'ko and N. A. Smirnov, *J. Phys.: Condens. Matter* **14** 6989 (2002).

[42] G. V. Sin'ko and N. A. Smirnov, *J. Phys.: Condens. Matter* **16** 8101 (2004).

[43] P. Söderlind, J. A. Moriarty and J. M. Wills *Phys. Rev. B* **53** 14063 (1996).

[44] K. J. Caspersen, A. Lew, M. Oritiz and E. A. Carter, *Phys. Rev. Lett.* **98** 15501 (2004).

[45] A. Landa, J. Klepeis, P. Söderlind, I. Naumov, O. Velikokhatnyi, L. Vitos and A. Ruban, *J. Phys. Chem. Solids* **67** 2056 (2006); *J. Phys.: Condens. Matter* **18** 5079 (2006).

[46] O. Gülseren and R. E. Cohen, *Phys. Rev. B* **65** 064103 (2002).

[47] R. E. Cohen, L. Stixrude and E. Wasserman, *Phys. Rev. B* **56** 8575 (1997).

[48] M. B. Kanoun, S. Goumri-Said, A. E. Merad, G. Merad, J. Cibert and H. Aouraq *Semiconduct. Sci. Technol.* **19** 1220 (2004).

[49] G. Steinle-Neumann, L. Stixrude and R. E. Cohen, *Phys. Rev. B* **60** 791 (1999).

[50] M. J. Mehl, B. M. Klein and D. A. Papaconstantopoulos, Chapt. 9 in "*Intermetallic Compounds"*, Vol. 11, Ed. by J. H. Westbrook and R. L. Fleischer (John Wiley and Sons Ltd. 1994).

[51] Y. Ding, R. Ahaja, J. Shu, P. Chow, W. Luo and H. Mao, *Phys. Rev. Lett.* ***98*** 085502 (2007).

[52] P. M. Marcus, H. Ma, and S. L. Qiu, *J. Phys.: Condens. Matter* **14,** L525 (2002).

[53] H. Ma, S. L. Qiu and P. M. Marcus, *Phys. Rev. B* **66,** 024113 (2002).

[54] L. Vocadlo, D. Alfe, M. J. Gillan, I. G. Wood, J. P. Brodholt, and G. D. Price, *Nature* **424** 536 (2003).

[55] L. Stixrude, R. E. Cohen, and D. J. Singh, *Phys. Rev. B* **50** 6442 (1994).

[56] S. S. Peng and H. J. F. Jansen, *J. Appl. Phys.* **69**, 6132 (1991).

[57] D. Spišák and J. Hafner, *Phys. Rev. B* **61**, 16129 (2000).

[58] D. Spišák and J. Hafner, *Phys. Rev. Lett.* **88**, 056101 (2002).

[59] T. Kraft, P. M. Marcus, M. Methfessel and M. Scheffler, *Phys. Rev. B* **48** 5886 (1993).

[60] P. Debye, *Ann. Phys.* **39**, 789 (1912).

[61] M. Blackman in *Handbrich der Physik,* vol. **7,** part 1, p. 325, ed. S. Flügge, (Springer, Berlin 1955).

[62] S. Narasimhan and S. de Gironcoli, *Phys. Rev. B* **65** 064302 (2002).

[63] J. Xie, S. de Gironcoli, S. Baroni, and M. Scheffler, *Phys. Rev. B* **59** 965 (1999).

[64] A. Debernardi, M. Alouani and H. Dreyssé, *Phys. Rev. B* **63** 064305 (2001).

[65] K. Takemura*, Phys. Rev. B* **60** 6171 (1999).

[66] K. Takemura, H. Yamawaki, H. Fujihisa and T. Kikegawa, *J. Phys: Condens. Matter* **14** 10563 (2002).

[67] K. Takemura, H. Yamawaki, H. Fujihisa and T. Kikegawa, *Phys. Rev. B* **65** 132107 (2002).

[68] G. Steinle-Neumann, L. Stixrude and R. E. Cohen, *Phys. Rev. B* **63** 054103 (2001).

[69] K. Takemura, *Phys. Rev. Lett.* **75** 1807 (1995).

[70] L. Fast, L. Ahuja, L. Nordström, J.M. Wills, B. Johansson and O. Eriksson, *Phys. Rev. Lett.* **79** 2301 (1997).

[71] D. L. Novikov, A. J. Freeman, N. E. Christensen, A. Svane and C. O. Rodriguez, *Phys. Rev. B* **56**, 7206 (1997).

[72] Z. Li and J. S. Tse, *Phys. Rev. Lett.* **85**, 5130 (2000).

[73] H. Olijnyk and A. P. Jephcoat, *Metall. Mater. Trans. A* **33** 743 (2002).

[74] H. Olijnyk and A. P. Jephcoat, *High Pressure Res.* **22** 43 (2002).